BRUNO GHIROTTO NUNES

# CHARACTERIZATION OF METABOLISM AND MITOCHONDRIAL DYNAMICS IN ASTROCYTES DERIVED FROM INDUCED PLURIPOTENT STEM CELLS OF MULTIPLE SCLEROSIS PATIENTS

# CARACTERIZAÇÃO DO METABOLISMO E DINÂMICA MITOCONDRIAL EM ASTRÓCITOS DERIVADOS DE CÉLULAS TRONCO PLURIPOTENTES INDUZIDAS DE PACIENTES COM ESCLEROSE MÚLTIPLA

SÃO PAULO
2021

BRUNO GHIROTTO NUNES

# CHARACTERIZATION OF METABOLISM AND MITOCHONDRIAL DYNAMICS IN ASTROCYTES DERIVED FROM INDUCED PLURIPOTENT STEM CELLS OF MULTIPLE SCLEROSIS PATIENTS

Dissertation presented to the Graduate Program in Immunology at the Institute of Biomedical Sciences of the University of São Paulo, aiming to obtain the title of Master of Science

Main field: Immunology

Supervisor: Prof. Dr. Niels Olsen Saraiva Câmara

Original version

SÃO PAULO
2021

CATALOGAÇÃO NA PUBLICAÇÃO (CIP)
Serviço de Biblioteca e informação Biomédica
do Instituto de Ciências Biomédicas da Universidade de São Paulo

Ficha Catalográfica elaborada pelo(a) autor(a)

Ghirotto Nunes, Bruno
Characterization of metabolism and mitochondrial dynamics in astrocytes derived from induced pluripotent stem cells of Multiple Sclerosis patients / Bruno Ghirotto Nunes; orientador Niels Olsen Saraiva Câmara. -- São Paulo, 2021.
118 p.

Dissertação (Mestrado) ) -- Universidade de São Paulo, Instituto de Ciências Biomédicas.

1. Esclerose Múltipla. 2. Neuroimunologia. 3. Dinâmica mitocondrial. 4. Metabolismo. 5. Células tronco pluripotentes induzidas. I. Olsen Saraiva Câmara, Niels, orientador. II. Título.

UNIVERSIDADE DE SÃO PAULO
INSTITUTO DE CIÊNCIAS BIOMÉDICAS

---

Candidato(a):

Titulo da Dissertação/Tese:

Orientador:

A Comissão Julgadora dos trabalhos de Defesa da Dissertação de Mestrado/Tese de Doutorado, em sessão publica realizada a **...../...../.....**, considerou o(a) candidato(a):

**(  ) Aprovado(a)  (  ) Reprovado(a)**

Examinador(a): Assinatura: .....
Nome: .....
Instituição: .....

Examinador(a): Assinatura: .....
Nome: .....
Instituição: .....

Examinador(a): Assinatura: .....
Nome: .....
Instituição: .....

Presidente: Assinatura: .....
Nome: .....
Instituição: .....

ICB USP

Cidade Universitária "Armando de Salles Oliveira", Butantã, São Paulo, SP - Av. Professor Lineu Prestes, 2415 - ICB III - 05508.000
**Comitê de Ética em Pesquisa em Seres Humanos - Telefone** (11) 3091-7733 - e-mail: cep@icb.usp.br

São Paulo, 16 de janeiro de 2020.

**PARECER 1460/CEPSH**
CAAE nº 26052519.9.0000.5467
Protocolo CEPSH-ICB nº 1512/19

O Comitê de Ética em Pesquisas em Seres Humanos do ICB, em 14/01/2020, **APROVOU** o projeto intitulado: "**Avaliação da dinâmica mitocondrial em astrócitos derivados de pacientes com Esclerose Múltipla**", do pesquisador: **Bruno Ghirotto Nunes**

Caberá ao pesquisador, em conformidade com a Resolução CNS nº 466/2012: 1) elaborar e apresentar a este Comitê, relatórios anuais (parciais e final) conforme modelo constante no site: ww2.icb.usp.br/icb/cepsh; 2) desenvolver o projeto conforme metodologia apresentada; 3) manter em arquivo sob sua guarda (impresso ou digital), por até 5 anos após conclusão da pesquisa, toda documentação relacionada a pesquisa; 4) encaminhar os resultados para publicação; 5) justificar ao CEP, via Plataforma Brasil, interrupção do projeto ou a não publicação de resultados; 6) finalizar o processo junto à Plataforma Brasil quando do encerramento deste projeto. O primeiro relatório deverá ser enviado, via Plataforma Brasil, até **14/01/2021**.

Atenciosamente,

Profa. Dra. **CAMILA SQUARZONI DALE**
Coordenadora do Comitê de Ética em
Pesquisas com Seres Humanos - ICB/USP

I dedicate this work to my grandfather, Renato Ghirotto (*in memoriam*), as a tribute to his career as a professor and the passion with which he always performed his duties. You will always be remembered by your kindness, intelligence and empathy. Thank you for showing me that happiness can be achieved in the simplest moments of life, when you do what you love.

**ACKNOWLEDGEMENTS**

To my advisor, professor Niels, for opening the doors of his lab to me and taking me as his student. Niels, you are outstanding as a scientist and as a person, my example of intelligence and empathy, always willing to help anyone who searches for you. Since I joined your lab, many doors have opened to me, I met so many incredible people and I learned a lot of new stuff that made me gain maturity at professional and personal levels. Besides an advisor, you have always been a friend, which I hope to last for a lifetime. Thank you for all the coffees and cakes you bring to us when you are inspired. I will always remember you wishing me "good night" when I arrived at the lab at 9AM with a sleepy face. Last but not least keep in mind that I will still beat you in the German lessons!

To my parents, Manuel and Renata for always being there for me whenever I needed them. My mother has always taught me to be authentic, to dream big and to be kind. My father is my example of resilience and honesty. Thank you both for always believing in me and for being such present parents. The completion of this step in my life is also your achievement. Love you!

To my grandmother Lidia, who is always one step ahead of her generation. Thank you for always showing so much affection and love to me.

To my grandmother Heloísa, whose life was lost to this terrible pandemic, that beyond all difficulties in her life, was always a strong and dedicated woman.

To all my friends, for being so present and so important in my life. Some special thanks go to Marcella, who has been a sister for me since undergraduation, and has helped me so much during these difficult times. I admire so much how you always reach out to everyone around you. You are very special to me. To Eloisa, with whom I got very close during my Master's, for our amazing talks, coffees and drinks together. To Paulo, for always being there for me when I needed him and for sharing his experience. I wish you all the best for this new chapter in your life and will certainly miss you! To Jean, who has always been an amazing friend, I hope to be able to visit you in Switzerland soon! To Barbara and Camila, for all the coffees and the laughs together. To Luís, our newest lab member, for the drinks and hangouts together. To Theresa, for the discussions and hangouts together, miss you a lot! To Maria Fernanda, our "Nanda", one of the most incredible scientists and persons I have ever met. To Cris Naffah, for all her help and our

nice talks. To Omar, who is a brilliant scientist and a very special person. To Matheus, for the coffees and discussions together. Finally, I want to thank all the other lab mates that are also amazing people: Mari, Laís, Vitor, Jeff, Nathalia, Araceli, Juliana, Daniel, Neto, Ingrid and Magaiver.

To Meire, our lab manager, for always helping us and for the great times together.

To my dearest friends since high school, Lara, Vitor, Fernanda, Alejandro and Pedro. Thank you for always sharing such amazing moments with me, love you!

To all my friends from undergraduation, especially Dione, Bianca, Giovanna and Arthur. Miss hanging out with you!

To professor Mayana Zatz, a brilliant scientist who has always opened her lab to me, thank you for collaborating with us during my master's. To Danyllo, who has been a mentor and a friend since I started my scientific journey, thank you for always helping me out, for the talks and for the laughs together. To Uirá Melo, thank you for our discussions and good times together, miss you! To the other friends from Mayana's lab and from the Human Genome Center, Ernesto, Luiz, Kayque, Kaid, Gerson, Heloísa, Lucas and Naila for helping me out and for the great talks.

To professor Enedina Oliveira, for helping us to obtain the patient's samples for this study and their clinical data.

To professor Alicia Kowaltowski, for collaborating with us, for the coffees and for the amazing discussions. I learned a lot from you! Special thanks to Camille, Julian and João for helping me with the metabolic assays and for the great talks. You are incredible!

To professor Glória Franco and especially Stella, for helping me out with bioinformatics analysis and for the amazing discussions in this fascinating field of biology.

To professor Carol Munhoz and her students Nilton and Regiane for giving us antibodies to perform the assays.

To professors Thiago Cunha, Alexandre Basso and Tatiana Rosenstock for their contributions in my qualification exam.

To professor Elia Caldini for assisting with electron microscopy analyzes

To all the patients who agreed to participate in this study, without your support it would not be possible.

To all employees of the Institute of Biomedical Sciences and the Human Genome Center, who make everything work well at these places. Thank you!

**FUNDING**

This Project received financial support from the São Paulo Research Foundation (FAPESP: grant #2018/23460-0). Additionally, we received support from Coordenação de Aperfeiçoamento de Pessoal de Nível Superior (CAPES) – Brazil – funding code 001.

**“Intelligence is the ability to adapt to change”**

**(Stephen Hawking)**

**RESUMO**

**GHIROTTO NUNES, B. Caracterização do metabolismo e dinâmica mitocondrial em astrócitos derivados de células tronco pluripotentes induzidas de pacientes com esclerose múltipla. 2021. 118 páginas. Dissertação (Mestrado em Imunologia) - Instituto de Ciências Biomédicas, Universidade de São Paulo, São Paulo, 2021.**

A Esclerose Múltipla (EM) é uma doença autoimune caracterizada por um quadro inflamatório crônico e progressivo no Sistema Nervoso Central (SNC), que resulta em um processo de neurodegeneração axonal, originando quadros de deficiência neurológica nos pacientes. Recentemente, estabeleceu-se que os astrócitos (células da glia) apresentam um papel chave na regulação das sinapses neuronais e na regulação dos processos inflamatórios e neurodegenerativos no SNC. Sabe-se também que os astrócitos são uma das maiores fontes de espécies reativas de oxigênio e isso está diretamente relacionado à regulação da função mitocondrial. Mitocôndrias modificam sua morfologia constantemente de acordo com as necessidades bioenergéticas da célula e alterações nos mecanismos de regulação podem desencadear processos neurodegenerativos. A EM dificilmente é representada em todas as suas apresentações clínicas por modelos animais, sendo que muitos estudos terapêuticos em modelos experimentais não conseguiram ser traduzidos para humanos devido às diferenças interespecíficas. Ainda, o estudo do papel de células residentes do SNC em pacientes de EM é dificultado por questões éticas. Nesse sentido, as células tronco pluripotentes induzidas (hiPSC), que podem ser reprogramadas a partir de amostras de sangue ou de pele dos pacientes e diferenciadas em qualquer população de células somáticas, surgem como uma abordagem poderosa para se investigar mecanismos moleculares que possam estar associados ao desenvolvimento de doenças complexas como a EM. Desta forma, neste trabalho formulamos a hipótese de que astrócitos derivados de hiPSC de pacientes com EM devem apresentar alterações de dinâmica e metabolismo mitocondrial que podem estar associadas às características fenotípicas da EM. De maneira sucinta, os astrócitos derivados de hiPSC foram obtidos e caracterizados com sucesso. Observamos diferenças basais entre os grupos tendo os astrócitos dos pacientes apresentado enriquecimento de genes associados à mitofagia e a processos neurodegenerativos, bem como de transporte de moléculas pela mitocôndria. Em seguida, observamos nesse mesmo grupo um aumento na produção de superóxido e uma diminuição da qualidade mitocondrial. Analisando funcionalmente as células por

meio da técnica de Seahorse observamos um aumento no metabolismo oxidativo e glicolítico nos astrócitos de pacientes, indicando um processo de estresse metabólico nessas células, além de uma diminuição significativa na eficiência bioenergética mitocondrial das mesmas. Por meio de microscopia eletrônica de transmissão analisamos a morfologia mitocondrial nos astrócitos e observamos um aumento significativo na fissão das mitocôndrias no grupo dos pacientes, corroborando nossos resultados de expressão gênica obtidos por PCR array. Ainda, ao encontro com os resultados anteriores, observamos uma diminuição no razão entre o DNA mitocondrial e o DNA nuclear. Como observamos um inchamento do retículo endoplasmático nos astrócitos de pacientes por microscopia eletrônica, fomos analisar a expressão de genes relacionados à via UPR (Unfolded Protein Response) bem como de genes ligados à regulação da resposta ao estresse mitocondrial e observamos que vários deles estão diminuídos significativamente nos astrócitos de pacientes, indicando um possível defeito na maquinaria celular de resposta ao estresse. Assim, nossos resultados sugerem um fenótipo de disfunção mitocondrial nos astrócitos derivados de pacientes com EM e abrem novas perspectivas para a modelagem da doença e futuras abordagens terapêuticas.

**Palavras-chave:** Esclerose Múltipla; neuroimunologia; células-tronco pluripotentes induzidas; dinâmica mitocondrial; metabolismo.

**ABSTRACT**

**GHIROTTO NUNES, B. Characterization of metabolism and mitochondrial dynamics in astrocytes derived from induced pluripotent stem cells of multiple sclerosis patients. 2021. 118 pages. Dissertation (Master's degree in Immunology) - Institute of Biomedical Sciences, University of São Paulo, São Paulo, 2021.**

Multiple sclerosis (MS) is an autoimmune disease characterized by a chronic and progressive inflammatory condition in the Central Nervous System (CNS), which results in an axonal neurodegeneration process, culminating in neurological deficiency in patients. Recently, it was established that astrocytes (glial cells) play a key role in the regulation of neuronal synapses, along with inflammatory and neurodegenerative processes in the CNS. It is also known that astrocytes are one of the major sources of reactive oxygen species and this is directly related to the regulation of mitochondrial function. Mitochondria constantly modify their morphology according to the bioenergetic needs of the cell and changes in these regulatory mechanisms can trigger neurodegenerative processes. MS is hardly represented in all its scope by animal models, and many therapeutic studies in experimental models have failed to be translated into humans due to interspecific differences. Still, the study of the role of CNS resident cells in MS patients is hampered by ethical issues. In this sense, induced pluripotent stem cells (hiPSC), which can be reprogrammed from patients' blood or skin samples and differentiated into any somatic cell population, appear as a powerful approach to investigate molecular mechanisms that may be associated the development of complex diseases like MS. Therefore, in this work we formulated the hypothesis that hiPSC-derived astrocytes from patients with Multiple Sclerosis should have changes in mitochondrial dynamics and metabolism that may be associated with the MS phenotype. In a brief manner, hiPSC-derived astrocytes were successfully obtained and characterized. We observed baseline differences between the control and patients' astrocytes, with enrichment of genes associated with mitophagy and neurodegenerative processes, as well as the transport of molecules through the mitochondria in MS astrocytes. Then, we observed in this same group an increase in superoxide production and a decrease in mitochondrial quality. Analyzing the cells functionally using the Seahorse technique, we observed an increase in oxidative and glycolytic metabolism in patients' astrocytes, indicating a process of metabolic stress in these cells, in addition to a significant decrease

in their mitochondrial bioenergetics efficiency. Using transmission electron microscopy, we analyzed the mitochondrial morphology in astrocytes and observed a significant increase in mitochondrial fission in the MS group, corroborating our gene expression results obtained by PCR array. Also, in line with the previous results, we observed a decrease in the ratio between mitochondrial DNA and nuclear DNA. As we observed a swelling of the endoplasmic reticulum in the astrocytes of patients by electron microscopy, we analyzed the expression of genes related to the UPR (Unfolded Protein Response) pathway as well as genes linked to the regulation of the response to mitochondrial stress and we observed that several of them are significantly decreased in patient astrocytes, indicating a possible defect in the cellular stress response machinery. Thus, our results suggest a phenotype of mitochondrial dysfunction in astrocytes derived from MS patients and open new perspectives for both disease modeling and future therapeutic approaches.

**Keywords**: Multiple Sclerosis; neuroimmunology; induced pluripotent stem-cells; mitochondrial dynamics; metabolism.

**LIST OF FIGURES**

**LIST OF TABLES**

**ABBREVIATIONS**

AD – Alzheimer's Disease
ADP - adenosine diphosphate
ALS – Amyotrophic Lateral Sclerosis
ATF4 – activating transcription factor 4
ATG5 – autophagy related 5
ATP – adenosine triphosphate
BAFF – B-cell activating factor
BBC3 – BCL-2 Binding Component 3
BCL-2 – B-cell lymphoma-2
BCL2L1 – BCL2 Like 1
BCS1L - BCS1 Homolog, Ubiquinol-Cytochrome C Reductase Complex Chaperone
BDNF – brain derived neurotrophic factor
c-Myc – cellular myelocytomatosis oncogene
CCL-2 – C-C motif chemokine ligand 2
CCL-20 - C-C motif chemokine ligand 20
CD8 – cluster of differentiation 8
CD20 - cluster of differentiation 20
CD38 - cluster of differentiation 38
CD80 – cluster of differentiation 80
CD86 - cluster of differentiation 86
CLPP - Caseinolytic Mitochondrial Matrix Peptidase Proteolytic Subunit
CNS – central nervous system
CNV – copy number variation
CRISPR – Clustered Regularly Interspaced Short Palindromic Repeats
CTLA-4 – cytotoxic T-lymphocyte associated protein 4
CXCL10 – C-X-C motif chemokine ligand 10
DARPP32 - dopamine- and cAMP-regulated phosphoprotein of 32 kDa
DCs – dendritic cells
DDIT3 – DNA damage inducible transcript 3
DMEM – Dulbecco's Modified Eagle's Medium
DMF - dimethyl fumarate
DMSO – dimethyl sulfoxide
DNA – deoxyribonucleic acid
Drp-1 – dynamin-related protein 1
EAE - Experimental Autoimmune Encephalomyelitis
EBs – embryoid bodies
ECAR – extracellular acidification rate
EDTA – ethylenediamine tetraacetic acid
ER – endoplasmic reticulum
ERO1A – endoplasmic reticulum oxidoreductase 1 alpha
FBS – fetal bovine serum
GDNF – glial cell derived neurotrophic factor
GFAP – glial fibrillary acid protein
GM-CSF – granulocyte-macrophage colony stimulating factor
HD – Huntington's Disease
HIF-1$\alpha$ - hypoxia-inducible factor 1-alpha

hiPSC – human induced pluripotent stem-cells
HLA – human leukocyte antigen
HMGB1 – high-mobility group box-1
HSPA9 – mitochondrial 70kDa heat shock protein
HSP60 - 60kDa heat shock protein (chaperonin)
ICAM-1 – intercellular adhesion molecule 1
IFNβ-1a - Interferon-Beta-1a
IFNβ-1b - Interferon-Beta-1b
IFN-γ – interferon gamma
IL – interleukin
iNOS – inducible-nitric oxide synthase
KLF4 – kruppel-like factor 4
LFA-1 – lymphocyte function-associated antigen 1
LONP1 – Lon Peptidase 1, mitochondrial
MAFG – Maf Bzip transcription factor G
MAT-2α – methionine adenosyltransferase 2 alpha
MCP-1 – monocyte chemoattractant protein 1
MCU – mitochondrial calcium uniporter
Mff – mitochondrial fission factor
MFI – mean fluorescence intensity
Mfn1 – mitofusin 1
Mfn2 – mitofusin 2
MHC – major histocompatibility complex
mi-RNA – micro ribonucleic acid
MS – multiple sclerosis
mt-DNA – mitochondrial DNA
mtPTP - Mitochondrial Permeability Transition Pore
NAD - Nicotinamide adenine dinucleotide
NADPH - Nicotinamide adenine dinucleotide phosphate
NCLX – Solute Carrier Family 8 Member B1
NDUFA5 - NADH:Ubiquinone Oxidoreductase Subunit A5
NF-κB - nuclear factor kappa B
NLRP3 - NACHT, LRR and PYD domains-containing protein 3
NLRC4 - NLR family CARD domain-containing protein 4
NO – nitric oxide
NPCs – neural progenitor cells
Nrf 2 – nuclear factor erythroid 2 related factor 2
OCT3/4 – octamer binding transcription factor ¾
OCR – oxygen consumption rate
Opa-1 – optic atrophy type 1
OXPHOS – oxidative phosphorylation
Parkin - Parkin RBR E3 Ubiquitin Protein Ligase
PBMC – peripheral blood mononuclear cells
PBS – phosphate buffered saline
PCR – polymerase chain reaction
PD – Parkinson's Disease
PGC-1α - Peroxisome proliferator-activated receptor gamma coactivator-1 alpha
RNA-seq – RNA sequencing

ROS – reactive oxygen species
RPMI – Roswell Park Memorial Institute Medium
RRMS – relapsing remitting multiple sclerosis
RT-qPCR – reverse transcription quantitative polymerase chain reaction
S1PR - sphingosine-1-phosphate receptor
S100-β – S100 calcium-binding protein beta
SNP – single nucleotide polymorphism
SOX2 – sex determining region Y box 2
SPMS – secondary progressive multiple sclerosis
SSEA-4 – stage-specific embryonic antigen 4
TLR3 – toll-like receptor 3
TGF-β - transforming growth factor beta
Th1 – T-helper 1
Th17 – T helper 17
UPR – unfolded protein response
VCAM-1 – vascular cell adhesion molecule 1
$\Delta\psi m$ – mitochondrial membrane potential

**ACRONYMS**

FDA – Food and Drug Administration

GEO – Gene Expression Omnibus

## SUMMARY

# 1. INTRODUCTION

## 1.1 Multiple Sclerosis

Multiple sclerosis is a chronic inflammatory disease that affects the central nervous system and currently affects more than two million people around the world [1]. A recent study made an epidemiological forecast of the incidence of MS in Brazil, showing that on average it affects 8.69/100.000 individuals, with a much higher prevalence in the South and Southeast than in the Northeast region, given that the disease affects the Caucasian population more frequently [2]. It is characterized by neurological deficits that are partial or fully recoverable, lasting from a few days to weeks. The average age of onset of symptoms is around 30 years old and approximately 25 years after diagnosis 50% of patients are permanently confined to a wheelchair. The symptoms are heterogeneous and can include sensory, vision and motor problems, as well as fatigue, pain and cognitive impairments [3].

MS is a complex and multifactorial disease. The knowledge of the genetic, environmental and lifestyle-related factors that are associated with the development of MS has been currently expanded. Environmental factors, such as smoking, diet, obesity and vitamin D intake are more determinant in susceptibility to the disease than genetic factors [4]. However, some genetic factors such as the differential expression of class II MHC haplotypes (HLA II in humans) contribute significantly to the predisposition to MS [5].

In agreement to an important autoinflammatory component in MS, a recent study showed that genetic variants in NLRP3 and NLRC4 inflammasomes influence both the susceptibility and severity of MS. The work shows that gain of function variants in the *NLRP3* and *IL1B* genes are directly associated with the severity and progression of the disease, suggesting that a constitutive activation of the NLRP3 inflammasome may be a risk factor to the development of more severe forms of MS. In this sense, the authors report that a SNP in the promoter region of *IL1B* that results in a gain of function is more frequent in the progressive forms of MS than in the relapsing-remitting ones. Still, it is shown for the first time that a SNP in the *NLRC4* intronic region, which leads to a loss of function, is more frequent in patients whose disease progression is slower and is related to a better response to IFN-γ therapy, being also more frequent in patients who are better

responders to therapy. This polymorphism leads to a decrease in *NLRC4* transcription in addition to a decrease in serum IL-18 levels, which seems to have a protective effect in MS [6].

There are two fundamental aspects in the progression of MS that must be considered: first, the neurologic manifestations of the disease are heterogeneous; second, most of the pathology manifests itself silently. Given that the disease generally affects individuals in their 20 to 30 years, uncertainties regarding the progression of symptoms negatively impact decisions both personally and professionally. Most patients start symptoms in a picture of Relapsing-Remitting Multiple Sclerosis (RRMS), which can last from years to decades, in which neuronal deficiencies are recurrent (about 1-2 times a year) but reversible and are characterized by demyelination and destruction of oligodendrocytes and axons, which occur as a result of an inflammatory process mediated by immune cells that enter the CNS. This relapsing phase lasts for a few months until a pro-resolving remitting phase occurs, characterized by a resolution of the inflammatory process and remyelination, which allows patients to recover their clinical condition, with reestablishment of the conduction of nerve impulses within the CNS. After 8 to 20 years, patients with RRMS may transition to a condition of Secondary Progressive Multiple Sclerosis (SPMS), in which neurological damage becomes progressive and irreversible. A transition from one frame of RRMS to another frame of SPMS has severe consequences for patients, leading to extremely severe cognitive and life quality issues [5].

## 1.2 Multiple Sclerosis immunopathology

It is well established that the immune system plays an essential role in MS progression by detecting induced expression of class II MHC molecules in macrophages, astrocytes, and microglial cells during MS [7]. Peripheral tolerance mechanisms mediated mainly by regulatory Foxp3+ T lymphocytes (Tregs) can inhibit the effector actions of autoreactive cells by several mechanisms, such as the release of antiinflammatory cytokines (IL-10, TGF-β, IL-35), apoptosis induction or through modulation of dendritic cells (DCs) via inhibitory receptors, such as CTLA-4. However, if this tolerance is broken in any way, autoreactive lymphocytes that recognize CNS antigens can be activated and become effector cells. Studies show that this cellular activation can occur by molecular mimicry, presentation of new autoantigens, recognition of a CNS antigen previously

phagocyted or even by stimulation of cytokines (bystander activation) [3]. In addition, environmental, genetic and infectious factors can contribute to this break in immunological tolerance. After activation, Th1, Th17 and $TCD8^+$ lymphocytes migrate to the CNS, leading to an inflammatory condition associated with tissue damage [3]. One of the most challenging questions regarding the immunopathology of MS concerns the origin of the immune response dysregulation, that is, if it starts directly in the immunocompetent cells of the CNS, with proinflammatory capacity (i.e. astrocytes and microglia) or if it is initiated in the periphery. In the first scenario, the first pathological event would occur within the CNS, in which an inflammatory state mediated by resident cells, especially astrocytes and microglia would lead to a release of CNS antigens that could be carried by antigen presenting cells (APCs) to the periphery. or drained directly to the lymph nodes. A proinflammatory autoimmune response would then be generated, mediated mainly by T lymphocytes, which would then migrate to the CNS and increase inflammation. The second model, in turn, suggests that the autoimmune response starts in the periphery, in the context of a systemic infection for example, and may eventually start inflammatory events in the CNS. Both scenarios result in a sort of positive feedback mechanism in which the tissue damage would lead to a greater release of CNS antigens to the periphery, causing greater activation and migration of autoreactive lymphocytes to the CNS and, consequently, increasing inflammation and tissue damage [4].

In an earlier stage of the disease, it is suggested that innate and adaptive immune cells may migrate from the periphery to the CNS via the blood-brain barrier, subarachnoid space or even via the choroid plexus. Upon entering the CNS, along with the resident cells (microglia and astrocytes), damage to axons and oligodendrocytes occurs, in addition to demyelination [3]. Recently, the existence of lymphatic vessels in the brain meninges has been discovered, characterizing another possible pathway for the activation of encephalitogenic immune cells, especially T lymphocytes, within the CNS. One study showed that removing meningeal lymphatic drainage in mice with Experimental Autoimmune Encephalomyelitis (EAE), an experimental model of MS, attenuates the clinical progression of the disease, but not does not lead to complete remission of the symptoms suggesting a direct participation of this pathway in the pathogenesis of EAE but without excluding other routes previously studied [8]. The later stage of MS progression is characterized by an exhaustion of adaptive immune cells. Therefore,

chronic inflammation, demyelination and progressive neurodegeneration damage are now mediated mainly by resident CNS cells with pro-inflammatory capacity, especially astrocytes and microglia [3].

Astrocytes, when stimulated by microglia, secrete the chemokine ligand CCL-2 and GM-CSF, contributing to an even greater recruitment and activation of microglial cells while producing reactive oxygen species (ROS), which intensify the process of neuronal degeneration. Astrocytes are still capable of inhibiting the differentiation of progenitor cells into oligodendrocytes, preventing neuron remyelination and are therefore key cells in the clinical course of MS [3]. There is a great amount of evidence in the literature supporting the existence of reactive astrocytes in patients with MS. In a study which aimed to understand the source of the chemokine MCP-1, important in recruiting T lymphocytes and monocytes, the researchers observed brain tissue slices from patients with the disease in the active and chronic demyelination phase and detected the presence of MCP-1 immunoreactive astrocytes, whereas the same result was not observed in perivascular and parenchymal macrophages [9]. Another study showed that in brain injuries in MS patients, activated astrocytes are BAFF producers, a factor that promotes the proliferation and activation of B lymphocytes, which could support an increase in the presentation of autoantigens coming from the CNS, leading to a worse MS progression [10]. Together, these studies demonstrate that astrocytes are activated in MS, especially in the phases of chronic demyelination and can directly impact disease progression.

## 1.3 Therapies for Multiple Sclerosis

MS is a complex disease, and no cure has been developed for it until today. For many years it was difficult to develop therapies for MS, given the limited knowledge on the pathological mechanisms that triggered it in combination with the extreme clinical variability observed in patients.

The therapeutic era in MS began with the FDA approval of Interferon-Beta-1b (IFNβ-1b) for the treatment of RRMS in 1993 [11]. A study published in 1996 [12] then showed that intramuscular injections of IFNβ-1a not only decreased the frequency of relapses in patients with RRMS but also decreased their weakness. Glatiramer acetate was the second injectable therapy approved for the treatment of RRMS in 1997, consisting of a mixture of peptides which mimic the basic myelin protein and thus competitively inhibit

the binding of immune cells to myelin [13]. Glatiramer acetate and new formulations of IFN-β constituted the therapeutic strategy adopted in the subsequent decade. The safety in the use of these drugs in humans is such that these treatments are still used to treat MS patients.

Even considering that RRMS patients responded positively to therapies with IFN-β and glatiramer acetate, their effect can be considered moderate, since they reduced the rate of relapses in only one third of the treated individuals, whereas several patients did not respond to them [11, 12, 13]. Therefore, more effective treatments have been developed over time, including therapies with monoclonal antibodies, being natalizumab the first developed. This antibody is able to block the adhesion of immune system cells, especially autoreactive T lymphocytes to the blood-brain barrier, preventing their migration to the CNS. Studies published in 1999 reported natalizumab as safe and effective in RRMS and SPMS patients, decreasing the number of active lesions in treated individuals [14]. Subsequent and larger-scale studies reaffirmed the same pattern of improvement in patients as seen in the first studies [15]. However, in 2005, three cases of patients who developed Progressive Multifocal Leukoencephalopathy (PML) during treatment with natalizumab [16] were described. In 2006, the FDA approved natalizumab therapy for patients with RRMS but with safety restrictions such as constant monitoring of patients, especially regarding the incidence of PML [17].

The treatment of RRMS has improved significantly since 2010, with the development of oral and non-injectable drugs effective in treating the disease. In comparison to previously available therapies, these drugs were either as effective or more while extending the available routes of application, satisfying patients. The first approved drug was fingolimod, a sphingosine-1-phosphate receptor (S1PR) antagonist, highly expressed in leukocytes and necessary for the escape of immune cells from lymph nodes. In this sense, fingolimod induces the retention of autoreactive T lymphocytes in the lymph nodes, preventing them from migrating into the CNS [18]. The second approved drug was teriflunomide, which inhibits the proliferation of T lymphocytes by blocking the pyrimidine synthesis pathway, decreasing the number of circulating lymphocytes [19]. The third drug approved by the FDA was dimethyl fumarate (DMF), an immunosuppressant that also decreases the number of circulating T lymphocytes,

especially TCD8 + [20]. All therapies were effective in clinical trials with RRMS patients, however fingolimod increased the susceptibility of some patients to infections [18].

Another oral drug known as cladribine has been developed for the treatment of RRMS, inducing apoptosis of lymphocytes, especially B cells, in patients. The drug had a lasting effect on treated individuals, suggesting that it promotes a prolonged remission of the disease without the need for short term therapy maintenance [21].

Recently, monoclonal antibodies known as ocrelizumab and rituximab have been developed, both targeting the CD20 molecule, found mostly on the surface of B lymphocytes [22, 23]. Ocrelizumab was approved by the FDA for the treatment of RRMS in 2017, after studies which showed that the therapy was more effective than IFNβ-1a in reducing disease progression [23].

Finally, in the last two or three years, studies have been trying to develop therapeutic strategies for SPMS such as autologous hematopoietic stem cell transplantation, which has managed to inhibit disease outbreaks and the formation of new lesions in patients [24] and an oral drug known as siponimod, which was approved by the FDA in 2019 for treating SPMS. This drug acts in a similar way to fingolimod, inhibiting S1PR and preventing the migration of autoreactive lymphocytes to the CNS and had positive effects in the patients' treatment, reducing the progression of the disease and being considered relatively safe, with very few side effects [25]. Together, these studies indicate that as much as there are therapies approved for MS, there is an urgent need for better understanding the molecular mechanisms behind the different forms of the disease so that new and increasingly effective treatments with less side effects may be developed.

## 1.4 Modeling neurologic diseases with hiPSC-derived cells

Among stem-cells, embryonic ones have stood out in studies in the biomedical field given their ability to differentiate in all cell types derived from the germ layer. Nevertheless, given the numerous ethical implications regarding their use, several researchers around the world started to look for alternative models that had the same differentiation capacity as embryonic cells. In this sense, the discovery that the state of pluripotency could be induced in fibroblasts or peripheral blood mononuclear cells (PBMCs) with the use of specific factors has revolutionized the field of medicine and opened new perspectives for both disease modeling and drug testing. This state is induced

by the overexpression of the factors Oct3/4, Sox2, Klf4 and c-Myc, which control the signaling pathways required for cellular reprogramming to a state of pluripotency, constituting the so-called induced pluripotent stem cells (hiPSC), which have unlimited self-renewal capacity and can differentiate to any type of human somatic cell. Currently, several reprogramming protocols for hiPSC use episomal or adenovirus-based vectors, to avoid the use of the c-Myc oncogene [26].

Prior to the establishment of the hiPSC technology, research in neurologic diseases was focused mainly on animal and cell culture models. Despite many important discoveries enabled using these models, they do not fully recapitulate human diseases for several reasons. Regarding animal models, species-related differences make it hard to translate study findings into humans, especially those focused on the development of new therapeutic strategies. Primary cells are, for instance, exceedingly difficult to be obtained fresh from brain tissues due to ethical implications, being most of the times replaced by post-mortem obtained samples, which lack blood and oxygen supply and are therefore distinct from CNS cells in steady-state conditions [27].

The use of hiPSC-derived cells to study neurological diseases has overcome the aforementioned disadvantages since they are obtained from human blood or skin samples, eliminating both the ethical and species-related differences issues. Additionally, hiPSC-derived cells maintain the genetic background from the donor sample and can therefore be used to investigate the functional effects of gene mutations in human diseases. Finally, the recent discovery of the CRISPR technology now allows stem-cell researchers to edit the hiPSC genome, either correcting or introducing specific gene mutations and studying their effects on differentiated cells, aiming to unravel disease mechanisms in a more precise way [27].

Regarding the CNS, hiPSC can be differentiated into several resident cell populations, such as neurons, astrocytes, oligodendrocytes and microglia, allowing researchers to study the phenotype of these cells in the context of several neurologic diseases such as Parkinson's, Alzheimer's, Amyotrophic Lateral Sclerosis and Huntington's, searching for pathology-associated molecular targets and screening for compounds that might dampen disease effects on these cells [26]. Nevertheless, it must be taken in consideration that hiPSC-disease modeling sometimes has limitations given that genetic and epigenetic variations may occur during hiPSC reprogramming, which

could lead to phenotypic differences between cell lines that are not disease-related or between clones generated from the same original cell line [27]. These changes can be overcome through using non-integrated hiPSC reprogramming methodologies such as episomal, Sendai viral and adenoviral vectors and plasmids, which maintain genome integrity during the process, instead of lentiviruses that integrate to the DNA and make the cell susceptible to SNPs and CNVs [27, 28] or using isogenic cells as controls in functional studies where a genetic mutation is involved, which can be achieved by correcting it in hiPSC using the CRISPR editing technology [27].

Finally, recent studies using hiPSC-modeling in neurologic diseases are exploring their potential to generate human brain organoids, which consist in tridimensional culture systems that mimic the human brain in developmental, morphological, transcriptional and epigenomic aspects that cannot be fully recapitulated by animal models, allowing researchers to study neurologic disease in a physiologically relevant context. This tool can be used to analyze in situ electrophysiology and calcium imaging of neuronal populations, as well as to explore molecular signatures of disease, even at a single cell level and to unravel intercellular interactions during neurodevelopment, such as the crosstalk between neurons and astrocytes. HiPSC-derived brain organoids have been used to model several diseases, such as Alzheimer's, Parkinson's, Huntington's and Autism [29].

### 1.4.1 Using hiPSC-derived astrocytes to study Multiple Sclerosis

In contrast to the abundant literature available in mouse models, the number of studies analyzing the reactivity of astrocytes in humans is reduced, mainly due to ethical implications, given the difficulty in obtaining biological samples from the CNS of individuals affected by neurological diseases. It must also be stated that there are significant differences between human and mouse astrocytes at the baseline level and in the face of inflammatory stimuli. In this context, the use of induced pluripotent stem cells appears as a technology to study molecular mechanisms of complex diseases such as MS in CNS resident cells [30].

Another relevant aspect to be considered is that the heterogeneity observed in several human diseases such as MS is hardly represented in its scope in animal models.

The generation of hiPSC from the same disease in its different clinical presentations opens doors to the discovery of molecular mechanisms that may be responsible for the transition to the most severe forms of the disease. In the case of MS, the discovery of mechanisms that are behind one of the disease presentations can assist in the development of drugs for the treatment of that phenotype [31].

Unlike another neurodegenerative diseases such as Parkinson's, Amyotrophic Lateral sclerosis, Alzheimer's and Huntington that have well described genetic mutations linked to their onset and have therefore been modeled through hiPSC-derived cells many times, MS is complex and involves both genetic and environmental factors, which makes it harder to find a consistent model that recapitulates disease aspects [32]. Nevertheless, disease-related alterations have already been demonstrated in hiPSC-derived neurons from sporadic cases of Schizophrenia [33], Alzheimer's Disease [34], Parkinson's Disease [35] and Amyotrophic Lateral Sclerosis [36], which raises the possibility whether hiPSC-derived CNS cells from MS patients, which are sporadic in their majority, could also display phenotypic abnormalities related to the disease.

There are very few studies in the literature which analyzed hiPSC-derived cells in the context of MS. It has been demonstrated that hiPSC from MS patients can efficiently be differentiated into functional neurons, astrocytes and oligodendrocytes [37, 38]. Interestingly, one recent study [39] demonstrated that hiPSC-derived neural progenitor cells from progressive MS patients have increased markers of cellular senescence and HMGB1 protein levels, inhibiting oligodendrocyte progenitor cells maturation into myelinating oligodendrocytes, which reaffirms the potential of using hiPSC technology to unravel MS pathogenic mechanisms. Regarding astrocytes there are just two studies available so far [40, 41] which derived these cells from MS patients' hiPSC but they reached very contradictory conclusions in relation to each other. One of them [40] analyzed the inflammatory reactivity of astrocytes to different inflammatory stimuli and observed no differences between secretion levels of proinflammatory cytokines between cells from controls and MS patients, suggesting that genetic risks for MS should be more linked to the regulation of immune response than directly to CNS resident cells. Although the authors do not report differences between hiPSC-derived astrocytes from controls and MS patients in a basal level, they essentially focus on transcriptomic changes between these cells and do not assess another functional aspects of these cells which are very

relevant to MS pathology, such as mitochondrial dysfunction along with the metabolic profiling of these astrocytes. The other study [41] showed instead that a genetic risk variant (rs7665090$^{G}$) on astrocytes which leads to a gain of function in NF-κB is related to a higher risk of developing MS. Interestingly, the authors also report impairments in metabolic parameters that are important to astrocyte homeostasis including glutamate uptake and lactate secretion in hiPSC-derived astrocytes bearing the risk variant. Therefore, in opposition to the previous study [40], their results demonstrated that MS risk is also influenced by dysregulated responses of CNS resident cells such as the astrocytes, which should play a significant role in establishing autoimmune inflammation within the CNS.

Despite several advances in the field of MS, there are many questions regarding the onset of the disease, its subtypes and different responsiveness to therapies which still need to be better elucidated. Therefore, the ability to obtain a specific phenotype of an MS patient on a laboratory dish appears as an alternative capable of overcoming most of the limitations of existing animal models of autoimmune demyelinating diseases, in addition to allowing the in-depth study of human CNS resident cells which were a priori very little accessible [31]. The specific analysis of these populations at the molecular level should, in a long-term perspective, allow the development of new therapeutic strategies for each subtype of MS, increasing the effectiveness of the treatments currently available

## 1.5 The role of astrocytes in Multiple Sclerosis

Astrocytes are the predominant glial cells in the CNS and are essential in maintaining homeostasis of several biological factors such as glutamate and extracellular potassium [42]. In addition, these cells communicate directly with other astrocytes and oligodendrocytes through communicating junctions, forming a connection network between glial cells [43].

Currently, it is known that astrocytes are key cells in the regulation of neuronal synapses, forming the so-called tripartite synapses, being able to regulate neuronal activity by releasing neurotransmitters such as glutamate, D-serine and ATP [44]. A single astrocyte can connect to several neuronal synapses at the same time, and it can also alter gene expression in neurons by releasing exosomal vesicles containing miRNA molecules. Furthermore, astrocytes can release neurotrophic factors and are metabolically linked to

neurons, providing the latter with lactate and antioxidant factors such as glutathione and thioredoxin. Finally, astrocytes also participate in the synthesis of some neurosteroids such as estrogen and dehydroepiandrosterone (DHEA), which modulate excitability and promote neuronal myelination [43].

Healthy astrocytes contribute to the maintenance of an antiinflammatory microenvironment in the CNS by the constitutive release of IL-10 and TGF-β, expression of the Fas ligand (FasL) molecule and induction of the expression of the inhibitory co-stimulation molecule CTLA-4 on the surface of T lymphocytes [43]. Astrocytes can be activated and become reactive upon the recognition of damage-associated molecular patterns (DAMPs) or pathogens (PAMPs), the first being the results of tissue damage to the CNS and the last from viral or bacterial infections, for example. When stimulated, astrocytes shift to a pro-inflammatory profile, increasing the release of cytokines such as TNF-α, IL-1β and IL-6, several chemokines including CCL2, CCL20 and CXCL10, neurotrophic factors (such as BDNF), adhesion molecules (LFA-1, ICAM-1 and VCAM-1), vascular endothelial growth factor (VEGF), ROS and reactive nitrogen species. Astrocytes activated with IFN-γ combined or not with TNF-α showed increased expression of MHC class II, co-stimulatory molecules CD80 and CD86 and adhesion molecules, suggesting that upon neuroinflammation these cells may contribute by displaying antigens to T lymphocytes. Finally, a cascade of proinflammatory cytokines in the CNS disrupts the metabolic and homeostatic functions of astrocytes, directly impacting neuronal activity due to changes in the availability of lactate and glutamate in the medium [43].

Like macrophages, astrocytes also receive a specific classification regarding their metabolic polarization profiles, being divided into A1, proinflammatory and A2, antiinflammatory [43, 45]. A1 astrocytes are induced by inflammatory stimuli and are abundant in diseases such as MS, being characterized by the abundant expression of the Complement System C3 protein and the release of ROS, TNF-α and CCL2, which promote neurodegeneration, inflammation and leukocyte recruitment to SNC, respectively. A2 astrocytes, in turn, are related to post injury and inflammatory processes neuronal regeneration processes, releasing neurotrophic factors such as BDNF and GDNF, in addition to their capacity to form astroglial scars [43].

Recent studies emphasize the proinflammatory role of astrocytes during neuroinflammation and suggest a key role for mitochondria in the regulation of these processes. One of them [46] showed that sphingolipid metabolism in astrocytes activates cytosolic phospholipase A2 (cPLA2) which is translocated to the mitochondrion, inducing the activation of a protein called MAVS (Mitochondrial Antiviral Signaling Protein), leading to its oligomerization and activation of subsequent downstream signaling pathways, which induce astrocyte proinflammatory activity via activation of the NF-κB transcription factor. Furthermore, the authors showed that the cPLA2-MAVS interaction controls the metabolism of astrocytes, decreasing the activity of the enzyme hexokinase 2 and consequently reducing glycolysis and lactate production, the latter essential for the metabolic regulation of neurons. The study identified that the drug Miglustat, which interferes with sphingolipid metabolism by inhibiting glucosylceramide synthesis, can suppress the activation of the cPLA2-MAVS-NF-κB pathway axis and consequently decrease the pathogenic activity of astrocytes, improving the progression of EAE, the animal model of MS [46]. The second study [47] by the same group performed an RNA sequencing of astrocytes from EAE mice and MS patients, demonstrating that they have a decrease in the expression of the antioxidant response regulating factor NRF2 (Nuclear factor erythroid 2- related factor 2) together with an increase in the expression of the MAFG transcription factor, which helps the MAT2α factor in DNA methylation and consequent inhibition of anti-inflammatory and antioxidant responses in cells. The inactivation of MAFG and MAT2α in astrocytes using the CRISPR technology resulted in improvement in the progression of EAE, with a decrease in the clinical score of the disease in mice, in addition to increasing antioxidant activity and decreasing proinflammatory signaling pathways in the cells. Interestingly, an analysis of the proinflammatory astrocyte clusters in both EAE and MS using bioinformatics tools identified the most significantly altered signaling pathways in these cells in the context of these diseases, with mitochondrial dysfunction appearing in both, although it was not deeply explored in this study [47]. These works together suggest that astrocytes actively participate in the pathology of MS and that mitochondria are closely linked to this process, indicating that there must be a better investigation and characterization of mitochondrial changes in astrocytes in these diseases, aiming at the discovery of new therapeutic targets.

## 1.6 Oxidative Stress and Neurodegeneration in Multiple Sclerosis

A possible mechanism to explain the neurodegeneration observed in the most advanced stages of MS is mitochondrial dysfunction, since mitochondria participate in intracellular calcium homeostasis and in the production of ATP and ROS and therefore failures in these organelles that occur as a secondary effect to the inflammatory process observed in the disease, results in energy imbalance whereas increasing the neuronal degeneration process [48, 49].

The CNS has a high-energy demand resulting mainly from neuronal oxidative metabolism to maintain its proper functioning, which makes it highly susceptible to mitochondrial dysfunctions, evidenced by the huge number of neurodegenerative diseases whose primary cause involve mutations in the mitochondrial DNA (mtDNA) or mutations in protein-coding genes that are essential for mitochondrial function, being examples Alzheimer, Parkinson and Amyotrophic Lateral Sclerosis [48, 50, 51].

The release of excessive amounts of ROS can be a consequence of mitochondrial dysfunction. The two major sources of ROS production by mitochondria are the complexes I and III of the mitochondrial electron transport chain in a process called reverse electron transport, which is induced in situations where there is a hyperpolarization of the mitochondrial membrane, which occurs during an inflammatory response for example. In this sense, stimulation of a cell with bacterial LPS induces an increase in the $\Delta\psi m$ that leads to the accumulation of succinate. This succinate starts to be oxidized by the enzyme succinate dehydrogenase, leading to an excessive production of ROS by the complex I of the mitochondrial electron chain, which, in turn, stabilizes the transcription factor HIF-1α, that acts by promoting an increase in glycolytic metabolism combined with a greater induction of pro-inflammatory cytokines such as IL-1β while suppressing the transcription of cytokines with a role in regulating the immune response, such as IL-10 [52].

In opposite to neurons, astrocytes have shown to display a higher glycolytic profile, producing high levels of lactate that are released and uptaken by neurons in a process known as the astrocyte-neuron lactate shuttle, a very important process in the regulation of brain energy metabolism [53]. Astrocytes in a steady-state condition possess a very efficient antioxidant machinery coordinated mainly by the Nrf2 transcription factor, with increased levels of glutathione precursors and enzymes that can detoxify ROS molecules

[53]. In the case of neurodegenerative diseases such as MS, mitochondrial dysfunctions in astrocytes directly impact the production of ROS and the metabolism of these cells, which can alter the regulation of neuronal synapses and increase the process of axonal neurodegeneration, worsening disease pathology [43]

## 1.7 Mitochondrial dynamics in the regulation of cell metabolism

Mitochondria are organelles with a highly-organized architecture. The mitochondrion is composed of two membranes, one external and one internal, the latter in which the electron transport chain is located. The main role of mitochondria in cells is the coupling of substrate oxidation by the tricarboxylic acid (TCA) cycle to oxidative phosphorylation (OXPHOS), which results in a high rate of ATP production (up to 36 molecules of ATP for each molecule of glucose). In addition, another important role of these organelles is the use of TCA cycle intermediates in anabolic or regulatory reactions. Nevertheless, mitochondrial metabolic activity also culminates in the production of mitochondrial ROS through monoelectronic reactions using molecular oxygen and generating anion superoxide and its dismutation product, hydrogen peroxide. These molecules can either function as cell signalers or promote cell damage, mainly through DNA damage, depending on their relative concentrations [54].

Contradictory to the original thoughts, mitochondria are not static organelles but highly dynamic, changing their bioenergetic patterns according to the metabolic needs of cells. Changes in mitochondrial morphology are coordinated by two key processes, fusion and fission. They guarantee the effective segregation of mitochondrial DNA as well as regulate the production levels of mitochondrial ROS, calcium homeostasis and OXPHOS. Mitochondrial fusion is a process still poorly understood, but it happens in 2 stages: first, the fusion of the outer membrane is regulated by the interaction between two GTPases proteins called mitofusins 1 and 2 (Mfn1 and Mfn2), while fusion of the inner membrane depends on another protein, Opa1. Mitochondrial fission is, in turn, induced in sites marked by actin or the endoplasmic reticulum, with the action of the adapter protein Mitochondrial fission factor, which recruits another protein, Drp-1 and the interaction between these proteins forms spirals that fragment the structure of the mitochondria [54].

Mitochondrial dynamics is also regulated by upstream transcription factors such as PGC-1α and HIF-1α. PGC-1α mediates mitochondrial biogenesis through the co-activation of Mfn2, one of the key mediators of mitochondrial fusion, recycling dysfunctional mitochondria and increasing the organelle numbers within the cells. HIF-1α, in the opposite direction, favors mitochondrial fission through phosphorylation at serine 616 of Drp-1, facilitating translocation this protein into the mitochondria and concomitant activation [55]. In the context of neurodegeneration, mitochondrial dysfunction is a hallmark of the pathology of several diseases, in which PGC-1α has shown to exert protective effects by upregulating mitochondrial biogenesis whereas HIF-1α is possibly related to increased mitochondrial fragmentation and stress, having therefore pathogenic effects [55, 56, 57]. It is important to point out that mitochondrial dynamics is an emerging field of research in neurodegenerative diseases and therefore the exact role played by these aforementioned transcription factors in regulating this process is still poorly understood.

In terms of cell metabolism, it has been originally demonstrated in T lymphocytes that mitochondrial dynamics regulate metabolic profiling of these cells. T memory cells rely mainly on β-oxidation to perform their functions, having increased number of fusioned mitochondria with elongated shape, which sustains the high mitochondrial metabolism demand of this subpopulation. On the other hand, T effector cells rely mainly on glycolysis, which might be facilitated by the increased number of fragmented mitochondria in this subpopulation. Genetic deletion of mitochondrial dynamics regulators in these immune cells resulted in metabolic alterations, indicating a role of this process in the regulation of cellular metabolism [54]. The role of mitochondrial dynamics in shaping the metabolism of other immune and non-immune cells should be further elucidated.

Mitochondria also play a key role in regulating calcium metabolism in cells. These organelles have the capacity to capture an enormous amount of calcium, albeit with a lower affinity than that presented by the endoplasmic reticulum, acting as buffers in cases of accumulation of the ion in the cytosol, which is extremely harmful to cells. The uptake of mitochondrial calcium occurs through a transporter known as MCU, a process that is also regulated by the mitochondrial membrane potential. However, an excessive accumulation of calcium in the mitochondria is extremely harmful to cells, since it induces

a phenomenon known as mitochondrial permeability transition, leading to the loss of the impermeability of the inner mitochondrial membrane together with the opening of a pore known as mtPTP, which leads to a release of the contents of the organelles into the cytosol, culminating in exacerbated cell death. This phenomenon has been reported in several diseases, such as stroke and in cases of liver inflammation. Mitochondrial dynamics play a key role in maintaining mitochondrial calcium transport, so that the Mfn2 protein mediates the interaction between mitochondria and the endoplasmic reticulum, regulates mitophagy and can increase the bioenergetic efficiency of cells. Also, changes in the morphology of mitochondria have been directly associated with the ability to capture cellular calcium, so that an increase in mitochondrial fusion, resulting in more elongated organelles through an increase in the expression of Mfn2, increases their efficiency in capturing calcium. On the other hand, induction of mitochondrial fission led to a decrease in baseline calcium levels as well as a decrease in calcium retention by the endoplasmic reticulum [58].

A failure in the mechanisms that regulate mitochondrial dynamics can result in dysfunctions in the mitochondria, associated with neurodegenerative processes. Fragmented mitochondria, which have undergone mitochondrial fission, generate more ROS, leading to increased neuronal degeneration. Astrocytes play an important role in the metabolism of glutathione, an important antioxidant that protects cells from the effects of free radicals and express the transcription factor Nrf2, which is also directly associated with the antioxidant response and is a molecular target of one of the main therapies indicated for patients with MS, dimethyl-fumarate [47, 59]. A study showed that upon proinflammatory stimuli such as LPS + IFN-γ and IL-1β, astrocytes modify their mitochondrial dynamics profile by increasing mitochondrial fission, with higher expression of Drp1, which results in greater production of ROS. In addition, the increased expression of Drp1 was shown to be dependent on iNOS activity, since inhibition of this enzyme inhibited the transition of mitochondria to a more fragmented state. Finally, this iNOS pathway, leading to the production of NO (RNS) and Drp1 expression, has been shown to act by signaling transduction of inflammatory stimuli into changes in mitochondrial morphology to a state of fission, which in turn further accentuates the NO production by astrocytes, contributing to increase the degenerative process [60].

In this sense, here we hypothesized that MS-derived astrocytes might have alterations in mitochondrial dynamics and metabolism that could be somehow related to the disease phenotype.

# 2. OBJECTIVES

## 2.1 Main

To characterize the mitochondrial dynamics and metabolism of hiPSC-derived astrocytes from controls and MS patients

## 2.2 Specific

i. Characterize the hiPSC, NPCs and astrocytes derived from controls and patients;
ii. Validate the hiPSC-derived cells technology as a reliable tool to study MS;
iii. Analyze the expression of genes related to mitochondrial metabolism and dynamics;
iv. Quantify the levels of proteins related to mitochondrial dynamics;
v. Visualize the mitochondrial morphology;
vi. Determine the metabolic profile of these cells; and
vii. Analyze ROS production.

# 3. MATERIALS AND METHODS

## 3.1 Experimental Design

An experimental design of our study protocol is illustrated below (Figure 1).

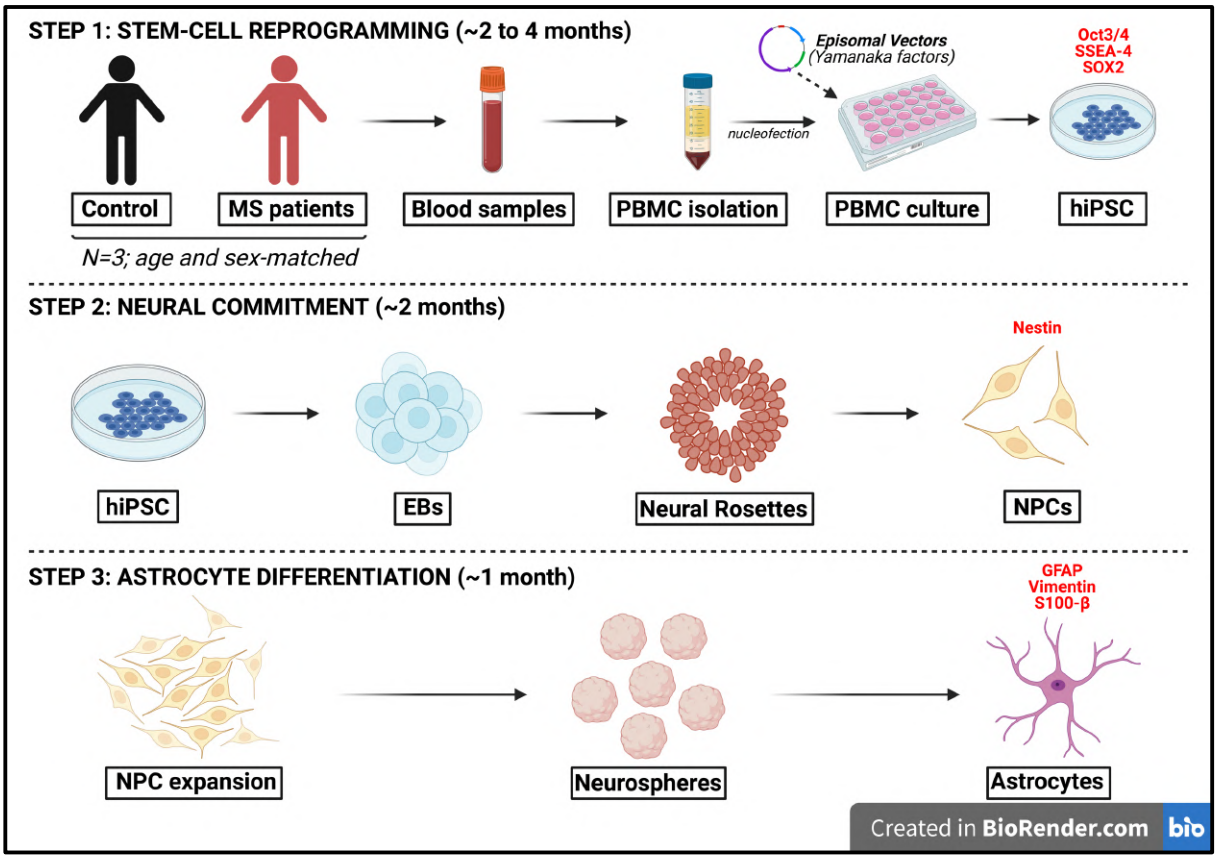


**Figure 1. Experimental Design.** The cell culture protocol consists of 3 main steps: Step 1, Stem-cell reprogramming, takes about 2 to 4 months to be completed. Blood samples were obtained from 3 MS patients and 3 age and sex-matched controls and used for isolation of PBMCs. The PBMCs were cultured and nucleofected with episomal vectors containing the Yamanaka factors required for cell reprogramming into hiPSC. To characterize the hiPSC we used the markers Oct3/4, SSEA-4 and SOX2; Step 2, Neural commitment, lasts usually 2 months. hiPSC were cultured in suspension as EBs, being exposed to neural differentiation factors and then plated to form neural rosettes. Rosettes were manually picked, expanded and dissociated, giving rise to the NPCs. Here, we characterized NPCs as Nestin⁺ cells; Step 3, Astrocyte differentiation, takes about 1 month and consists of NPCs expansion and culture in suspension as neurospheres, being exposed to astrocyte differentiation factors. Neurospheres are then plated and give rise to astrocytes, which were the cells used for further experiments in this study. We used GFAP, Vimentin and S100-β as astrocyte markers. The figure was generated using Biorender.

## 3.2 Ethics

All human procedures in this study as well as the inclusion and the exclusion criteria and the consent forms were approved by the Ethics Committee on Human

Research of the Institute of Biomedical Sciences – University of São Paulo, under the protocol number 1460/CEPSH and register number CAAE nº 26052519.9.0000.5467.

### 3.3 Patients

Samples from three Multiple Sclerosis patients were obtained at the Demyelinating Diseases Department at the São Paulo School of Medicine, federal University of São Paulo located at Rua Pedro de Toledo, nº 650 - Vila Clementino, São Paulo, SP – Brazil. The inclusion and exclusion criteria for the selection of the patient cohort are outlined below.

***Inclusion Criteria:*** 1. Adults of both sexes aged 18 years or older; 2. Consent forms signed at the Demyelinating Diseases Department, Federal University of São Paulo; 3. Multiple Sclerosis patients who were not using immunosuppressive drugs, such as Azathioprine, Cyclophosphamide, Mitoxantrone, Cyclosporine and Methotrexate, were included.

***Exclusion Criteria:*** 1. Age below 18 years; 2. Use of immunosuppressive drugs, such as Azathioprine, Cyclophosphamide, Mitoxantrone, Cyclosporine and Methotrexate, since they can interfere with the analyzes of this project; 3. Pregnant or lactating patients; 4. Patients with significant medical or surgical conditions, psychiatric disorders or who need any medication or treatment that may interfere with the progress of this study; 5. Patients who underwent another experimental treatment protocol prior to donation of the samples.

**Table 1. Clinical data of MS patients studied.** Legend: M – male; F – Female; OCB – oligoclonal bands of immunoglobulin G in the cerebrospinal fluid; N/A – not available.

| *Initials* | *Birth date* | *Gender* | *Diagnosis* | *Relapses* | *First Symptom* | *OCBs* | *Medication* | *Time of Symptoms* |
|---|---|---|---|---|---|---|---|---|
| ***P.C.*** | 09/21/1959 | M | RRMS | 10 | Brainstem | Positive | None | 29 years |
| ***A.M.*** | 08/26/1985 | F | RRMS | 1 | Spine | N/A | IFNβ-1a | 4 years |
| ***E.P.*** | 05/10/1965 | F | RRMS | 4 | Sensitive | N/A | None | 21 years |

## 3.4 Controls

Samples from three healthy individuals, age and sex-matched with the MS patients were collected at the Human Genome and Stem Cell Research Center at the University of São Paulo, located at Rua do Matão, nº106 - Butantã, São Paulo.

***Inclusion Criteria:*** 1. Adults of both sexes aged 18 years or older; 2. Informed Consent Form signed at the Human Genome and Stem Cell Research Center University of São Paulo; 3. Individuals without serious comorbidities such as chronic diseases (diabetes, decompensated dyslipidemia, recent infectious disease, among others).

***Exclusion Criteria:*** 1. Age below 18 years; 2. Pregnant or lactating women; 3. Individuals with significant medical or surgical conditions, psychiatric disorders or who need any medication or treatment that may interfere with the progress of this study; 4. Individuals who have undergone another treatment protocol.

## 3.5 PBMC isolation

PBMCs were isolated using density gradient centrifugation. First, we added 3mL of a medium containing 2mM filtered EDTA in 1x PBS to 5mL of blood to prevent coagulation of the samples. Then, 3mL of Ficoll-Paque (GE healthcare, USA) was added to a 10mL Leucosep tube (Greiner Bio-one, Austria) and centrifuged at 1000g for 10 minutes, room temperature. The previously diluted blood was then added to the Leucosep tube and centrifuged at 400g for 30 minutes without break, room temperature. Following centrifugation, the plasma layer was removed and the white cells ring formed (PBMCs) was transferred to a new 15mL falcon tube. The tube was completed with the same medium containing EDTA and PBS to 15mL and centrifuged at 300g for 10 minutes, room temperature. Then, the supernatant was discarded, resuspended in 15mL of the same medium and centrifuged at 200g for 15 minutes (this step was repeated twice). The supernatant was discarded, the cells were resuspended in 5mL of the same medium and then counted. Finally, samples were centrifuged at 200g for 15 minutes, the supernatant was discarded and cells were resuspended at a density of 3-5x$10^6$ per cryovial in RPMI medium containing 10% DMSO.

### 3.6 PBMC expansion

PBMCs were thawed in a water bath at 37°C, transferred to a 15mL falcon tube containing 9mL of 1x PBS and 20% FBS (Gibco, USA) and then centrifuged for 10 minutes at 400g, room temperature. The supernatant was discarded and resuspended in 1mL of erythroblast medium consisting of Stemspan medium (Stemcell technologies, Canada) supplemented with 50ng/mL recombinant human stem-cell factor (R&D systems, USA), 2U/mL of human erythropoietin (R&D systems, USA), 1μM of dexamethasone (Sigma-Aldrich, USA), 40ng/mL of insulin-like growth factor 1 (Miltenyi, Germany), 10ng/mL of interleukin-3 (Miltenyi, Germany) and 10μg/mL of gentamicin (Life technologies, USA). Then, the resuspended cells were transferred to a 24-well ultra-low attachment plate (Corning, USA) and incubated at 37°C with 5% $CO_2$. Amplification of the cells consisted in flushing them twice a day, every day using a Pasteur pipette for the next 10 days to avoid their differentiation into erithrocytes. The cells were tested for mycoplasma contamination using the MycoAlert kit (Lonza, Switzerland).

### 3.7 hiPSC reprogramming

Prior to reprogramming, the PBMCs were flushed and transferred to a falcon tube at a density of $1x10^6$ cells to perform the nucleofection protocol. Nucleofection was performed using 2μg of each episomal plasmid (non-integrating) containing the Yamanaka factors required for induction of cell pluripotency (pCXLE-hOCT3/4-shp53; pCXLE-hSK; pCXLE-hUL, all from Addgene, USA) and a mix of 82μL of nucleofection solution and 18μL of supplement (Lonza human nucleofection kit, VPA-1003, Switzerland). The next day following nucleofection, cell medium was changed (using erythroblast medium) to remove nucleofection reagent and dead cells. Three days after nucleofection, cells were plated on irradiated murine embryonic fibroblasts (Millipore — A24903, USA) in embryonic stem cell medium (DMEM/F12 supplemented with 2mM GlutaMAX, 0.1mM non-essential amino acids, 100μM 2-mercaptoethanol, 20% knockout serum, all from Life Technologies, USA) containing 10ng/mL basic human fibroblast growth factor, 0.25mM sodium butyrate, 0.5mM valproic acid, 2μM thiazovivin, 0.5μM PD0325901, and 2μM SB431542, all from Tocris Bioscience, UK). The colonies of hiPSCs

were manually picked and then transferred to 60mm petri dishes coated with matrigel (Corning — 354277, USA) and cultured in Essential 8 medium (Life Technologies-A1517001, USA) with 100µg/mL of Normocin (InvivoGen-ant-nr-1). Rho-associated protein kinase (ROCK) inhibitor (Y-27362, Tocris Bioscience, UK) was added to the medium after colony selection and every time the cells were splitted. The E8 medium + normocin was used to expand the cells and was changed every day. Some hiPSC were frozen using CryoStor freezing medium (Stem cell technologies, Canada). One clone was selected for each subject for further characterization and study.

## 3.8 hiPSC characterization

### 3.8.1 Multiplex Ligation-dependent Probe Amplification (MLPA)

Multiplex Ligation-dependent Probe Amplification (MLPA) is a multiplex PCR method that is used to detect chromosomal abnormalities in cells. It detects abnormal copy numbers in chromosomal candidate regions using DNA samples. MLPA is subdivided into 5 main steps: 1 – denaturation of the DNA followed by hybridization of the probes; 2 – probe ligation (the probe ligation products correlate with the number of target sequences in the DNA sample); 3 – probe amplification through a PCR reaction that has the probe sequence as a target; 4 – fragment separation using capillary electrophoresis, being the PCR products separated by length and each fragment being associated to a given MLPA probe; 5 – data analysis [61].

The total genomic DNA was extracted from hiPSCs using the DNeasy Blood and Tissue kit (QIAGEN – 69504, Germany), according to the manufacturer's instructions. MLPA analysis was performed using subtelomeric kits (P036 and P070; MRC - Holland). The PCR products were detected by the ABI3130 Genetic Analyzer (Applied Biosystems, USA) using capillary electrophoresis and the generated raw data was analyzed through the GeneMarker software (Softgenetics, USA).

### 3.8.2 Analysis of pluripotency markers using confocal microscopy

hiPSC were plated in matrigel (Corning — 354277, USA) coated Lab-tek 8-well chamber slide systems (Thermo Fisher, USA) at a density of $4x10^4$ cells per well in

Essential 8 medium (Life Technologies-A1517001, USA) with 100µg/mL of Normocin (InvivoGen-ant-nr-1). Two days after, the medium was removed and cells were fixed with a solution of 4% paraformaldehyde (PFA) in 1x PBS for 15 minutes at room temperature followed by 3 washes with 1x PBS. After that, cells were permeabilized with a solution of 0,01% Triton X-100 (Bio-rad laboratories, USA) in 1x PBS for 30 minutes at room temperature followed by 3 washes with 1x PBS. Then, cells were blocked using a solution of 5% bovine serum albumin in 1x PBS for 1 hour at room temperature followed by 3 washes with 1x PBS. Then, the cells were incubated overnight with primary antibodies at 4 ° C followed by 3 washes with 1x PBS and subsequently labeled with a secondary fluorescent antibody for 1 hour at 4 ° C, followed by 3 washes with 1x PBS. Finally, hiPSCs were incubated with DAPI (4', 6-diamidino-2-phenylindole) (1:2000) for 1 minute at room temperature followed by 1 wash with 1x PBS. The slides were mounted with Vectashield (Vector Laboratories, USA), dried, sealed and the analysis was performed using the Zeiss LSM 800 confocal microscope. Quantification of percentage of positive cells was performed using the FIJI software.

**Table 2. Antibodies used to characterize hiPSC through confocal microscopy**

| ***Antibodies*** | ***Type*** | ***Brand*** | ***Catalog*** | ***Dilution*** |
|---|---|---|---|---|
| *anti-SSEA-4 APC* | Conjugated | R&D Systems | FAB1435A | 1:100 |
| *rabbit anti-OCT4 policlonal* | Primary | Abcam | ab19857 | 1:100 |
| *AF488 goat anti-rabbit IgG* | Secondary | Life | A11034 | 1:1000 |

### 3.8.3 Analysis of pluripotency markers using RT-qPCR

Total RNA was isolated from hiPSCs using the RNeasy mini kit (QIAGEN – 74104, Germany), according to the manufacturer's instructions. The purity of the RNA was analyzed using quantification on the NanoDrop ND-1000 Spectrophotometer (NanoDrop Technologies) and the integrity validated using a 1% agarose electrophoresis gel. The synthesis of cDNA was performed with an initial amount of 2000 ng RNA using the M-MLV Reverse Transcriptase System (Promega, USA). Using a 0.2 mL tube, 2000 ng of RNA, 2.5 µL of DNAse, 5 µL of 10X Reaction Buffer and 1 µL of DNase-RNAse free were placed in

each sample for digestion of contaminating DNA. The samples were placed in a Mastercycler EP gradient S (Eppendorf, Germany) with a first cycle of 30 minutes at 37°C and were then incubated for 5 minutes on ice. After incubation, the samples were returned to the thermocycler in a cycle of 10 minutes at 65 ° C followed by another 5 minutes on ice. Finally, a mixture containing 1 µL BSA (20 µg / mL), 10 µL of M-MLV Buffer 5X, 10 µL of dNTP, 2 µL of Oligo DT and 2 µL M-MLV reverse transcriptase was applied to perform the last cycling in the thermocycler programmed for 1 hour at 37 ° C followed by a 65 ° C step for 10 minutes. At the end, the samples were stored at - 20 ° C and diluted 20X until used. The quantitative PCR reaction was performed with 0.5µL (500nM) of the forward primer, 0.5µL (500nM) of the reverse primer, 1µL of purified water, 5µL of SYBR Green Master Mix (Applied Biosystems – 4368577, USA) and 3µL of the previously diluted cDNA, totalizing 10µL per well. All reactions were performed on MicroAmp Optical 8-Tube Strips (Applied Biosystems, USA) plates on the QuantStudio 12K Flex Real-Time PCR System device (Applied Biosystems, USA). All samples were analyzed in technical triplicates, being the *GAPDH* gene chosen as the normalizer and quantification performed by the 2-ΔΔCT method. All primers were previously stored in a 100µM stock concentration, that was further diluted 10x (10µM) to use, being the 500nM concentration in the final reaction titrated in the laboratory for optimized results. A table of the used primers is shown below (Table 3).

**Table 3. Primers used to characterize hiPSC through RT-qPCR**

| ***Genes*** | **Primer forward (5'-3')** | **Primer reverse (5'-3')** |
|---|---|---|
| *OCT4* | TCCCATGCATTCAAACTGAGG | CCAAAAACCCTGGCACAAACT |
| *NANOG* | TGGACACTGGCTGAATCCTTC | TGGACACTGGCTGAATCCTTC |
| *SOX2* | GCTACAGCATGATGCAGGACCA | TCTGCGAGCTGGTCATGGAGTT |
| *GAPDH* | ACAACTTTGGTATCGTGGAAGG | GCCATCACGCCACAGTTTC |

## 3.9 Differentiation of hiPSC to NPCs

hiPSCs were maintained for 3 days in Essential 8™ medium (Life Technologies-A1517001, USA) with 100µg/mL of Normocin (InvivoGen-ant-nr-1). When the cell dish reached approximately 80% confluency, the medium was changed to NB [DMEM/F12 medium containing 0.5% of N2 supplement and 1% of B27 supplement (both from Thermo Fisher, USA) and 100µg/mL of Normocin (InvivoGen-ant-nr-1)] plus 2µM dorsomorphin and 2µM of SB431542 (both from Tocris) for 2 days. Afterwards, colonies were detached from the plate and cultured in suspension as embryoid bodies (EBs) in ultra-low attachment 6-well plates (Corning, USA) with the same medium (day 0), which was also replaced the next day (day 1). From day 2 on, the medium was changed to NB supplemented with 20ng/mL of human recombinant basic fibroblast growth factor (bFGF) and 20ng/mL of human recombinant epidermal growth factor (EGF) (both from Peprotech, USA) every 2 days for 1 week. The EBs were then plated in 60mm matrigel (Corning — 354277, USA) coated petri dishes and expanded using the NB+bFGF+EGF medium, with regular changes every 2 days, until neuronal rosettes appeared in the plates. Emerged rosettes were manually picked and plated into new 60mm matrigel coated dishes, being expanded using the same medium, with regular changes every 2 days, until the cells reached maximal confluency. Then, cells were dissociated using Accutase (Gibco, USA), centrifuged and resuspended in NB+bFGF+EGF medium, being plated into 60mm matrigel coated petri dishes for further expansion or frozen using CryoStor freezing medium (Stem cell technologies, Canada).

## 3.10 NPC characterization through confocal microscopy

NPCs were plated in matrigel (Corning — 354277, USA) coated Lab-tek 8-well chamber slide systems (Thermo Fisher, USA) at a density of $4x10^4$ cells per well and subjected to the exact same procedure described in section 3.8.2. The conjugated antibody used to characterize the NPCs was an Alexa-Fluor 647 mouse anti-Nestin (1:100 dilution, BD biosciences, catalog 560393, USA). Quantification of percentage of positive cells was performed using the FIJI software.

### 3.11 Differentiation of NPCs to astrocytes

NPCs were expanded using NB medium supplemented with 20ng/mL of bFGF and 20ng/mL of EGF (both from Peprotech, USA), with regular medium changes every 2 days until the cells reached confluency. Then, on day 0 the NPCs' monolayer was detached after two washes with 1x PBS followed by scraping and cultured in suspension as neurospheres in ultra-low 6-well plates (Corning) under agitation at 94 RPM at 37 °C and 5% CO2 with the same medium. On day 1, the medium was changed to eliminate death cells and on day 3 the neurospheres' medium was changed to Astrocyte Basal Medium plus supplements (FBS, Ascorbic Acid, Insulin, EGF and glutamine, Lonza, Switzerland) and 100μg/mL of Normocin (InvivoGen-ant-nr-1). The medium was changed every 2 days for 14 days under agitation, and on day 16, the neurospheres were seeded in a double-coated plate with poly-ornithine (10μg/mL, Sigma-Aldrich, USA) and laminin (5μg/mL, Gibco, USA). Astrocytes emerged from the attached spheres, and cells were detached using accutase and expanded using ABM medium with regular media changes every 2 days. When the plates reached confluency, the neurospheres were aspirated and the cells were dissociated with Accutase (Gibco, USA), filtered through a 40μm cell-strainer (Corning, USA) and transferred to matrigel coated 60mm petri dishes with ABM medium plus supplements and normocin. Astrocytes were then subjected to the experimental procedures, being used from passages 2 to 4 in order to avoid cellular senescence.

### 3.12 Astrocyte characterization through confocal microscopy

Astrocytes were plated in matrigel (Corning — 354277, USA) coated Lab-tek 8-well chamber slide systems (Thermo Fisher, USA) at a density of $4x10^4$ cells per well and subjected to the exact same procedure described in section 3.8.2. Quantification of percentage of positive cells was performed using the FIJI software.

**Table 4. Antibodies used to characterize astrocytes through confocal microscopy**

| *Antibodies* | *Type* | *Brand* | *Catalog* | *Dilution* |
|---|---|---|---|---|
| *Mouse anti-GFAP* | Primary | Sigma | G3893 | 1:100 |
| *Mouse-anti Vimentin* | Primary | DAKO | M7020 | 1:100 |
| *AF488 goat anti-mouse IgG* | Secondary | Life | A11001 | 1:250 |
| *AF594 donkey-anti mouse IgG* | Secondary | Life | A21203 | 1:250 |

### 3.13 PCR Array

The RT² Profiler PCR Array System is one of the most reliable and accurate tools to analyze the expression of a given panel of genes related to a biological pathway simultaneously, with high sensitivity, specificity and a wide linear dynamic range. Here we chose the Human Mitochondria PCR array (QIAGEN, PAHS-087Z, Germany) that contains several genes related to the mitochondrial dynamics, metabolism and ion transport, being therefore a very useful tool to have insights about the mitochondrial function and regulation in astrocytes derived from the MS patients compared to the controls.

First, the total RNA was isolated from the astrocytes using the RNeasy mini kit (QIAGEN – 74104, Germany), together with on column DNAse digestion using the RNAse-free DNAse set (QIAGEN, 79254, Germany) according to the manufacturer's instructions. The purity of the RNA was analyzed using quantification on the NanoDrop ND-1000 Spectrophotometer (NanoDrop Technologies) and the integrity validated using a 1% agarose electrophoresis gel. An amount of 500ng of RNA was used to synthesize the cDNA, as recommended by the manufacturer, using the RT² First Strand Kit (QIAGEN, 330401, Germany). The first step consisted in eliminating genomic DNA from the samples using 2μL of genomic elimination (GE) buffer in 500ng of RNA diluted in RNAse free water, totalizing 10μL reaction volumes per tube.The samples were then incubated for 5 minutes at 42°C in a Mastercycler EP gradient S (Eppendorf, Germany) thermocycler followed by a 1 minute incubation on ice. Then, a mix composed by 4μL of 5x buffer BCR, 1μL of control P2 primers, 2μL of RE3 RT mix and 3μL of RNAse-free water was added to the tubes, totalizing 10μL per tube, followed by two incubation cycles: 42°C for 15 minutes and 95°C

for 5 minutes. Then, 91μL of RNAse free water was added to each tube and the samples were stored at -20°C until used. The RT-qPCR reaction was performed using the $RT^2$ SYBR Green ROX qPCR Mastermix (QIAGEN, 330524, Germany). One plate was used for each subject analyzed in this research, totalizing 6 plates (3 controls and 3 MS patients) and the reaction mix per plate consisted in 1350μL of 2xRT Sybr Green mastermix, 102μL of the previous cDNA synthesis reaction and 1248μL of RNAse free water, being 25μL of this mix added in each well of the plate. The reactions were performed on the QuantStudio 12K Flex Real-Time PCR System device (Applied Biosystems, USA).

Data analysis was performed on the GeneGlobe software (QIAGEN, Germany), being the beta-2-microglobulin gene (*B2M*) chosen to normalize all the samples. The Ct threshold was standardized throughout the plates, as recommended by the manufacturer and the fold regulation threshold used during the analysis was 1.5. Genes with undetermined $Ct_s$ in at least one sample were excluded from the analysis. Enrichment analysis of the upregulated genes was performed using the EnrichR software [62, 63] (Maayan Laboratory, Mount Sinai School of Medicine, NY, USA) using the KEGG pathways human 2019, GO Biological Process 2018 and GO Molecular Function 2018 databases.

### 3.14 Analysis of Mitotracker and Mitosox using flow cytometry

Mitotracker Green FM (Thermo Fisher, M7514, USA), Mitotracker Deep Red (Thermo Fisher, M22426, USA), Mitosox Red (Thermo Fisher, M36008, USA) and LIVE/DEAD fixable aqua dead cell stain kit (Thermo Fisher, L34957, USA) were the probes used in the flow cytometry analysis. Mitotracker Green FM is a green-fluorescent stain that localizes to mitochondria in live cells independently of the $\Delta\psi m$. Mitotracker Deep Red is a $\Delta\psi m$-dependent far-red fluorescent stain that localizes to mitochondria in live cells and has therefore been used as an indicator of $\Delta\psi m$ in cells [64]. The ratio between the Mitotracker Deep Red MFI and the Mitotacker Green MFI has already been used as an indicator of mitochondrial quality [65], which is the main reason why we chose to combine these two probes in our analysis. Mitosox is a reliable indicator of ROS production as when oxidized by superoxide it produces red fluorescence. Finally, LIVE/DEAD stain is an indicator of cell death as it enters in necrotic cells and reacts with cellular amines becoming fluorescent.

For flow analyzes of mitochondria, cells were initially treated with Accutase (Gibco, USA), washed with 1x PBS, centrifuged at 1500rpm at room temperature for 5 minutes and then resuspended in a staining solution of 1x PBS and 200nM of Mitotracker Green, 200nM of Mitotracker Red, 5µM of Mitosox and 0.2% LIVE/DEAD. Then, cells were incubated at 37°C for 20 minutes, centrifuged at 1500rpm, room temperature, for 5 minutes, washed once with 1x PBS, centrifuged again and resuspended in 200µL for flow cytometry analysis. Flow cytometry analysis was performed on a BD FACSCanto™ II Cell Analyzer (BD, USA) with the following voltages: 287v for the forward scatter (FSC), 435v for the side-scatter (FSC), 347v for FITC (Mitotracker Green), 363v for PE (Mitosox), 330v for APC (Mitotracker Deep Red) and 522v for AmCyan (LIVE/DEAD). For each sample, we acquired 200000 events. Analysis of frequency and MFI of the probes in the samples was performed using the FlowJo software (Flow Jo, LLC, USA).

Gating was performed in single cells/live cells/positive populations for each marker, as determined by the unstained control and for Mitosox the positive control using 1mM of hydrogen peroxide (Sigma Aldrich, USA) for 10 minutes at 37°C prior to probe staining to stimulate ROS production in the cells. Our gating strategy is demonstrated below (Figure 2).

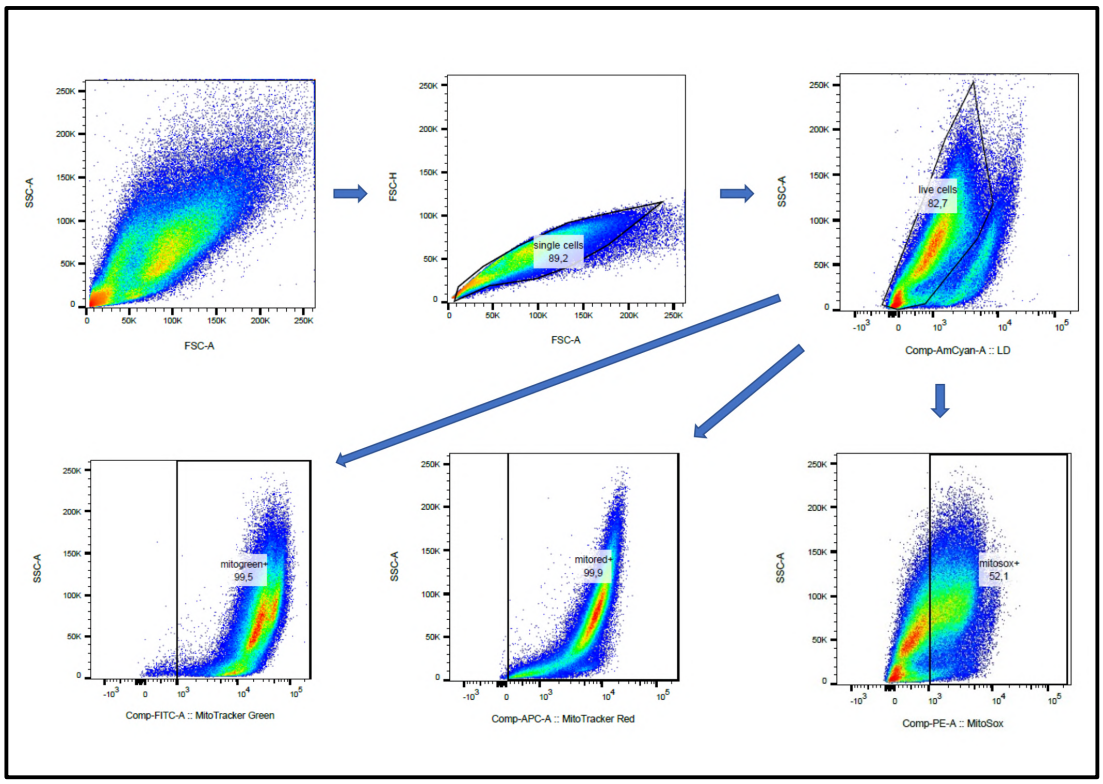

**Figure 2. Gate strategy for flow cytometry experiments.** Cells were gates as single cells to remove doublets from the analysis and then inside this gate we selected the unstained population for the LIVE/DEAD (AmCyan), which is representative of live cells. Inside the live cell gate, we selected the positive populations for Mitotracker Green (FITC), Mitotracker Deep Red (APC) and Mitosox (PE) based on the unstained control and the hydrogen peroxide positive control for Mitosox (frequency of positive cells). MFI was analyzed inside each of these positive populations for the probes using the FlowJo software.

### 3.15 Seahorse Analyzes

To analyze the mitochondrial function in the astrocytes derived from MS patients and controls we performed the OCR and ECAR tests using the XF24 analyzer (Seahorse Technology, Agilent, USA) to evaluate mitochondrial respiration and glycolysis in these cells, respectively.

#### 3.15.1 Oxygen Consumption Rate

We first seeded 40000 cells per well on a matrigel (Corning, USA) coated Seahorse XF24 cell plate (Agilent, USA) 2 days before the experiment in 500μL of ABM medium plus supplements (Lonza, Switzerland). The day before the experiment, the cartridge was hydrated using 1mL of Seahorse XF Calibrant Solution (Agilent, USA) at 37°C in an incubator without $CO_2$. Before measurements, cells were washed 3 times and incubated for 1 h at 37°C in an incubator without $CO_2$ with 500 μl respiratory medium (pH 7.4) consisting of DMEM (Gibco, USA) supplemented with 25 mM glucose (Sigma, USA) plus 1 mM pyruvate (Sigma, USA) and 2 mM glutamine (Gibco, USA). The respiratory medium lacked sodium bicarbonate and FBS, aiming to optimize the analysis. After equipment calibration, baseline respiration measurements were followed by 1μM of oligomycin (Sigma, USA) addition to determine ATP-linked and proton leak-driven respiration. 2,4-Dinitrophenol (2,4-DNP) was used in a concentration of 500μM as a mitochondrial uncoupler to induce the maximal respiratory capacity. Non-mitochondrial respiration was determined after the addition of 1μM rotenone plus 1μM antimycin A, which inhibit the complexes I and III of the mitochondrial electron transport chain, respectively. We injected all compounds diluted in 70μL of medium. All respiratory modulators were previously titrated, as recommend by the manufacturer. ECAR values correspond to baseline respiration measurements, before oligomycin addition. All plates were

normalized to protein content using the BCA kit (Thermo, USA). Analysis was performed in the Wave software (Agilent, USA), with the calculation parameters below (Table 5)

**Table 5. Seahorse XF Cell Mito Stress Test Parameter Equations**

| ***Parameter Evaluated*** | ***Equation*** |
|---|---|
| *Non-mitochondrial OCR* | Minimum rate measurement after Rotenone/Antimycin |
| *Basal OCR* | Last measurement before oligomycin - Non-mitochondrial OCR |
| *Maximal OCR* | Maximum measurement after 2,4-DNP – Non-mitochondrial OCR |
| *Proton Leak OCR* | Minimum measurement after oligomycin – Non-mitochondrial OCR |
| *ATP-linked OCR* | Last measurement before oligomycin - Minimum measurement after oligomycin |
| *Spare Capacity* | Maximal OCR – Basal OCR |
| *Coupling efficiency* | (ATP-linked OCR/Basal OCR) x 100 |
| *ECAR* | Average of basal ECAR measurements before oligomycin |
| *Bioenergetic Health Index* | (Spare capacity x ATP-linked OCR)/ (Proton leak OCR x Non-mitochondrial OCR) |

### 3.15.2 Extracellular Acidification Rate

We first seeded 40000 cells per well on a matrigel (Corning, USA) coated Seahorse XF24 cell plate (Agilent, USA) 2 days before the experiment in 500µL of ABM medium plus supplements (Lonza, Switzerland). The day before the experiment, the cartridge was hydrated using 1mL of Seahorse XF Calibrant Solution (Agilent, USA) at 37°C in an incubator without $CO_2$. The reaction medium used in this test consisted of Seahorse XF minimal DMEM medium (Agilent, USA) supplemented with 1mM glutamine (Gibco, USA). The medium is free of sodium bicarbonate, glucose, has low buffering capacity and low phenol red levels, which makes it ideal for this specific ECAR assay. Before measurements, cells were washed 3 times and incubated with the reaction medium (pH 7.4) at 37°C in an incubator without $CO_2$. After equipment calibration, baseline respiration measurements were followed by injection of 10mM Glucose (Sigma, USA) aiming to analyze basal glycolysis. Then, 1µM of oligomycin (Sigma, USA) was used to inhibit the ATP synthase, shutting down OXPHOS and allowing the cells to reach their maximal glycolytic capacity. Finally, the last injection consisted of 50mM 2-Deoxi-D-glucose (2-DG) (Sigma, USA)

which inhibits glycolysis by competitive binding to the hexokinase enzyme to determine whether the ECAR rates were indeed related to glycolysis. We injected all compounds diluted in 70μL of medium. All respiratory modulators were previously titrated, as recommend by the manufacturer. All plates were normalized to protein content using the BCA kit (Thermo, USA). Analysis was performed in the Wave software (Agilent, USA), with the calculation parameters below (Table 6).

**Table 6. Seahorse XF Cell Glycolysis Stress Test Parameter Equations**

| ***Parameter Evaluated*** | ***Equation*** |
|---|---|
| *Glycolysis* | Maximum measurement after glucose – Last measurement before glucose |
| *Glycolytic Capacity* | Maximum measurement after oligomycin – Last measurement before glucose |
| *Glycolytic Reserve* | Glycolytic Capacity - Glycolysis |
| *Glycolytic Reserve (%)* | (Glycolytic Capacity/Glycolysis) x 100 |
| *Non-Glycolytic Acidification* | Last measurement before glucose |

### 3.16 Glucose and lactate measurement

The metabolites analysis was performed using $5x10^5$ cells, which were seeded on matrigel-coated 12 well plates (Corning, USA). Two days (48 hours) later, the lactate and glucose measurements of the astrocyte supernatants were performed with enzymatic tests from Labtest Diagnóstica (Minas Gerais, Brazil) following the protocol established by the supplier. The absorbance was obtained using a Biotek's Synergy HTX® equipment (Vermont, USA) at a wavelength of 542nm or 550 nm.

### 3.17 Protein Quantification

To quantify proteins for Western-Blot or from the Seahorse plates we used 500 μL of RIPPA Lysis Buffer 1X solution (Merck, Germany) combined with phosphatase and protease inhibitors (1 tablet of each inhibitor for 10ml of RIPPA) (Roche, Switzerland) every $2x10^6$ cells. The RIPPA solution (pH 7.4) consisted of: 0.5M Tris-HCl, 1.5M Sodium Chloride, 2.5% deoxycholic acid, 10% nonyl phenoxypolyethoxylethanol (NP-40) and 10mM EDTA. After adding the solution to the pellet cells, they were incubated for 15 minutes on ice (4 ° C) for future quantification by the BCA kit (Thermo Fisher, USA)

following the manufacturer's instructions, ending with storage of samples at -80 ° C until use. BSA standard curves were used for normalization of the samples, as recommend by the manufacturer.

### 3.18 Transmission Electron Microscopy

To perform electron microscopy assays, at least $1x10^6$ astrocytes were used. Cells were treated with Accutase (Gibco, USA), centrifuged and fixed in a 2% glutaraldehyde solution (Ladd Research Industries, USA), dissolved in 0.15M phosphate buffer at pH 7.2, followed by postfixation in 1% osmium tetroxide (Ladd Research Industries, USA), and block staining in 1% aqueous uranyl acetate (Ladd Research Industries, USA). The samples were embedded in a polyester resin, thin sectioned with a LKB ultratome, double-stained by uranyl acetate and lead citrate (Ladd Research Industries, USA), and examined with a Jeol 1010 (Tokyo, Japan) electron microscope.

At least 10 individual cells per group (astrocytes from controls and MS patients) were analyzed. Mitochondrial morphology was assessed using the ImageJ software and quantified using two parameters previously reported to indicate changes in mitochondrial dynamics [58]: the automated mitochondrial aspect ratio and the mitochondrial roundness generated by the software. Additionally, cell areas were individualized and for each analyzed image the ratios between the area of individual mitochondria/cell area were determined.

### 3.19 RT-qPCR

Total RNA was isolated from the astrocytes using the RNeasy mini kit (QIAGEN – 74104, Germany), according to the manufacturer's instructions. The purity of the RNA was analyzed using quantification on the NanoDrop ND-1000 Spectrophotometer (NanoDrop Technologies) and the integrity validated using a 1% agarose electrophoresis gel. The synthesis of cDNA was performed with an initial amount of 2000 ng RNA using the M-MLV Reverse Transcriptase System (Promega, USA). Using a 0.2 mL tube, 2000 ng of RNA, 2.5 µL of DNAse, 5 µL of 10X Reaction Buffer and 1 µL of Dnase-RNAse free were placed in each sample for digestion of contaminating DNA. The samples were placed in a Mastercycler EP gradient S (Eppendorf, Germany) with a first

cycle of 30 minutes at 37°C and were then incubated for 5 minutes on ice. After incubation, the samples were returned to the thermocycler in a cycle of 10 minutes at 65 ° C followed by another 5 minutes on ice. Finally, a mixture containing 1 µL BSA (20 µg / mL), 10 µL of M-MLV Buffer 5X, 10 µL of dNTP, 2 µL of Oligo DT and 2 µL M-MLV reverse transcriptase was applied to perform the last cycling in the thermocycler for 1 hour at 37 ° C followed by a 65 ° C step for 10 minutes. At the end, the samples were stored at – 20 ° C and diluted 20X until used. The quantitative PCR reaction was performed with 0.5µL (500nM) of the forward primer, 0.5µL (500nM) of the reverse primer, 1µL of purified water, 5µL of SYBR Green Master Mix (Applied Biosystems – 4368577, USA) and 3µL of the previously diluted cDNA, totalizing 10µL per well. All reactions were performed on MicroAmp Optical 8-Tube Strips (Applied Biosystems, USA) plates on the QuantStudio 12K Flex Real-Time PCR System device (Applied Biosystems, USA). All samples were analyzed in technical duplicates, being the *RPLP0* gene chosen as the normalizer and quantification performed by the 2-ΔΔCT method. The mitochondrial/nuclear DNA ratio was calculated as *16S/RPLP0* expression. All primers were acquired from Thermo Fisher, USA and previously stored in a 100µM stock concentration, that was further diluted 10x (10µM) to use, being the 500nM concentration in the final reaction titrated in the laboratory for optimized results. A table of the used primers is shown below (Table 7).

**Table 7. Primers used in RT-qPCR**

| ***Genes*** | **Primer forward (5'-3')** | **Primer reverse (5'-3')** |
|---|---|---|
| *RPLP0* | CCTCATATCCGGGGGAATGTG | GCAGCAGCTGGCACCTTATTG |
| *16S* | GCCTTCCCCCGTAAATGATA | TTATGCGATTACCGGGCTCT |
| *ATF4* | GTCCCTCCAACAACAGCAAG | CTATACCCAACAGGGCATCC |
| *DDIT3* | AGCCAAAATCAGAGCTGGAA | TGGATCAGTCTGGAAAAGCA |
| *HSP60* | ACTCGGAGGCGGAAGAAA | TGTGGGTAACCGAAGCATTT |
| *HSPA9* | GGAAGCTGCTGAAAAGGCTA | CTTGGGTCCAGAAGAATCCA |
| *ERRO1A* | AGCGGCACAGAGGTGCT | TGTAGTCTTGGGAAAAGCCTG |
| *LONP1* | CCCGCGCTTTATCAAGATT | AGAAAGACGCCGACATAAGG |

| | | |
|---|---|---|
| *CLPP* | CTCTTCCTGCAATCCGAGAG | GGATGTACTGCATCGTGTCG |
| *PGC1A* | CCAAAGGATGCGCTCTCGTTCA | CGGTGTCTGTAGTGGCTTGACT |
| *HIF1A* | TATGAGCCAGAAGAACTTTTAGGC | CACCTCTTTTGGCAAGCATCCTG |
| *S100B* | GAAGAAATCCGAACTGAAGGAGC | TCCTGGAAGTCACATTCGCCGT |

### 3.20 Western-Blotting

Protein samples previously quantified were submitted to Laemmli Buffer 4X and 0.015g DDT for each 100 µL of dye. Subsequently, the samples were denatured by heating (94°C/1h) Thermoblock EppendorfTM (Hamburg, Germany). With 50 µg of each denatured sample, an electrophoretic separation was performed using an SDS-PAGE gel, for 90 min at 120v. In the next step, the gel containing the samples was transferred (semi-dry) to a nitrocellulose membrane (GE Healthcare, Chicago, USA) through the BIORAD Trans-Blot® TurboTM Sytem standard program (California, USA). After transfer, the membranes were blocked for 1h at room temperature (TBST 1x with 2% milk powder), washed 3 times with TBST 1X every 5 minutes under agitation. After washing, the membranes were incubated with the primary antibody of rabbit anti-DRP1 (ab184247, Abcam) at a dilution of 1:1000 and mouse anti- β-Actin (8H10D10, Cell Signaling Technology, USA) at a dilution of 1:5000. Both antibodies were diluted in a 1X TBST solution containing 2% BSA. After incubation at 4 ° C overnight, the membranes were washed three times again in TBST and subjected to the secondary antibodies for 1h at room temperature. Secondary antibodies were anti-rabbit (SAB3700861-2MG) and anti-mouse (A9044-2ML) at a 1:5000 dilution in TBS-T 1X (0.1% Tween-20) (Sigma-Aldrich, USA). After 3 washes, the membranes were revealed with SuperSignal Chemiluminescent Substrate (Thermo Fisher, USA) and read using the LAS-500 equipment (GE Healthcare, USA). The quantification was made based on the pixels of the bands, which were measured by the ImageJ software.

### 3.21 Bioinformatics analysis

### 3.21.1 Data acquisition and quality control evaluation

Libraries deposited in the GEO, accession number GSE120411, from healthy donors' hiPSC-derived astrocytes without stimulation or stimulated with TNF-α (10ng/mL, for 24 hours) were selected. The reads were downloaded and converted to the fasta format using the fasterq-dump v2.10.8 tool (https://github.com/ncbi/sra-tools/wiki/HowTo:-fasterq-dump). Quality assessment was performed with the FastQC v0.11.4 program (Babraham Bioinformatics, UK) and the results were visualized with the MultiQC v1.8. dev0 program (available at https://multiqc.info/). The adapters were removed using Trimmomatic v0.39 (available at http://www.usadellab.org/) with the parameters ILLUMINACLIP: /TruSeq3-SE. fa: 2: 30: 10 MINLEN: 90. The parallelization of the processes was carried out with the GNU Parallel software (available at https://www.gnu.org/).

### 3.21.2 Differential Expression Analysis

The kallisto v0.43.1 program (available at https://github.com/pachterlab) was used to perform the pseudo-alignment and quantification of the transcripts, with the parameters --single -l200 -s20 -b100 and using, for this purpose, the human transcriptome GRCh38.p13 v35 made available by GENCODE. Using the DESeq2 v1.30.1 package (available at https://bioconductor.org/packages) in R v4.0.3 (R Studio, Inc), differential transcript expression was performed between samples without stimulation and with TNF- stimulation. Transcripts that presented $\log_2$ fold change>1 or <-1 and FDR <0.05 were considered differentially expressed. The hierarchical clustering of the differentially expressed transcripts was performed with the pheatmap package v1.0.12 (R Studio, Inc) and the graphics with the package ggplot2 v3.3.3 (R Studio, Inc).

### 3.21.3 Functional Analysis

Transcripts found differentially expressed were filtered and only the protein-coding ones were selected. Then, Gene Ontology biological processes enrichment analysis was performed on the upregulated and downregulated transcripts, focusing on

mitochondrial alterations, to see the enriched and repressed processes, respectively. The analysis was performed using the EnrichR software (Ma'ayan Laboratory, USA).

Gene Set Enrichment Analysis was performed with the package fgsea v1.16.0 on R (available at https://bioconductor.org/packages) for Reactome biological pathways. Biological pathways with $p < 0.05$ were considered significant. Only genes whose transcripts are classified as protein coding were used in the analyzes. The ggplot2 v3.3.3 package (R Studio, Inc) was used to create the graphics.

### 3.22 Statistical analyzes

Differences between groups were first analyzed using Kolmogorov-Smirnov normalization test. If both groups tested positive, then unpaired two-tailed Student's t tests were used to compare the groups. If one of the groups tested negative on the normalization test, we selected the nonparametric Mann-Whitney test to compare the groups. The p values were provided in their exact value in the figures, being considered significant when $p<0.05$. Data are represented as mean ± standard error, as indicated in the figures. All graphs and analyzes were generated using the GraphPad Prism Software.

# 4. RESULTS

## 4.1 hiPSC characterization

We reprogrammed hiPSC from PBMCs of controls and MS patients successfully. First, we analyzed all the cells using confocal microscopy and observed that hiPSC from both control and MS groups stained positive for the pluripotent markers OCT4 (nuclear) and SSEA-4 (surface) (Figure 3A). Then, to detect if the hiPSC clones selected from each subject presented chromosomal abnormalities we used the MLPA technique. We observed that both control (Figure 3B) and MS (Figure 3C) hiPSC clones did not present copy number variations in the chromosomes, either duplications or deletions, indicating that these clones could be used for further steps of this study. Finally, using RT-qPCR we analyzed the expression of 3 pluripotency genes: *SOX2* (Figure 3D), *OCT4* (Figure 3E) and *NANOG* (Figure 3F) and observed no significant differences between the control and MS groups, indicating that the reprogramming process worked well.

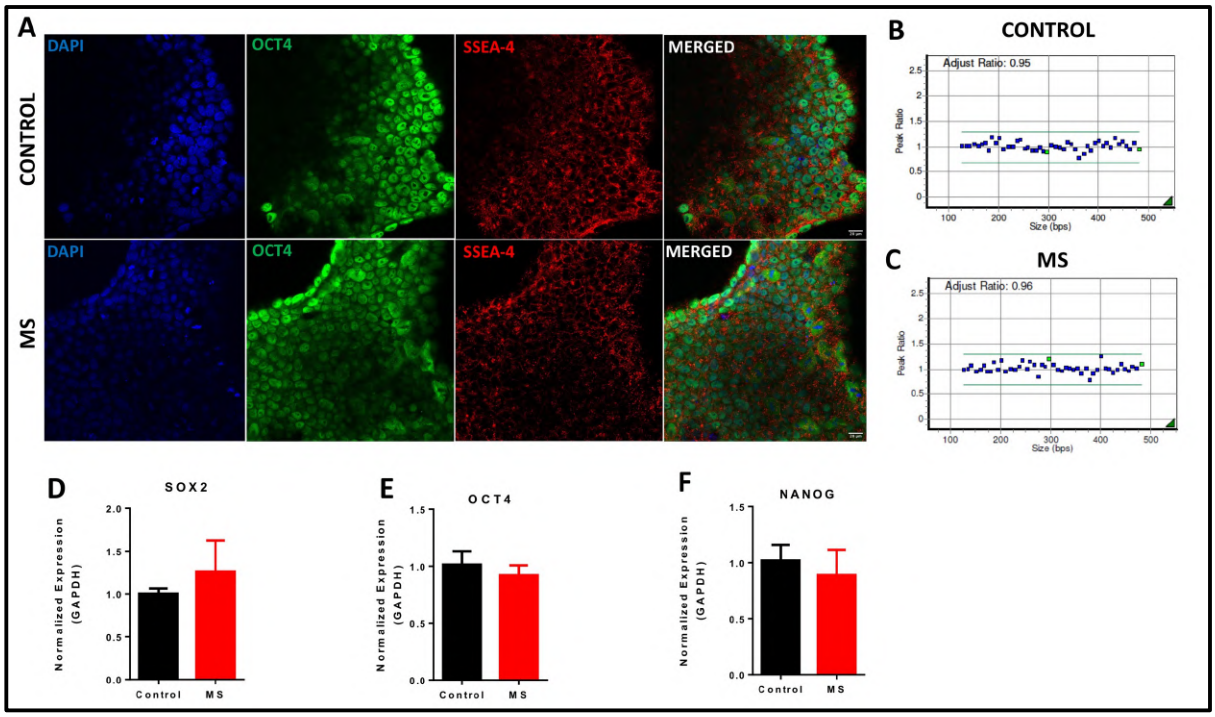


**Figure 3. hiPSC characterization. A –** Panel of confocal microscopy analysis for the pluripotency markers OCT4 (green), SSEA-4 (red) and DAPI (blue) for nuclear staining. The top line is representative of the results obtained for the control group and the bottom line is representative of the results obtained for the MS groups. Scale bar = 20μm. N=3 controls and 3 patients. **B and C –** Representative MLPA analysis for the control and MS groups, respectively, using the P036 and P070 kits (MRC – Holland). N=3 controls and 3 patients. **D-F** – Expression analysis of the pluripotency genes *SOX2* (**D**), *OCT4* and *NANOG* (**F**) using RT-qPCR, normalized to *GAPDH*. N=3 controls and 3 patients, analyzed in technical triplicates in two independent experiments. Data in panels D-F are represented as the mean ± standard error.

## 4.2 NPC characterization

Following hiPSC characterization, we proceeded with the differentiation to NPCs, which were characterized by confocal microscopy analysis using Nestin as a marker. Nestin is an intermediate filament which was originally described to be expressed in neural stem-cells [66]. We observed that all cell lines expressed Nestin (Figure 4A), with no differences in the frequency of positive cells between control and MS groups (Figure 4B), indicating that the differentiation process was successful in all cell lines used in this study.

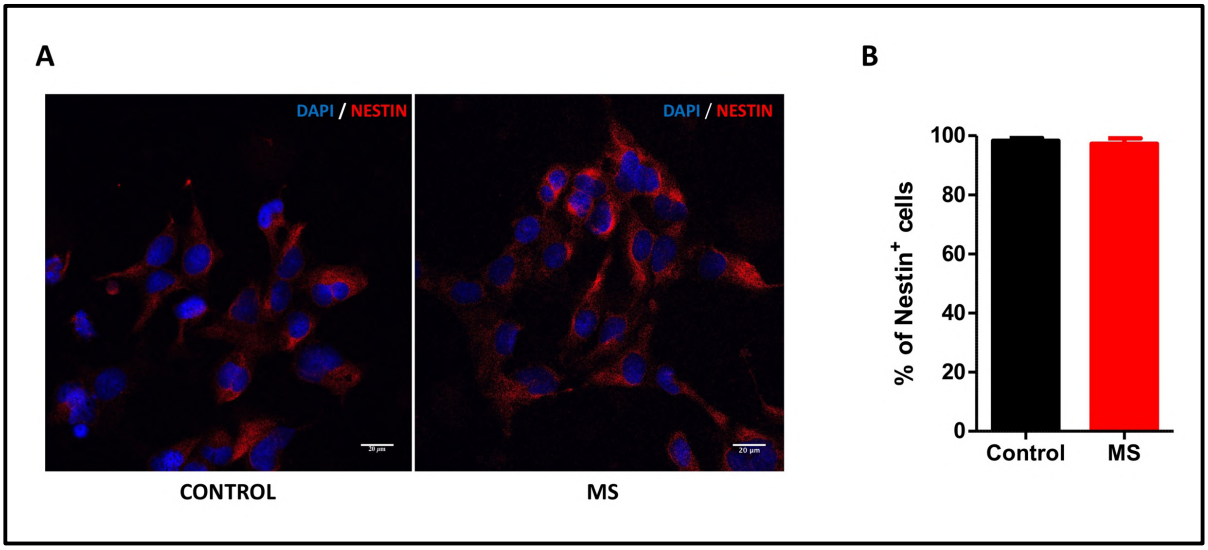


**Figure 4. NPC characterization. A –** Panel of confocal microscopy analysis for the NPC marker Nestin (red) and DAPI (blue) for nuclear staining. The left panel is representative of the control group and the right panel is representative of the MS group. Scale bar = 20µm. **B –** Quantification of the frequency (%) of Nestin positive cells between the groups using the ImageJ software. N=3 controls and 3 MS patients, with at least 4 images of each of the subjects' NPC lines being analyzed for both groups in two independent experiments. Data in panel B is represented as the mean ± standard error.

## 4.3 Astrocyte characterization

Following NPC characterization, the astrocyte differentiation protocol was performed. Astrocytes were first characterized by staining with antibodies for the intermediate filaments GFAP and Vimentin using confocal microscopy, as published before [67, 68], and showed positivity for both markers in the control and MS groups (Figure 5A), with no differences in the frequency of GFAP (Figure 5B) and Vimentin (Figure 5C) positive cells between them. We also used RT-qPCR to analyze the expression

of the *S100B* gene, another classical marker of astrocytes [67] and observed no significant differences between the control and MS groups (Figure 5D), indicating that astrocyte differentiation was performed successfully and cells were ready for the experimental procedures of this study. All markers were analyzed 30 days after the start of the differentiation protocol. Cell viability was analyzed using Trypan-Blue (Gibco, USA) staining prior to the experiments in Countess automated cell counter (Thermo, USA).

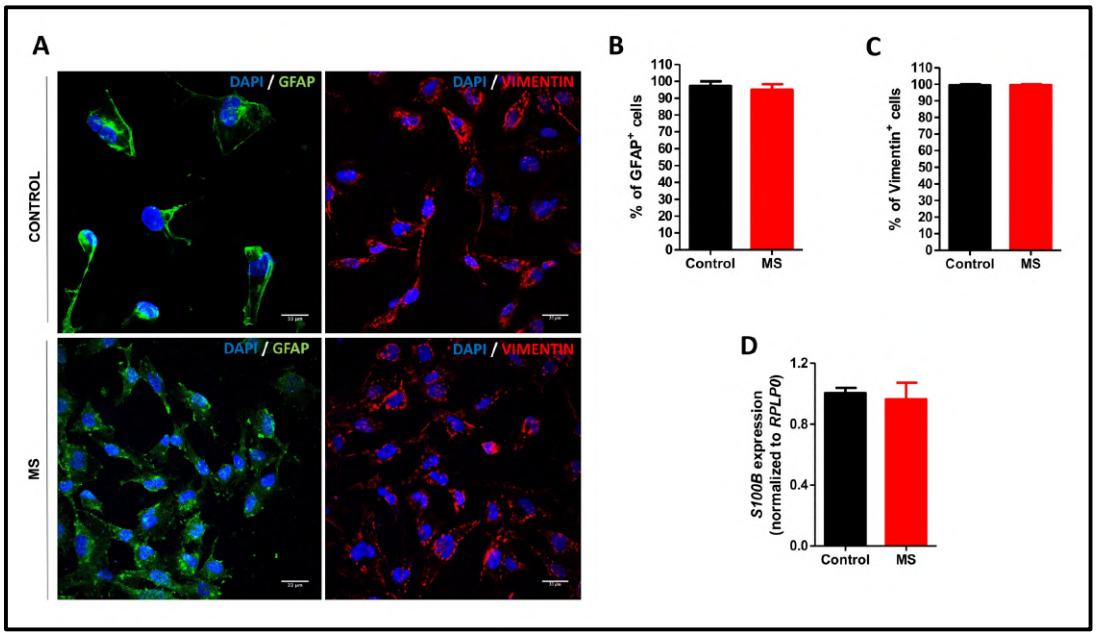


**Figure 5. Astrocyte characterization. A –** Panel of confocal microscopy analysis for GFAP (green), Vimentin (red) and DAPI (blue) for nuclear staining. The top line is representative of the results obtained for the control group and the bottom line is representative of the results obtained for the MS groups. Scale bar = 33µm. **B and C–** Quantification of the frequency (%) of GFAP and Vimentin positive cells, respectively between the groups using the ImageJ software. N=3 controls and 3 MS patients, with at least 4 images of each of the subjects' astrocyte lines being analyzed for both groups in two independent experiments. **D** – Expression analysis of the *S100B* astrocyte marker using RT-qPCR. N=3 controls and 3 patients, analyzed in technical triplicates in two independent experiments. Data in panels B-D are represented as the mean ± standard error.

## 4.4 MS astrocytes show altered expression of mitochondrial related genes

Using the differentiated astrocytes from controls and MS patients, we performed a PCR array analysis of genes related to human mitochondria (Qiagen, PAHS-087Z, Germany). The genes in this array include regulators and mediators of mitochondrial molecular transport, including metabolites required for proper functioning of the electron transport chain, OXPHOS, mitochondrial membrane potential and polarization. Additionally, intrinsic apoptosis pathway related genes, indicators of cellular damage and

stress, are also included. The gene list also targets transport of previously folded and translated proteins through the outer and inner mitochondrial membranes and also into the mitochondrial matrix. Therefore, the PCR array represents a reliable technique to assess further insights on mitochondrial biology in the astrocytes from MS patients and controls. A list containing all off the PCR array genes is attached (Supplementary table 1, page 105).

We observed an upregulation of 18 genes in our analysis and a downregulation of one gene (*BCL2*) in astrocytes derived from MS patients compared to controls. The gene most upregulated was *UXT*, followed by *TOMM20*, *SH3GLB1*, *GRPEL1*, *SLC25A27*, *MFN1*, *SLC25A5*, *SLC25A16*, *FIS1*, *IMMP2L*, *SLC25A20*, *SLC25A24*, *DNM1L*, *TIMM8A*, *MPV17*, *SOD1*, *LRPPRC* and *SLC25A30* (Figure 6, A and B).

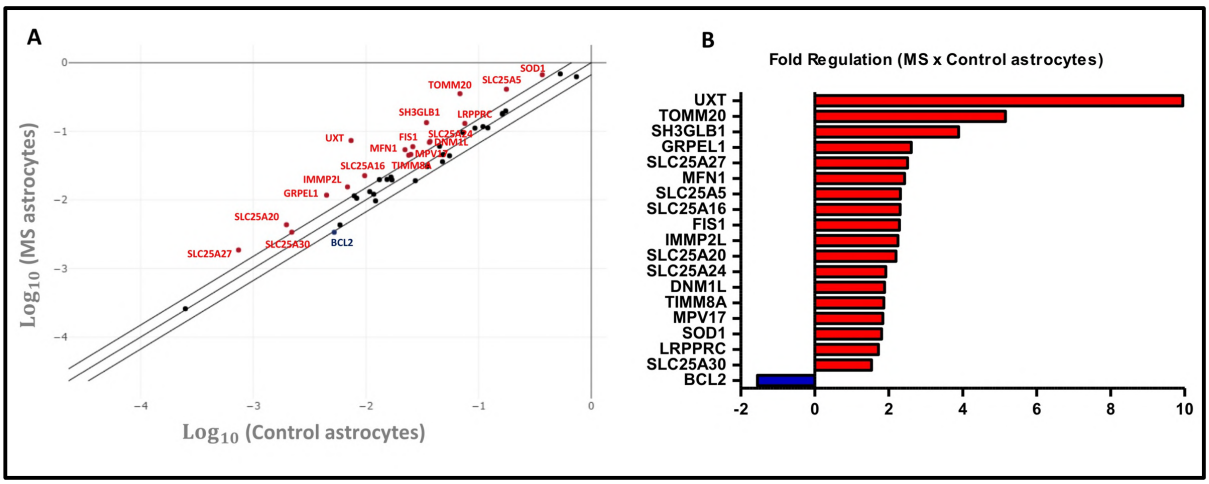


**Figure 6. Human mitochondria PCR array analysis. A** – Scatter plot showing the upregulated (red dots) and downregulated (blue dots) genes in MS astrocytes compared to controls. The middle diagonal line represents a fold regulation of 1 and the 2 diagonal bordering lines represent the threshold fold regulation of 1.5 considered in the analysis. Black dots are representative of genes that were neither above or below the threshold. The y-axis represents the fold regulation values for the MS astrocytes group in a $\log_{10}$ scale. The x-axis represents the fold regulation values for the control astrocytes group in a $\log_{10}$ scale. **B** – Bar graph of absolute fold regulation values of genes in MS astrocytes, compared to the control group. Red bars represent upregulated genes and blue bars represent downregulated genes. N=3 controls and 3 MS patients. Expression was normalized to the beta 2 microglobulin housekeeping gene.

To facilitate the data interpretation and to give insights into biological pathways that could be altered in MS astrocytes compared to controls, we performed an enrichment analysis on the 18 upregulated genes shown in Figure 6 using the Kyoto Encyclopedia of Genes and Genomes (KEGG) 2019 human database (Figure 7). We observed a significant enrichment of 8 pathways, related mostly to cell death, mitochondrial dysfunction and

neurodegeneration. Mitophagy was the most enriched among them, followed by Peroxisome, Necroptosis, NOD-like receptor signaling pathway, Huntington disease, Protein export, Prion diseases and Amyotrophic Lateral Sclerosis.

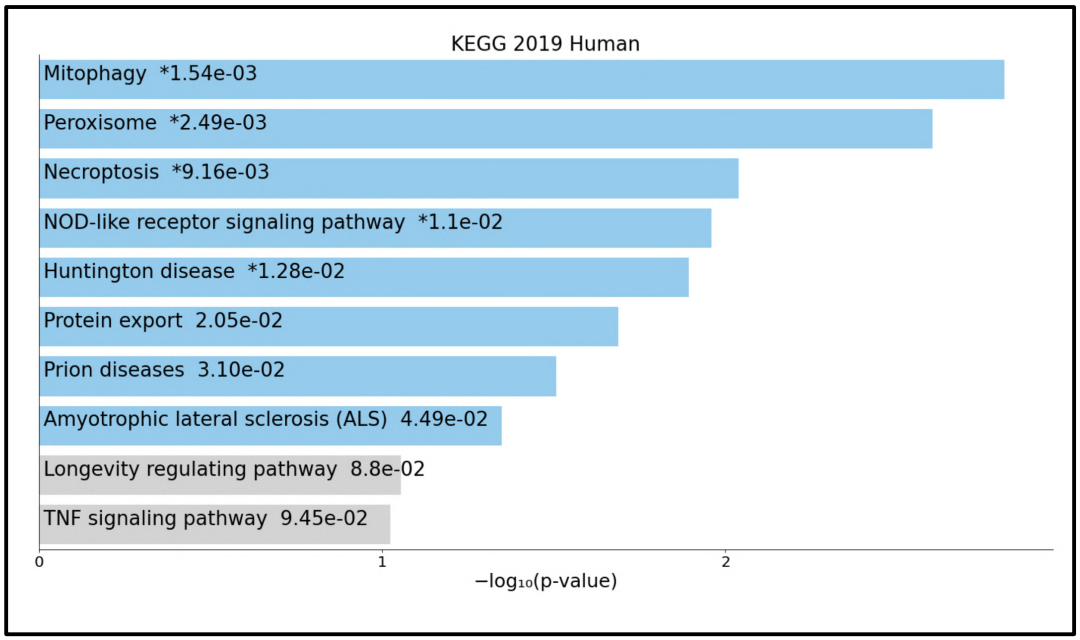


**Figure 7. Pathway enrichment analysis of PCR array upregulated genes.** Enrichment analysis was performed on the 18 upregulated genes shown in figure 6 using the KEGG 2019 human database. The bar chart shows the top 10 enriched terms in the chosen library, along with their corresponding p-values. Colored bars correspond to terms with significant p-values (<0.05). An asterisk (*) next to a p-value indicates the term also has a significant adjusted p-value (<0.05). The analysis was performed using the EnrichR software.

Next, we performed an enrichment analysis on the same 18 upregulated genes (Figure 6) to assess biological processes that could be regulated by them using the Gene Ontology (GO) Biological Process 2018 database. The top 10 enriched terms are shown in Figure 8. The most significant process was mitochondrial transport (GO:0006839), followed by mitochondrion organization (GO:0007005), protein targeting to mitochondrion (GO:0006626), positive regulation of intrinsic apoptotic signaling pathway (GO:2001244), establishment of protein localization to mitochondrion (GO:0072655, establishment of mitochondrial localization, microtubule-mediated (GO:0034643), membrane fusion (GO:0061025), purine ribonucleotide transport (GO:0015868), adenine nucleotide transport (GO:0051503) and peroxisome fission (GO:0016559). Supplementary table 2 (page 107) contains a list of the other significant enriched biological processes found in this analysis. Among them are another relevant processes such as mitochondrial fragmentation involved in apoptotic process

(GO:0043653), mitochondrion transport along microtubule (GO:0047497), negative regulation of endoplasmic reticulum calcium ion concentration (GO:0032471), ornithine transport (GO:0015822), carnitine transport (GO:0015879), positive regulation of mitochondrial calcium ion concentration (GO:0051561), dynamin family protein polymerization involved in mitochondrial fission (GO:0003374), cellular response to superoxide (GO:0071451), positive regulation of autophagosome assembly (GO:2000786), organelle transport along microtubule (GO:0072384), apoptotic mitochondrial changes (GO:0008637), positive regulation of mitochondrial fission (GO:0090141), necroptotic process (GO:0070266), positive regulation of autophagy (GO:0010508), regulation of oxidative stress-induced intrinsic apoptotic signaling pathway (GO:1902175), release of cytochrome c from mitochondria (GO:0001836), mitochondrial calcium ion homeostasis (GO:0051560), hydrogen peroxide metabolic process (GO:0042743), mitochondrion disassembly (GO:0061726), autophagy of mitochondrion (GO:0000422), positive regulation of reactive oxygen species metabolic process (GO:2000379) and interleukin-12-mediated signaling pathway (GO:0035722).

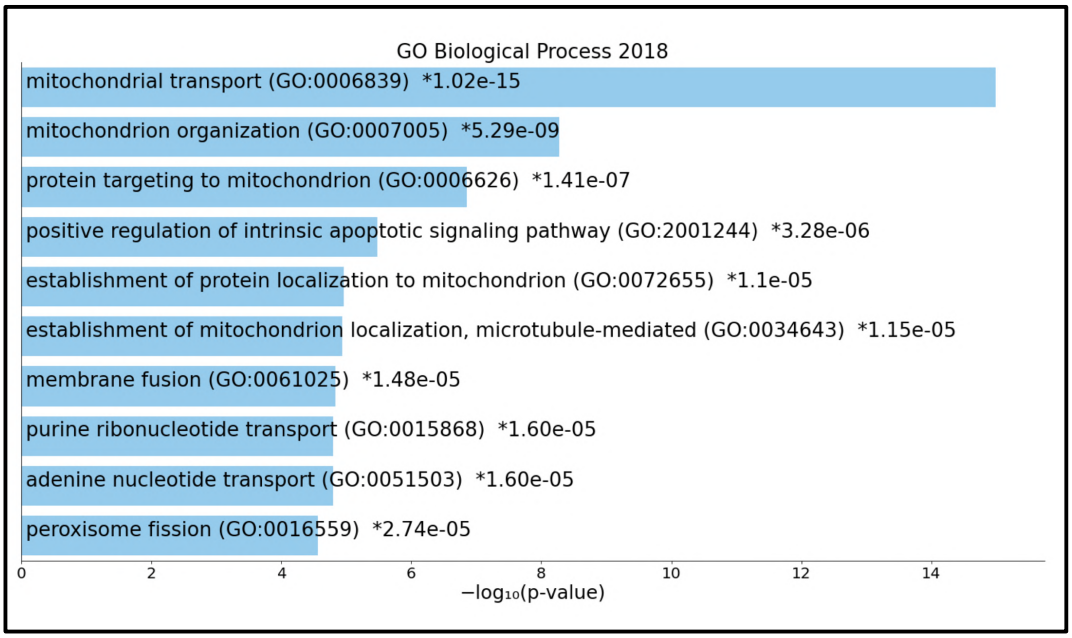


**Figure 8. Process enrichment analysis of PCR array upregulated genes.** Enrichment analysis was performed on the 18 upregulated genes shown in figure 6 using the GO Biological Process 2018 database. The bar chart shows the top 10 enriched terms in the chosen library, along with their corresponding p-values. Colored bars correspond to terms with significant p-values (<0.05). An asterisk (*) next to a p-value indicates the term also has a significant adjusted p-value (<0.05). The analysis was performed using the EnrichR software.

Finally, we performed an enrichment analysis on the same 18 upregulated genes (Figure 6) to assess their molecular function using the Gene Ontology (GO) Molecular Function 2018 database. The top 10 enriched terms are shown in Figure 9. The most significant term was adenine nucleotide transmembrane transporter activity (GO:0000295), followed by ADP transmembrane transporter activity (GO:0015217), ATP transmembrane transporter activity (GO:0008514), antiporter activity (GO:0015297), beta-tubulin binding (GO:0048487), microtubule binding (GO:0008017), tubulin binding (GO:0015631), protein phosphatase 2B binding (GO:0030346) and L-ornithine transmembrane transporter activity (GO:0000064). Supplementary table 3 (page 111) contains a list of the other significant enriched terms found in this analysis. Among them are important terms like Rac GTPase binding (GO:0048365), copper ion binding (GO:0005507), carnitine transmembrane transporter activity (GO:0015226) and amino-acid betaine transmembrane transporter activity (GO:0015199).

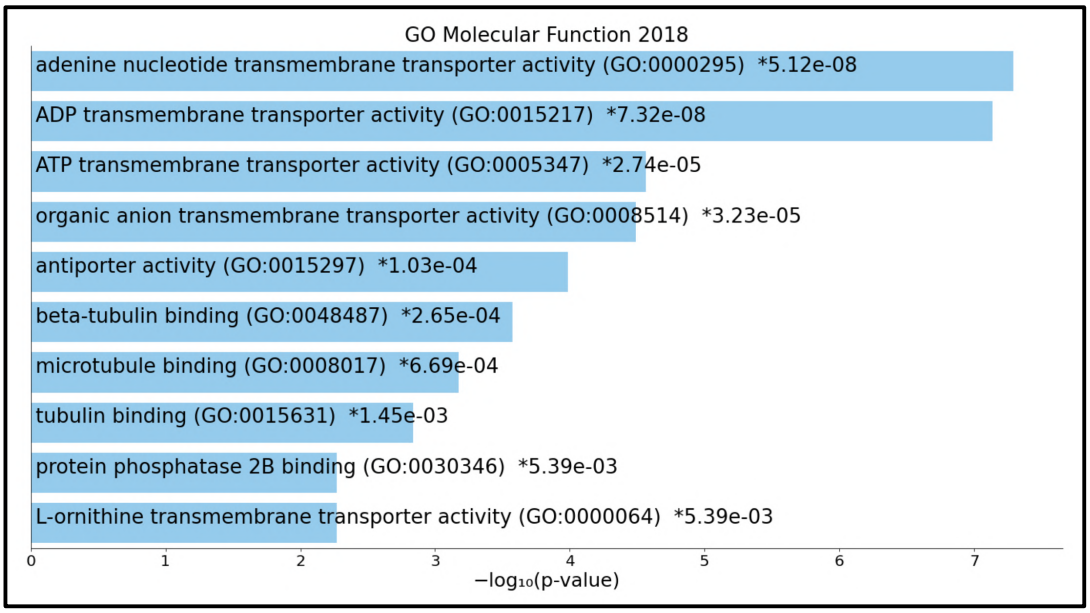


**Figure 9. Function enrichment analysis of PCR array upregulated genes.** Enrichment analysis was performed on the 18 upregulated genes shown in figure 6 using the GO Molecular Function 2018 database. The bar chart shows the top 10 enriched terms in the chosen library, along with their corresponding p-values. Colored bars correspond to terms with significant p-values (<0.05). An asterisk (*) next to a p-value indicates the term also has a significant adjusted p-value (<0.05). The analysis was performed using the EnrichR software.

## 4.5 MS astrocytes have increased mitochondrial fragmentation

Increased mitochondrial fragmentation in CNS resident cells, such as astrocytes and microglia, has already been shown to propagate neuroinflammation and

neurodegeneration [69]. Therefore, after assessing the expression of mitochondrial function related genes in the astrocytes, we analyzed the mitochondrial morphology using transmission electron microscopy to evaluate possible changes in these organelles' dynamics.

We first observed an increased swelling of the ER in the MS astrocytes (Figure 10A, bottom line), which has already been associated to ER stress [70]. Next, we analyzed changes in mitochondrial dynamics quantitatively and observed an increased mitochondrial roundness, an index with a 0-1 scale in which 1 indicates a perfect circular shape, in the patient's cells (Figure 10B). Also, this was coupled with a decrease in the mitochondrial aspect ratio (the proportion between width and height) (Figure 10C). Fragmented mitochondria are in fact characterized by an increased circularity and decreased aspect ratio [58], indicating an increased mitochondrial fission in the MS astrocytes, in accordance with the biological process enrichment analysis of the upregulated PCR array genes (Supplementary table 2). Finally, we observed a decreased mitochondrial/cell area ratio in the astrocytes from the MS group (Figure 10D), which is suggestive of a disruption of the mitochondrial content. This is in line with our pathway (Figure 7) and biological process enrichment analysis (Supplementary table 2), which highlighted mitophagy and autophagy of mitochondria, respectively, in the MS group.

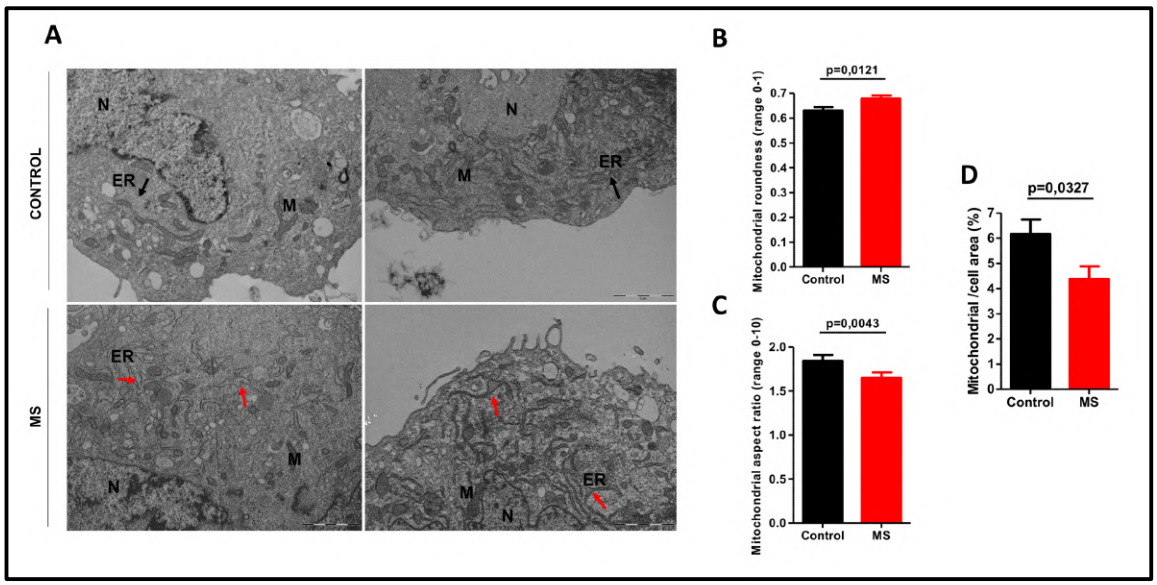


**Figure 10. Mitochondrial morphology analysis in astrocytes. A** – Panel of electron microscopy analysis. The top line is representative of the results obtained for the control group cells and the bottom line is representative of the results obtained for the MS group cells. Scale bar = 2µm. The black arrows indicate the ER in the control group and the red arrows indicate the ER in the MS cells. N: nucleus, ER: endoplasmic reticulum, M: mitochondria. **B** – Quantification of mitochondrial roundness in control and MS astrocytes. **C**

- Quantification of mitochondrial aspect ratio in control and MS astrocytes. **D** – Quantification of the mitochondrial/cell area as a percentage in control and MS astrocytes. N=10 individual cells per group. Data in panels B-D are represented as the mean ± standard error. Quantification was performed using the ImageJ software. Unpaired two-tailed Student's t tests or Mann-Whitney tests were used to compare the groups using GraphPad Prism.

## 4.6 Analysis of DRP1 protein levels

As we observed increased mitochondrial fission in the MS astrocytes, both at gene and morphology levels we used *western blotting* to assess the DRP1 protein expression in these cells, as it is one of the key regulators of mitochondrial fission [55]. We observed no significant differences between the groups, although a slight increase in DRP1 levels that could have biological meaning is observed in the cells derived from the MS patients (Figure 11, A and B).

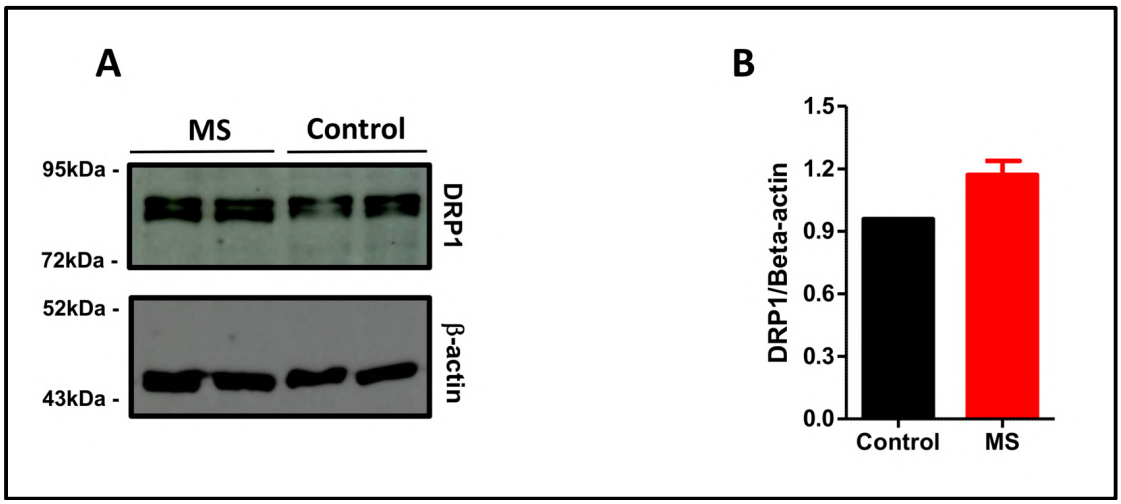


**Figure 11. Analysis of DRP1 protein levels. A –** Representative Western-Blot membrane for DRP1 (top panel, predicted molecular weight = 83kDa) and β-actin (bottom panel, predicted molecular weight = 45kDa). The first two samples in the membrane are from the MS astrocytes and the last two samples are from the control cells. **B** – Quantification of DRP1 protein levels, normalized to β-actin, analyzed using ImageJ software. Data in **B** is represented as the mean ± standard error. These data are representative of cells from N=2 controls and 2 patients from one experiment.

## 4.7 MS astrocytes show decreased mitochondrial DNA content and impaired activation of the mitochondrial unfolded protein and stress response pathways

Our electron microscopy findings demonstrated a decreased mitochondrial/cell area ratio (Figure 10D). Therefore, we complemented this analysis by assessing the mitochondrial/nuclear (mt/n) DNA ratio using RT-qPCR. In accordance with our previous results, we observed a significantly decreased mt/n DNA ratio in MS astrocytes compared

to controls (Figure 12A), which is suggestive of a disruption of the mitochondrial content and is also in line with our PCR array findings (Figure 7 and Supplementary table 2).

The mitochondrial UPR (UPR) and integrated stress response (mtISR) pathways promote protective outcomes in cells with mitochondrial dysfunction, inducing mitochondrial proteostasis [71-74]. These pathways comprise mitochondria-located chaperones and proteases that induce the degradation or proper folding of damaged mitochondrial proteins, regulating both the quality and functioning of the organelles. Among mitochondrial UPR and ISR related transcripts (Figure 12B-F) we observed a significant decrease in the expression of *ATF4* (Figure 12C), *HSPA9* (Figure 12E) and *HSP60* (Figure 12F), along with a significantly decreased expression of the mitochondrial proteases *LONP1* (Figure 12G) and *CLPP* (Figure 12H) in MS astrocytes. Together, these results indicate an impaired activation of these pathways in the patient's cells.

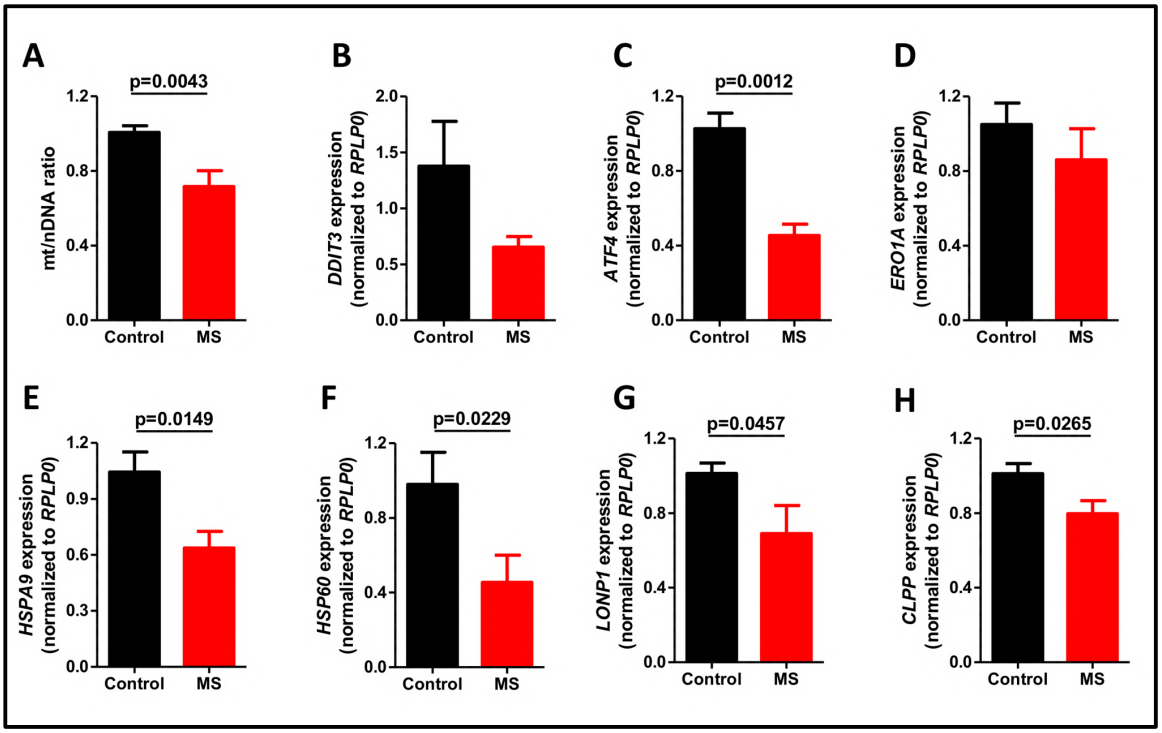


**Figure 12. Analysis of mitochondrial content and integrated stress response genes. A** – Mitochondrial (*16S*) to nuclear (*RPLP0*) DNA ratio estimative by RT-qPCR. **B-F** Relative expression of mitochondrial UPR and ISR related transcripts *DDIT3* (**B**), *ATF4* (**C**), *ERO1A* (**D**), *HSPA9* (**E**) and *HSP60* (**F**). **G-H** Relative expression of mitochondrial proteases *LONP1* (**G**) and CLPP (**H**). All genes were normalized to the housekeeping gene *RPLP0*. N=3 controls and 3 patients, analyzed in technical triplicates in two independent experiments. Data are represented as the mean ± standard error. Unpaired two-tailed Student's t tests or Mann-Whitney tests were used to compare the groups using GraphPad Prism.

## 4.8 Mitotracker fluorescence suggests increased mitochondrial mass and number of actively respiring mitochondria in MS astrocytes

After analyzing the previous parameters in the astrocytes, we performed flow cytometry analyzes of mitochondria using the mitochondria-localized probes Mitotracker (Thermo Fisher, USA) to have an idea of mitochondrial function. We used Mitotracker Green as an indicator of mitochondrial mass, and the $\Delta\psi$m-dependent Mitotracker Deep red as an indicator of actively respiring and ROS-producing mitochondria in the cells, as previously published [65]. In terms of frequency of positive cells, we did not observe differences between control and MS astrocytes for both Mitotracker Green (Figure 13A) and Mitotracker Deep Red (Figure 13C). On the other hand, although at the margin of being statistically significant (p=0.0649), when analyzing the mean fluorescence intensity of these markers, we observed an increased MFI of both Mitotracker Green (Figure 13B) and Mitotracker Deep Red (Figure 13D) in MS astrocytes compared to controls, indicating a possible biological effect in which the patients' cells should have increased mitochondrial mass and respiration, together with ROS production.

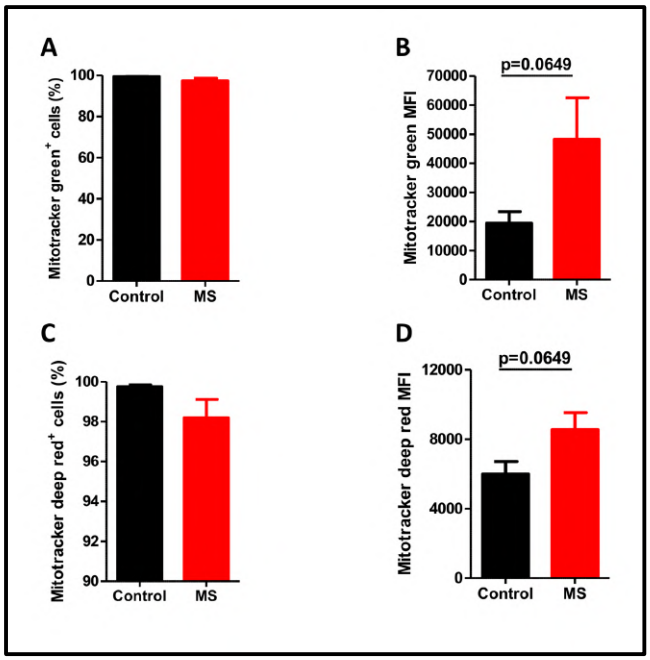


**Figure 13. Analysis of mitochondrial function using Mitotracker. A** – Quantification of Mitotracker Green positive cells between the astrocytes from controls and MS patients. **B** – Quantification of Mitotracker Green mean fluorescence intensity between the groups. **C** – Quantification of Mitotracker Deep Red positive cells between the astrocytes from controls and MS patients. **D** – Quantification of Mitotracker Deep Red mean fluorescence intensity between the groups. Data are represented as the mean ± standard error. N=3

controls and 3 patients, analyzed in technical duplicates in two independent experiments. Flow cytometry analysis was performed using the FlowJo software. Unpaired two-tailed Student's t tests or Mann-Whitney tests were used to compare the groups using GraphPad Prism.

## 4.9 MS astrocytes have increased ROS and decreased mitochondrial quality

To have further insights into the quality and functioning of mitochondria, as well as to specifically analyze ROS production in the astrocytes from both groups, we deepened into the mitochondrial flow cytometry analyzes. The ratio between the Mitotracker Deep Red MFI and the Mitotracker Green MFI has previously been reported as an indicator of mitochondrial quality in the cells [65]. Therefore, we analyzed this parameter in the astrocytes and observed a decreased mitochondrial quality in the MS astrocytes (Figure 14A), which is in line with the biological processes found enriched in the PCR array analysis (Supplementary table 2).

Next, to quantify ROS production in the astrocytes from both groups we used Mitosox (Thermo Fisher, USA), which is an indicator of superoxide production in cells. We observed no significant differences between the frequency of Mitosox$^+$ cells between the groups (Figure 14B), however we found a significant increase in the Mitosox MFI in MS astrocytes (Figure 14C), indicating that these cells have higher superoxide production. Interestingly, superoxide related biological processes have been found enriched in MS astrocytes in our analysis (Supplementary table 2).

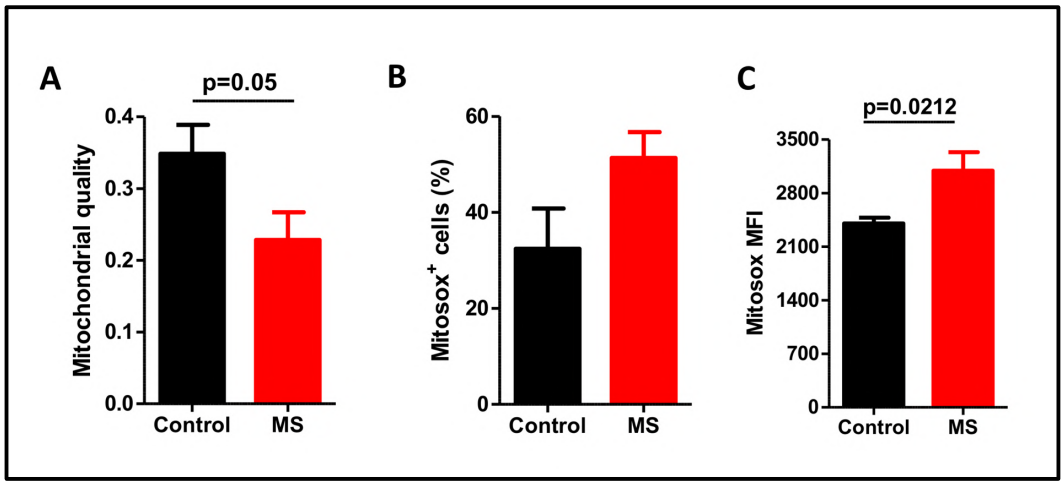


**Figure 14. Analysis of mitochondrial quality and ROS production. A** – Quantification of mitochondrial quality between the astrocytes from controls and MS patients. This index is the ratio between the Mitotracker Deep Red MFI and the Mitotracker Green MFI. **B** – Quantification of Mitosox positive cells between the astrocytes from controls and MS patients. **C** – Quantification of Mitosox mean fluorescence

intensity between the groups. Data are represented as the mean ± standard error. N=3 controls and 3 patients, analyzed in technical duplicates in two independent experiments. Flow cytometry analysis was performed using the FlowJo software. Unpaired two-tailed Student's t tests or Mann-Whitney tests were used to compare the groups using GraphPad Prism.

## 4.10 MS astrocytes uptake higher amounts of glucose

Next, to have a first idea of the metabolic profile of the astrocytes, we measured glucose and lactate from the cells' supernatants. As mentioned before, in steady-state astrocytes display a more glycolytic profile and provide lactate to neurons, fueling their metabolism through the astrocyte-neuron lactate shuttle [53].

We observed a significant decrease in glucose levels in MS astrocytes (Figure 15A), which indicates that they uptake more glucose from the medium. On the other hand, no differences in lactate production were observed between control and MS astrocytes in a basal level (Figure 15B).

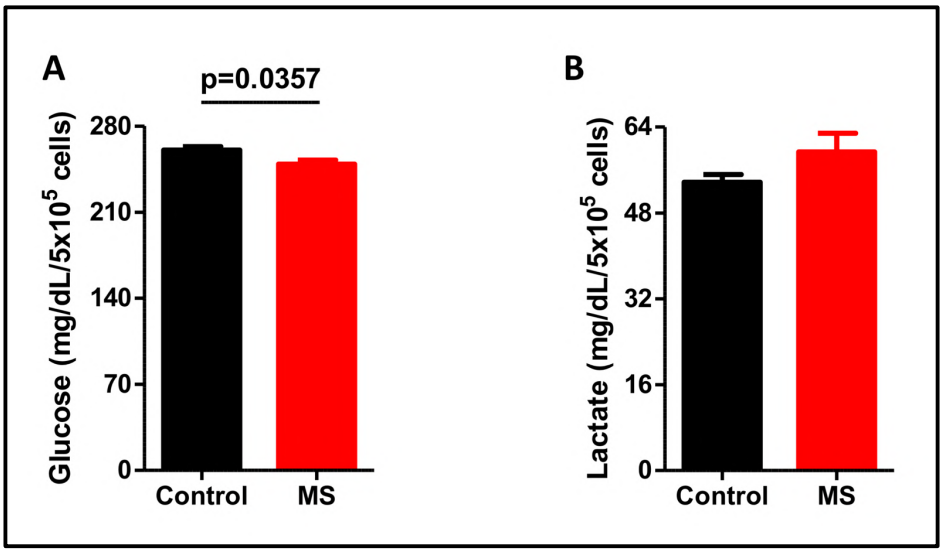


**Figure 15. Analysis of metabolites in astrocyte supernatants.** Cells were plated at a density of $5x10^5$ and 48 hours after, the supernatant was collected for metabolite analyzes. **A** Quantification of the amount of glucose in the supernatant of the astrocytes in mg/dL. **B** Quantification of the amount of lactate in the supernatant of the astrocytes in mg/dL . Unpaired two-tailed Student's t tests or Mann-Whitney tests were used to compare the groups using GraphPad Prism. N=3 controls and 3 patients, analyzed in technical triplicates in two independent experiments. Data are represented as the mean ± standard error.

## 4.11 No differences in PGC-1α and HIF-1α gene expression between the groups

As we observed changes in mitochondrial morphology (Figure 10) and in glucose uptake (Figure 15A) in MS astrocytes, we analyzed the expression of the *PPARGC1A* and *HIF1A* genes related to the transcription factors PGC-1α and HIF-1α, respectively. These are two transcription factors that are involved in the upstream regulation of mitochondrial dynamics and in the regulation of the metabolic profiling of the cells.

Our analysis showed no significant differences between the groups for both *HIF1A* (Figure 16A) and *PPARGC1A* (Figure 16B) genes.

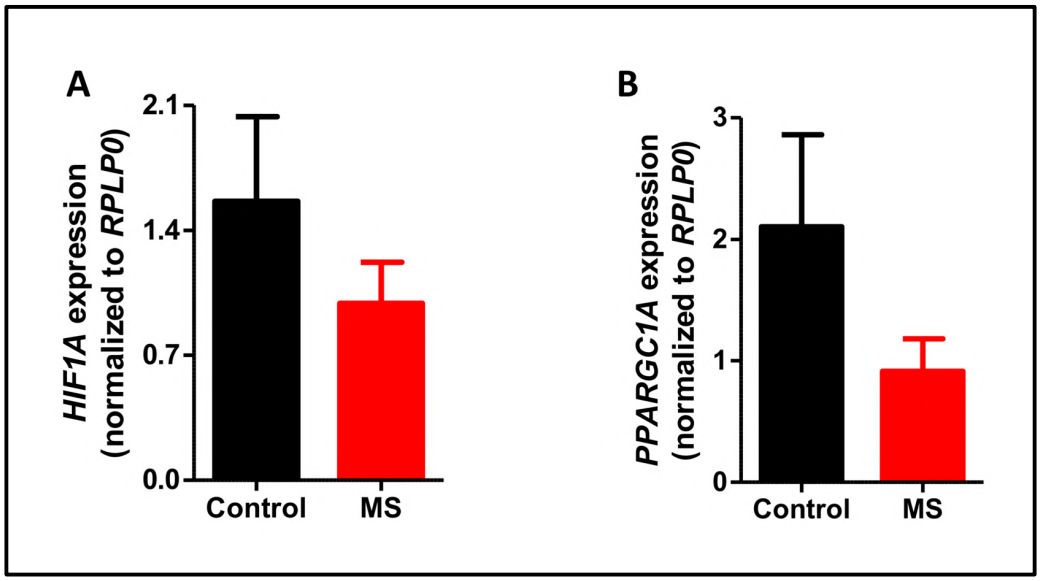


**Figure 16. Analysis of mitochondrial dynamics regulator genes. A -** Relative expression of *HIF1A* gene. B - Relative expression of *PPARGC1A* gene All genes were normalized to the housekeeping gene *RPLP0*. N=3 controls and 3 patients, analyzed in technical triplicates in two independent experiments. Data are represented as the mean ± standard error. Unpaired two-tailed Student's t tests or Mann-Whitney tests were used to compare the groups using GraphPad Prism.

## 4.12 MS astrocytes display increased oxidative profile and decreased mitochondrial bioenergetics health

One of our key objectives in the study was to determine the metabolic profile of the astrocytes from both groups. As we observed increased glucose uptake in MS astrocytes (Figure 15A), we deepened the metabolic analysis using a much more reliable tool to assess mitochondrial function in intact cells, the Seahorse (Agilent, USA) technology, which allows measurements of mitochondrial respiration without the need for isolating mitochondria in non-homeostatic conditions.

We first performed the Mitostress test, which is the gold standard assay for analyzing mitochondrial function through measuring the OCR of cells (Figure 17A). Among the analyzed parameters, the assay indicated an increased Non-Mitochondrial OCR (Figure 17B), increased Maximal OCR (Figure 17D), increased Proton Leak OCR (Figure 17E) and decreased Bioenergetic Health Index (Figure 17J) in MS astrocytes compared to controls, suggesting higher oxidative metabolism in these cells. The Bioenergetic Health Index has been previously indicated as biomarker for mitochondrial health and functionality in cells, in a way that the lower it is, the higher mitochondrial dysfunction and oxidative damage the cell has [75, 76]. This is in line with our PCR array findings (Supplementary table 2) in which superoxide and mitochondrial damage related processes were found enriched in the MS astrocytes and the increased superoxide production seen in this same group (Figure 14C). Interestingly, we also observed a significant basal ECAR (Figure 17I) in MS astrocytes, which is suggestive of enhanced glycolytic metabolism.

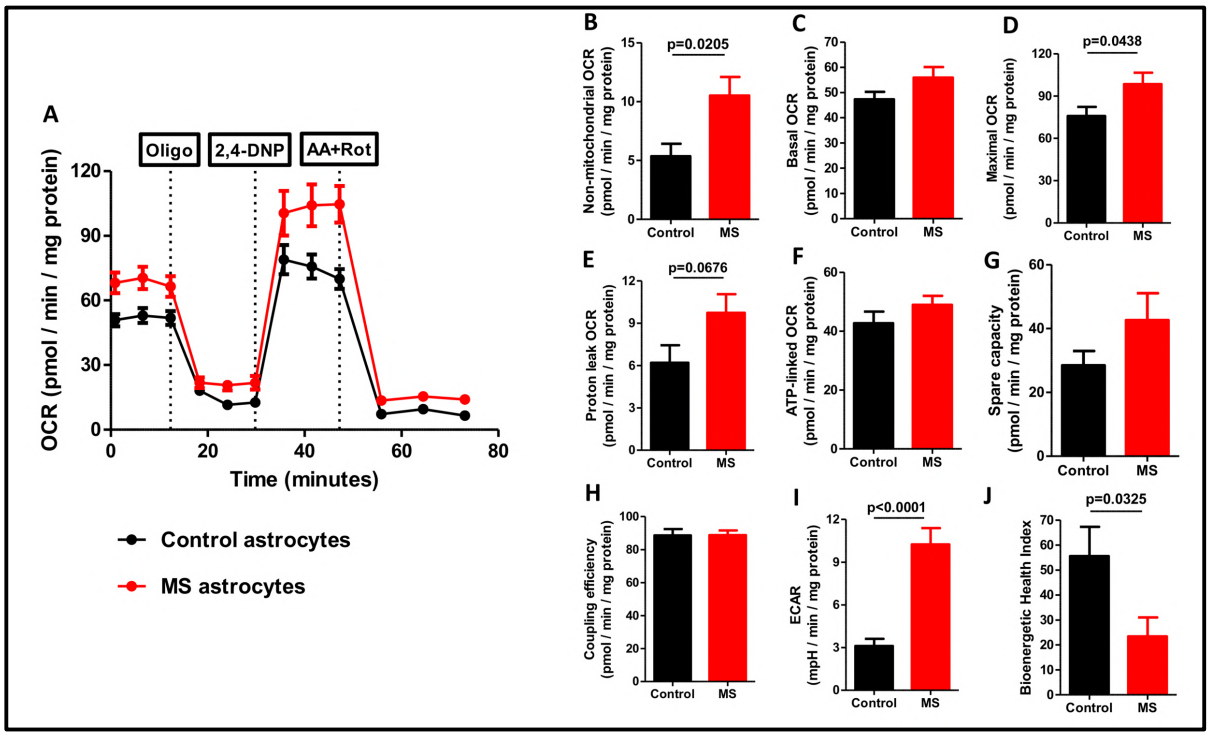


**Figure 17. Mitostress test analysis. A** – Curves showing the overall OCR for control and MS astrocytes. Oligo: Oligomycin, 2,4-DNP: 2,4-dinitrophenol, AA+Rot – antimycin-A plus Rotenone. **B** – Quantification of the non-mitochondrial OCR. **C** – Quantification of the basal OCR. **D** – Quantification of the maximal OCR. **E** – Quantification of the proton-leak OCR. **F** – Quantification of the ATP-linked OCR. **G** – Quantification of the spare-capacity. **H** – Quantification of the coupling efficiency. **I** – Quantification of the ECAR. **J** – Quantification of the bioenergetic health index. Data are representative of N=3 controls and 3 patients, with cells analyzed in quadruplicates in three independent experiments. Analysis was performed using the Wave software. All

data were normalized to cell protein content. Data are represented as the mean ± standard error. Unpaired two-tailed Student's t tests or Mann-Whitney tests were used to compare the groups using GraphPad Prism.

## 4.13 MS astrocytes display increased glycolytic reserve rate

As we observed a very significant basal ECAR in our Mitostress OCR analysis (Figure 17I), we used the Seahorse technology to specifically assess glycolytic metabolism in the astrocytes using the Glycolysis stress test.

We observed a significant increase in non-glycolytic acidification (Figure 18E) and glycolytic reserve rate (%) (Figure 18F) in MS astrocytes compared to controls, which is suggestive of increased extracellular acidification from other sources rather than glycolysis and increased response to energetic requirements such as ATP demands in the cells, respectively.

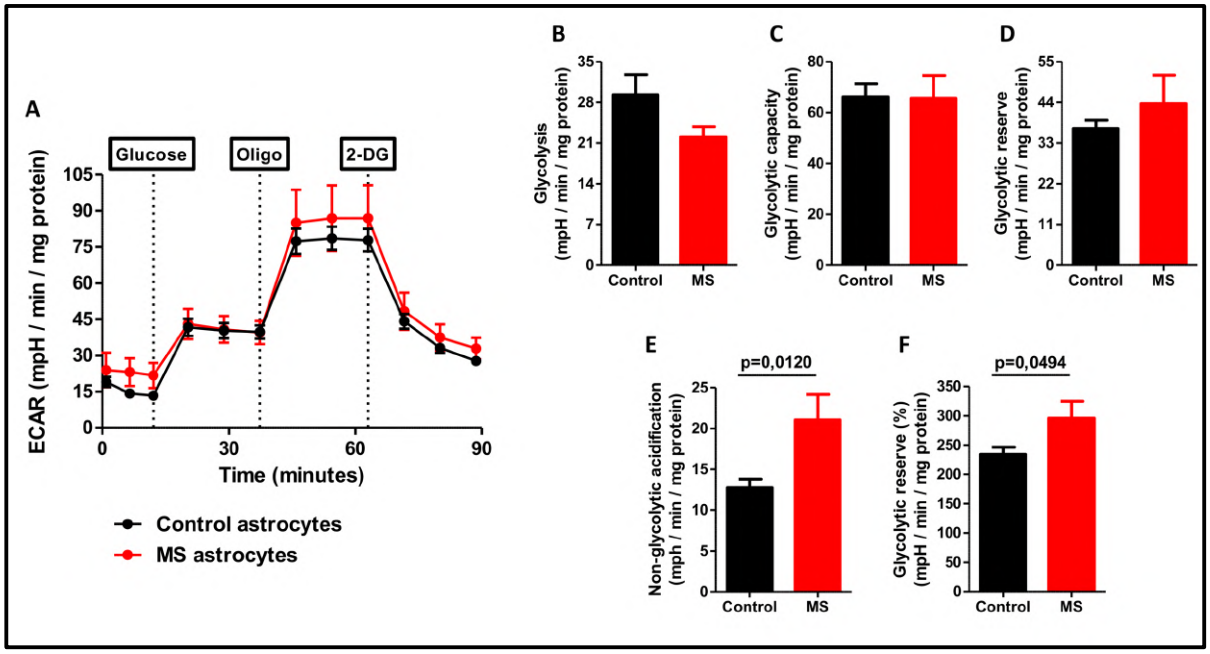


**Figure 18. Glycolysis stress test analysis. A** – Curves showing the overall ECAR for control and MS astrocytes. Oligo: Oligomycin, 2-DG: 2-Deoxi-D-glucose. **B** – Quantification of glycolysis. **C** – Quantification of glycolytic capacity. **D** – Quantification of glycolytic reserve. **E** – Quantification of non-glycolytic acidification. **F** – Quantification of the glycolytic reserve rate (%). Data are representative of N=3 controls and 3 patients, with cells analyzed in quadruplicates in two independent experiments. Analysis was performed using the Wave software. All data were normalized to cell protein content. Data are represented as the mean ± standard error. Unpaired two-tailed Student's t tests or Mann-Whitney tests were used to compare the groups using GraphPad Prism.

### 4.14 Bioinformatics RNA-seq analysis shows several mitochondria-related changes in hiPSC-derived astrocytes stimulated with TNF-α

Finally, we used a publicly available RNA sequencing database (GEO accession number GSE120411) to compare the transcriptome of hiPSC-derived astrocytes from healthy donors in a basal level and upon stimulation with TNF-α (10ng/mL, for 24 hours), a classically MS-related cytokine [77], focusing on mitochondrial changes between these groups. TNF-α is a cytokine related to the pathology of several neurological disorders [78], therefore analyzing the transcriptome of hiPSC-derived astrocytes activated with this cytokine could give us some further insights on the mitochondria-related pathways that can be altered in these cells in a more general context of neuroinflammation We first observed that TNF induced a very distinct transcriptomic signature in hiPSC-derived astrocytes, with a massive upregulation of several transcripts (Figure 19A). The type and number of transcripts differentially expressed are shown in detail in supplementary figure 1 (page 112).

Additionally, when performing biological processes enrichment analysis on the upregulated and downregulated protein-coding transcripts obtained from the RNA-seq analysis (Figure 19B), focusing on mitochondria, we observed among enriched pathways release of cytochrome c from mitochondria (GO:0001836), apoptotic mitochondrial changes (GO:0008637), positive regulation of release of cytochrome c from mitochondria (GO:0090200), regulation of release of cytochrome c from mitochondria (GO:0090199), dynamin family protein polymerization involved in mitochondrial fission (GO:0003374), regulation of protein insertion into mitochondrial membrane involved in apoptotic signaling pathway (GO:1900739), intrinsic apoptotic signaling pathway in response to oxidative stress (GO:0008631), positive regulation of autophagy (GO:0010508) and positive regulation of purine nucleotide metabolic process (GO:1900544) in TNF-α stimulated hiPSC-derived astrocytes. Interestingly, the mitochondrial membrane organization (GO:0007006) process appeared significantly repressed in the TNF group as well. Altogether, these results are in line with our findings in MS astrocytes (Supplementary table 2 and Figure 10), suggesting increased mitochondrial dysfunction and fission in human astrocytes in the context of neuroinflammation.

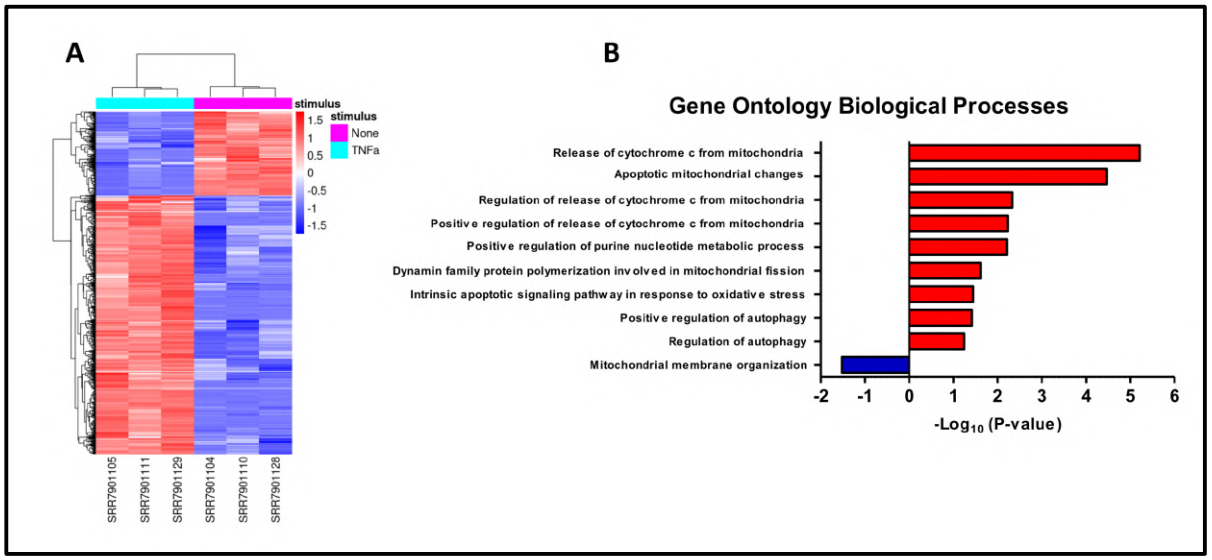


**Figure 19. Bioinformatics RNA-seq analysis. A** – Heatmap of the differentially expressed transcripts, filtered by FDR<0.05. Light blue lines on top indicate TNF-α activated iPSC-derived astrocytes and the pink line indicates cells with no stimulation -α (10ng/mL, for 24 hours), N= 3 for each group. The z scores (-1.5 to 1.5) color scale is shown at right. Transcripts that presented $\log_2$ fold change>1 or <-1 and FDR <0.05 were differentially expressed. **B** – Transcripts found differentially expressed were filtered and only the protein-coding ones were selected. Then, Gene Ontology biological processes enrichment analysis was performed on the upregulated and downregulated transcripts, focusing on mitochondrial alterations, to see the enriched and repressed processes, respectively. The analysis was performed using the EnrichR software. All processes are demonstrated in a $-\log_{10}$(P-value) scale. Data were obtained from the GSE12041 dataset.

Next, we analyzed expression of several transcripts and highlighted those related with mitochondrial function (Figure 20A). Many protein-coding, mitochondrial-related transcripts were found upregulated in the TNF-treated astrocytes, including *SOD2*, *SLC25A22*, *SLC25A28*, *NDUFA5*, *CD38*, *CASP8*, *BCL2*, *BCL2L1* and *BBC3*. Among the downregulated transcripts in this same group there are *TAZ*, *NEFL*, *BCS1L* and *APC2*. Then, we performed Gene Set Enrichment Analysis and analyzed the biological pathways differentially regulated in the groups (Figure 20B). Among the enriched pathways, we highlight some: apoptosis; trafficking of AMPA receptors; glutamate binding, activation of AMPA receptors and synaptic plasticity; negative regulation of the PI3K/AKT network; dimerization of procaspase-8; caspase activation via extrinsic apoptotic signaling pathway; regulation of TP53 activity; signaling by GPCR; SLC transporter disorders; antiviral mechanism by IFN-stimulated genes; programmed cell death; DDX58/IFIH1-mediated induction of interferon alpha/beta and ISG15 antiviral mechanism. Among the repressed pathways, we highlight cell cycle and DARPP-32 events. Altogether, these

results are in line with our PCR array findings in MS astrocytes, with upregulation of several mitochondrial transporter and apoptosis-related genes and pathways in the TNF-activated hiPSC-derived astrocytes.

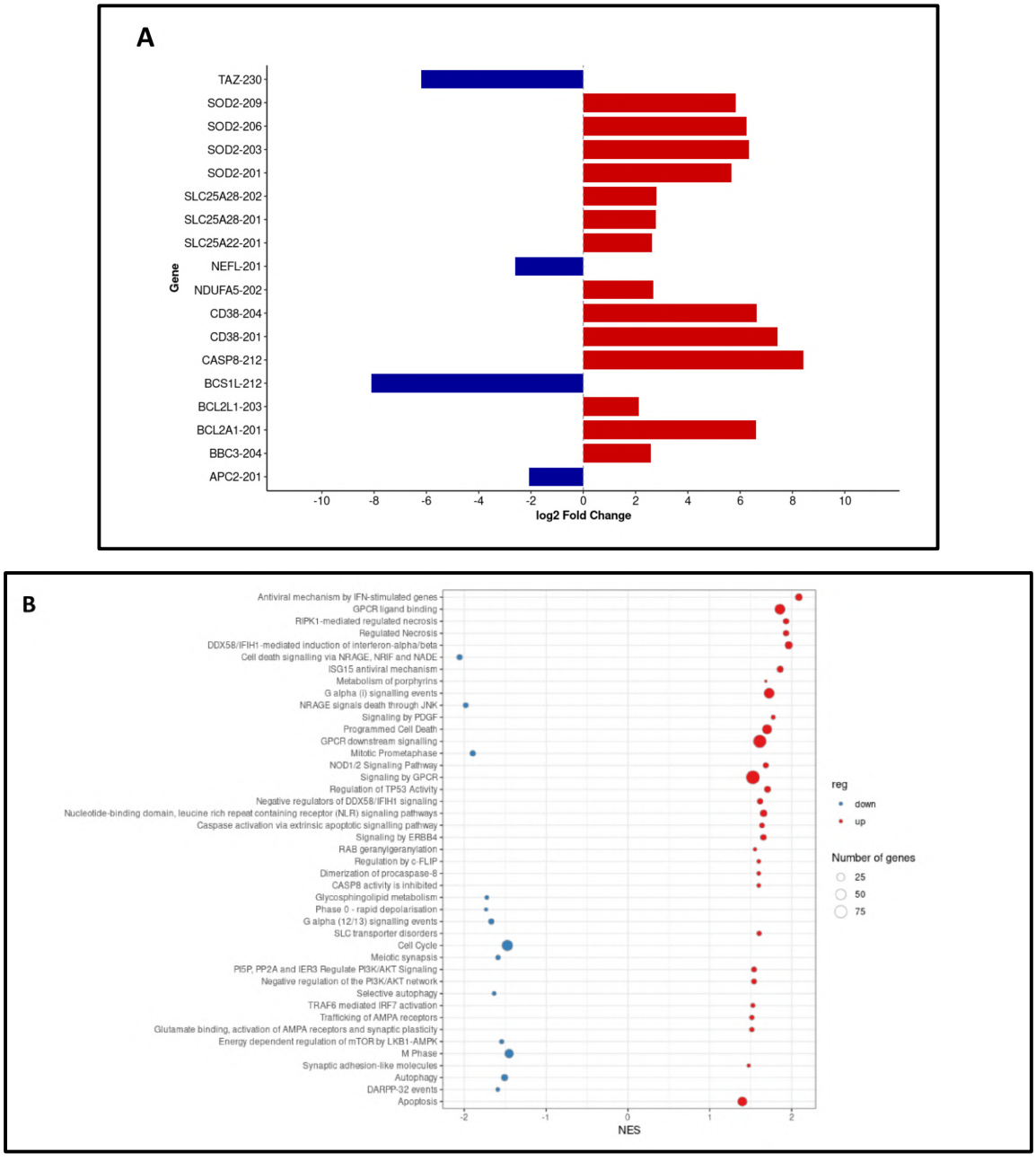


**Figure 20. Analysis of mitochondria-related transcripts and GSEA. A** – Expression of protein-coding genes related to the mitochondrial biology. The differential expression represented in a $\log_2$ Fold Change scale, filtered by FDR<0.05. **B** – Gene-set Enrichment Analysis (GSEA) using Reactome database for biological pathways. Enriched pathways are shown in red and repressed pathways are shown in blue. The circle size represents the number of genes associated to each specific pathway. NES – normalized enrichment score. N=3 cell lines for each group of hiPSC-derived astrocytes, unstimulated or TNF-activated. Biological pathways with p <0.05 were considered significant. Data were obtained from the GSE12041 dataset.

# 5. DISCUSSION

MS is a complex disease with mechanisms that are not fully recapitulated by animal models, along with the interspecific differences that make it very hard to translate study findings into humans [26, 27]. Here we used the human induced pluripotent stem cell technology to derive astrocytes from 3 RRMS patients compared with 3 sex and age-matched controls as an attempt to find differences between them that could recapitulate some disease aspects, focusing mainly on mitochondrial dynamics and cell metabolism.

First, we were able to successfully derive and characterize the astrocytes starting from MS patients' hiPSC, which is accordance with the very few previously published studies using the hiPSC-derived cells to model MS [37-41].

There are only two studies in the literature that analyzed hiPSC-derived astrocytes from MS patients, which reached very different conclusions [40-41]. While the first [40] suggested that MS alterations should be more linked to alterations in immune response genes rather than those occurring within the CNS, with no differences observed in cytokine profiles of control and MS astrocytes in a basal level, the second [41] suggested exactly the opposite, that is, the resident CNS cells should play a significant role in the development of MS, acting in synergy with peripheral immune cells to promote autoimmune neuroinflammation. Although this study [41] analyzed some metabolic parameters in astrocytes bearing a NF-κB gain of function variant, such as the glutamate and glucose uptake together with lactate production, they do not assess cell metabolism in more details nor mitochondrial functionality and morphology within these cells.

The role played by mitochondria in the regulation of cell metabolism extends far beyond the production of ATP during OXPHOS. Besides this canonical role, the organelles can participate in the pathology of several neurologic diseases through modulation of mitochondrial morphology, mitophagy, generation of oxidants, interactions with the ER and regulation of Calcium metabolism [79]. One hallmark of neurodegeneration is the activation of CNS resident cells such as the astrocytes and microglia, which produce a lot of proinflammatory cytokines along with mitochondrial ROS and signaling molecules [45-47], demanding a lot in terms of energy and therefore highlighting the importance of the proper regulation of mitochondrial bioenergetics in these cells. In this context, the changes in mitochondrial morphology, known as mitochondrial dynamics, have been

demonstrated to shape the cells' energy metabolism according to their bioenergetics demands towards a more glycolytic or oxidative profile [54]. Besides that, mitochondrial dynamics play a significant role in the regulation of neuroinflammation, as it regulates the formation of mitochondria-ER associated membranes, mitophagy and programmed cell death [80]. Importantly, several mitochondrial changes have already been found in Multiple Sclerosis patients [81-83], reaffirming the importance of these organelles to the pathology of the disease.

In this context, we first analyzed mitochondria-related genes using PCR array in MS and control hiPSC-derived astrocytes to have deeper insights on mitochondrial biology in these cells (Figure 6). The most upregulated gene in MS astrocytes was *UXT*. Interestingly, UXT protein has already been associated with enhanced NF-κB activity, composing the NF-kB enhanceosome and regulating its nuclear functions [84]. NF-κB has been shown to regulate the metabolic response to inflammation and basal metabolism in astrocytes modulating both glycolysis and OXPHOS pathways [85]. Additionally, it has also been demonstrated that UXT induces mitochondrial aggregation by regulating the microtubular cytoskeleton through the interaction with LRPPRC, a protein involved in mitochondrial trafficking, also found upregulated in MS astrocytes in our analysis. Mitochondrial aggregation has already been associated with TNF-related pathways activation [86, 87], suggesting it as an inflammation-dependent mechanism. Finally, increased activation of UXT has been linked to cell death [87, 88]. We also observed in this group an increased expression of the mitochondrial dynamics regulators *MFN1* (fusion), *FIS1* and *DNM1L* (mitochondrial fission), suggesting mitochondrial morphology changes in MS astrocytes. Several mitochondrial transporter genes from the Solute Carrier 25 (SLC25) family were also found upregulated in MS astrocytes, which has already been suggested as a marker for mitochondrial dysfunction in the brain [89]. *SOD2*, which was also found upregulated in MS astrocytes, is the mitochondrial superoxide dismutase and increased *SOD2* has already been linked to the activation of astrocytes [90], as a way to dampen the oxidative damage caused by superoxide generation. The antiapoptotic *BCL2* appeared downregulated in MS astrocytes. Curiously, BCL2 has already been associated to the regulation of mitochondrial fusion [91-93], however it failed to exert protective outcomes in the release of cytochrome c from the mitochondria, a process known to induce apoptosis in cells [94]. There was also upregulation of the *SH3GLB1* gene in MS

astrocytes, which has already been associated to the promotion of autophagy [95] and to the maintenance of mitochondrial morphology [96]. The expression of the mitochondrial translocases of the outer and inner mitochondrial membrane, *TOMM20* and *TIMM8A*, respectively, which regulate import of cytosolic proteins into the mitochondria [97] was also found upregulated in MS astrocytes, together with the ADP/ATP nucleotide exchanger *GRPEL1*, which has also been linked to the regulation of cellular stress responses [98], suggesting an increased bioenergetics demand in these cells. An upregulation of the mitochondrial peptidase *IMMP2L* was also observed in MS astrocytes. Interestingly, IMMP2L has been directly associated with the production of the DIABLO, which is a protein linked to apoptosis in cells [99]. Finally, we observed increased expression of *MPV17* in MS astrocytes, that is associated with the mtDNA maintenance [100].

To have more biological insights of the PCR array results, we used pathway enrichment analysis on the upregulated genes (Figure 7) and observed that the most enriched one was mitophagy, which is related to mitochondrial quality control through the removal of damaged mitochondria of cells and is tightly associated with mitochondrial dynamics, being regulated by the DRP-1, OPA-1 and MFN2 proteins that play a role in autophagosome formation [80]. Although mitophagy is usually found impaired in neurodegenerative diseases, such as Parkinson's and Alzheimer's [80], it has been demonstrated that MS patients display significant increased levels of mitophagy and autophagy markers in both serum and cerebrospinal fluid [101], indicating a pathological role of these pathways to the disease. The researchers also observed a positive correlation between ATG5 and Parkin concentrations, suggesting that mitophagy and autophagy are associated pathways in MS. In this sense, another study from the same group [102] further demonstrated that serum and cerebrospinal fluid concentrations of ATG5 and Parkin are greater in gadolinium-positive MS patients than in the negative ones, suggesting that the interplay between mitophagy and autophagy correlates with the active MS disease phase. In line with these data, here we found another evidence that could suggest increased mitophagy in MS-derived astrocytes, which were the decreased mitochondrial/cell area ratio observed in transmission electron microscopy (Figure 10D) and the decreased mitochondrial/nuclear DNA ratio (Figure 12A). Importantly, the molecular mechanisms that regulate this mitophagic/autophagic crosstalk during MS remain to be further

elucidated. We also observed enriched pathways related to other neurological diseases such as Huntington, Amyotrophic Lateral Sclerosis and Prion diseases, suggesting that MS astrocytes have pathways related to neurodegenerative processes. Additionally, the peroxisome pathway was found enriched in MS astrocytes and peroxisomes have shown to play a role in the regulation of mitochondrial β-oxidation [103] and redox balance [104], therefore being important in metabolism and homeostasis in cells. Finally, we observed enrichment of necroptosis in the patient derived-astrocytes, which was already shown to be implicated in MS pathology [105].

We also performed enrichment analysis on the PCR array MS upregulated genes to see biological processes that could be correlated with them (Figure 8 and Supplementary Table 2). We found several enriched processes related to mitochondrial organization and transport of ADP and aminoacids, which is suggestive of increased bioenergetics demands in the MS astrocytes. Interestingly, dynamin polymerization involved in mitochondrial fission appeared enriched in MS astrocytes, which is in line with the increased mitochondrial fragmentation we observed in electron microscopy analysis (Figure 10A-C). Increased mitochondrial fragmentation has already been described in the experimental mouse model of MS, EAE [106], and increased DRP-1 levels were found in active lesions from MS patients [107]. Nevertheless, this study is, to the best of our knowledge, the first one describing alterations in mitochondrial morphology in astrocytes derived from MS patients using the hiPSC technology. We also observed, as previously discussed, enriched processes related to the regulation of apoptosis and mitophagy in MS astrocytes, suggesting that these pathways should contribute to the disease pathology. We found also that processes related to the negative regulation of Calcium amounts in the ER and positive regulation of this ion concentration in the mitochondria. While the elucidation of the role of mitochondrial calcium uptake in the regulation of brain energy metabolism is at its beginning, it has already been reported that a mitochondrial Calcium overload may occur due to decreased levels of the mitochondrial sodium/calcium exchanger NCLX and this enhances mitochondrial dysfunction, leading to increased mitochondrial ROS production and increasing neurodegeneration in Alzheimer's disease patients and animal models [108]. Finally, we observed pathways related to ROS enriched in MS astrocytes, what could be reaffirmed by the increased levels of mitochondrial superoxide we detected in these cells (Figure 14C). Finally, the molecular function

enrichment analysis (Figure 9) also suggest an increased ADP, ATP and aminoacid transporters activity and cytoskeleton rearrangement in MS astrocytes, probably involved with mitochondrial trafficking in these cells. Altogether, these enrichment results provide supportive evidence for increased mitochondrial dysfunction and cell bioenergetics demand in MS astrocytes, highlighting several pathways that can be associated to disease mechanisms.

As our morphological analysis (Figure 10A-C) showed increased mitochondrial fission we analyzed the levels of DRP-1 protein in astrocytes. Although no significant changes were observed, a slight tendency of increased DRP-1/β-actin ratio could be observed (Figure 11B), that could reach statistical significance if the number of patients and experiments were increased. Despite the increased mitochondrial fragmentation already discussed, our electron microscopy analysis revealed increased ER dilation in MS astrocytes, which has already been implicated as a feature of cellular stress and damage [109]. In this context, we analyzed the expression of genes related to the mitochondrial unfolded protein and integrated stress response pathways, that are key regulators of mitochondrial proteostasis, having usually protective outcomes to the cells, and observed a significant decrease in *ATF4*, *HSPA9*, *HSP60*, *LONP1* and *CLPP* genes. It has already been demonstrated that enhancing mitochondrial proteostasis has positive effects in Alzheimer's disease through delaying amyloid-β-induced proteotoxicity [110]. Mitochondrial UPR activation has already been shown in brain diseases [74] and its chronic activation can lead to cellular damage [111]. Here, we suggest that the activation of the protective machinery induced by the mitochondrial UPR and integrated stress response pathways is impaired in MS astrocytes and this leads to increased mitochondrial and cellular damage, although these mechanisms need to be explored in more details. In line with this, the expression of the mitochondrial protease CLPP, one of the key inducers of the mitochondrial integrated stress response, was found significantly downregulated in MS patients' lesions compared to controls [112].

Our flow analysis using Mitotracker suggested, although not significantly, an increased MFI of Mitotracker Green and Deep Red in MS astrocytes, which have been used as indicators of mitochondrial mass, in a $\Delta\psi$m-independent and dependent manner, respectively [64, 65]. Nevertheless, here we observed a disruption of the mitochondrial content in the MS astrocytes, as indicated by electron microscopy (Figure 10D) and qPCR

(Figure 12A) analysis. Therefore, taking in consideration all our findings in this study, here we suggest the interpretation of increased Mitotracker fluorescence as increased number of fragmented mitochondria, which are relatively smaller in shape and should therefore occupy a decreased area in MS astrocytes, and can mediate processes that culminate in mtDNA depletion [113], as observed.

As HIF-1α and PGC-1α have been implicated in the transcriptional regulation of mitochondrial dynamics and metabolism [55], we analyzed their expression in the astrocytes (Figure 16) and observed no meaningful differences between the groups. Although we did not analyze their protein levels, this suggests that there should be other upstream transcriptional regulators which can modify mitochondrial dynamics in the astrocytes. In this sense, our PCR array analysis demonstrated downregulation of *BCL-2*, which plays a role in the promotion of mitochondrial fusion [91-93] and might therefore explain the morphological changes in MS astrocytes' mitochondria observed here. When analyzing the metabolic profile of the cells we also observed a significant decrease in glucose levels in the MS astrocyte supernatant together with a slight increase in lactate, although not significant. Glucose is uptaken by cells through specific glucose transporters (GLUTs) and usually follow 3 different pathways: glycolysis, pentose-phosphate pathway and glycogenesis [53]. The glycolysis final product, pyruvate, can either be converted into lactate in the cytosol by lactate dehydrogenase or enter the mitochondria, where it is transformed in acetyl-CoA by pyruvate dehydrogenase and fuels the TCA cycle, resulting in increased OXPHOS and ATP production. Alternatively, one of the intermediary glycolytic products, glucose 6-phosphate, can enter the pentose-phosphate pathway, resulting in NADPH production or can be stored as glycogen, in this case specifically in astrocytes [53].

In this context, here we used the Seahorse technology to have insights on astrocyte utilization of the two-major energy-producing metabolic pathways in the cells, OXPHOS and glycolysis. Our OCR analysis using the Mitostress assay (Figure 17) first indicated increased non-mitochondrial OCR in MS astrocytes. This parameter has already been associated to inflammatory enzymes such as the NADPH oxidases, lipoxygenases and cyclo-oxygenases as well as with increased ROS, being therefore an indicator of damaged bioenergetics health in the cells [75]. Additionally, we observed an increased maximal OCR in MS astrocytes, which is suggestive of increased oxidative metabolism. In this

sense, increased Complex IV activity and oxidative stress markers levels were found increased specifically in astrocytes in lesions from MS patients, highlighting the several energy demanding processes played by these cells in disease pathology, which could explain the enhanced mitochondrial activity [82]. We also observed increases in the basal ECAR in MS astrocytes, which can be suggestive of increased glycolysis, since the assay medium already contained glucose, but without the addition of sodium bicarbonate. Finally, we observed a significant decrease in the Bioenergetic Health Index in MS astrocytes, which is suggestive of higher levels of unhealthy mitochondria. Accumulation of unhealthy mitochondria leads to increased superoxide formation and mtDNA damage [75]. Interestingly, we in fact observed in this study increased superoxide levels in MS astrocytes (Figure 14C) together with a decreased mitochondrial/nuclear DNA ratio (Figure 12A), corroborating these speculations.

When analyzing ECAR specifically through the Glycolysis stress test (Figure 18) we observed an increased non-glycolytic acidification in MS astrocytes, probably due to increased activity of the TCA cycle because of increased mitochondrial respiration, generating carbon dioxide molecules that can lead to acidification the medium or even by the increased proton leak suggested by the mitostress test analysis, which would lead to the same effects through the increased release of hydrogen protons [114]. We also observed a significant increase in the glycolytic reserve rate in MS astrocytes, which can be related to increased cell energy demands due to the several molecules produced by astrocytes during MS. Interestingly, the metabolic activity and levels of the glycolytic enzymes enolase and pyruvate-kinase was found increased in the cerebrospinal fluid of MS patients, together with higher levels of aldolase and lactate dehydrogenase [115]. In opposite direction, a more recent study [116] indicated the presence of Glyceraldehyde 3-phosphate dehydrogenase (GAPDH)-reactive antibodies in the cerebrospinal fluid of MS patients, which could inhibit GAPDH activity, having therefore direct implications for glycolysis as a preferential metabolic pathway to fuel brain resident cells during MS.

In terms of metabolic pathways related to MS, the TCA cycle associated proteins α-ketoglutarate [117, 118] and citrate [118] were a long time ago found to be increased in MS patients. Also, the levels of another TCA-related enzyme, aconitase, was also found to be upregulated in MS patients [119]. Regarding OXPHOS, decreased expression of the ATP synthase gene was already found in MS patients [120], together with increased

enzymatic activities of complexes I-V of the Electron Transport Chain [119]. Another study [81] found defects in proteins related to mitochondrial respiratory complex III, such as cytochrome c oxidase (COX) and COX-1. Altogether, these observations demonstrate that alterations in mitochondrial metabolism are correlated with MS pathology and here we could detect changes in mitochondrial function and metabolism using our hiPSC-derived astrocyte model, that mimicked several disease mechanisms and can therefore open new therapeutic avenues and drug-screening platforms for MS.

At the end, we analyzed RNA-seq data of hiPSC-derived astrocytes activated with TNF-α using bioinformatics to have further insights on mitochondrial metabolism and function in a more general context of human neuroinflammation, since this cytokine is altered in several neurologic diseases [78]. When performing biological processes enrichment analysis on the up and downregulated transcripts we found several terms related to mitochondria which were highlighted in figure 19B. Interestingly, in accordance with our findings for the MS astrocytes we found apoptotic mitochondrial changes, autophagy and mitochondrial fission enriched in the TNF-stimulated astrocytes, indicating that these mitochondrial dysfunction changes might be extended to astrocytes in the context of another brain diseases, which should be further validated. When analyzing specifically genes related to mitochondrial function (Figure 20A) we observed an upregulation of mitochondrial transporters from the SLC25 family in TNF-stimulated astrocytes, as we did for the MS-derived ones. Also, we observed increased expression of the mitochondrial SOD2 in this group, which suggests that superoxide mediated oxidative damage is also a cellular pathological mechanism upon TNF-stimulation, as it was demonstrated here for MS astrocytes. The *NDUFA5* gene, also found upregulated in TNF-stimulated astrocytes, is a part of the mitochondrial respiratory complex I, which suggests that increased oxidative metabolism can be triggered in human astrocytes in the contexts of inflammation. This is in line with our OCR findings for MS astrocytes as well as with the already mentioned studies indicating increased activity of the respiratory complexes in MS [119]. Also, the apoptosis mitochondria-related BCL-2 family genes BCL2, BCL2L1 and BBC3 were found upregulated in TNF-stimulated astrocytes, corroborating some of our findings for MS astrocytes. The $NAD^+$ase CD38, which has already been associated to the promotion of mitochondrial dysfunction [121], was also found upregulated in TNF-activated astrocytes. Among the downregulated genes in TNF-stimulated astrocytes we

found *NEFL*, whose disruption in cells has already been associated to the induction of mitochondrial fission [122]. We also found the gene *TAZ* downregulated in TNF-astrocytes, which is related to the mitochondrial transacylase Taffazin, a protein that is involved in the production of the phospholipid cardiolipin, a key component of the inner mitochondrial membrane [80]. Finally, the *BCS1L* gene, whose absence has been associated to mitochondrial respiratory complex III deficiency [123], was also found significantly downregulated in TNF-stimulated astrocytes. Interestingly, as mentioned before, deficiencies in this same complex have already been reported in MS patients [81].

Finally, we performed Gene-Set Enrichment Analysis (Figure 20B) to have insights on biological pathways that could be differentially regulated in TNF-astrocytes. We observed several enriched pathways related to: the regulation of intrinsic apoptosis in these cells; glutamate α-amino-3-hydroxy-5-methyl-4-isoxazolepropionic acid (AMPA) receptor activation, that has already been implicated in the promotion of mitochondrial fission [124]; SLC transporter disorder; negative regulation of the PI3K/AKT-network, a signaling pathway which has been associated to the induction of mitochondrial fusion [125] and suppression of BAX translocation to the mitochondria [126]; type I interferon antiviral responses, that have been already associated to metabolic shifts towards OXPHOS and β-oxidation in cells [127] and that can be triggered by the release and recognition of mitochondrial damage associated molecular patterns in the context of necroptosis for example, which has implications for neuroinflammation, since glial cells and neurons display type I interferon receptors, being able to amplify the inflammatory cascade within the CNS [80]. We highlighted two pathways found to be significantly repressed in TNF-stimulated astrocytes, which are DARPP32-mediated events, that have been related to, in association with BCL-2, the inhibition of apoptosis [128] and cell-cycle, which is tightly coupled to the regulation of mitochondrial fission through the cyclin B1–cyclin-dependent kinase (CDK), linking mitochondrial and nuclear division.

Interestingly, these findings in the transcriptome of hiPSC-derived astrocytes activated with TNF-α correlated with the ones found in MS derived astrocytes, indicating that neuroinflammatory processes can induce shared molecular mechanisms of disease in astrocytes. In this sense, here we provide several genes and pathways in astrocytes that could be further validated as therapeutical targets for neurologic diseases.

## 6. CONCLUSIONS

In summary, our findings indicate that:

- hiPSC-derived cells can be used as a reliable tool for MS studies;

- MS hiPSC-derived astrocytes mimic several disease features *in vitro*;

- MS hiPSC-derived astrocytes have increased oxidative stress;

- MS hiPSC-derived astrocytes have enhanced oxidative and glycolytic metabolism;

- MS hiPSC-derived astrocytes have increased mitochondrial fragmentation;

- MS hiPSC-derived astrocytes can have shared molecular disease mechanisms with other neurologic diseases;

- Since the balance between mitochondrial fusion and fission is a key process in the regulation of astrocyte metabolism, we propose that mitochondrial dynamics and metabolism in astrocytes can be targeted in future MS therapeutic approaches.

A summary of the findings of this study is shown below (Figure 21):

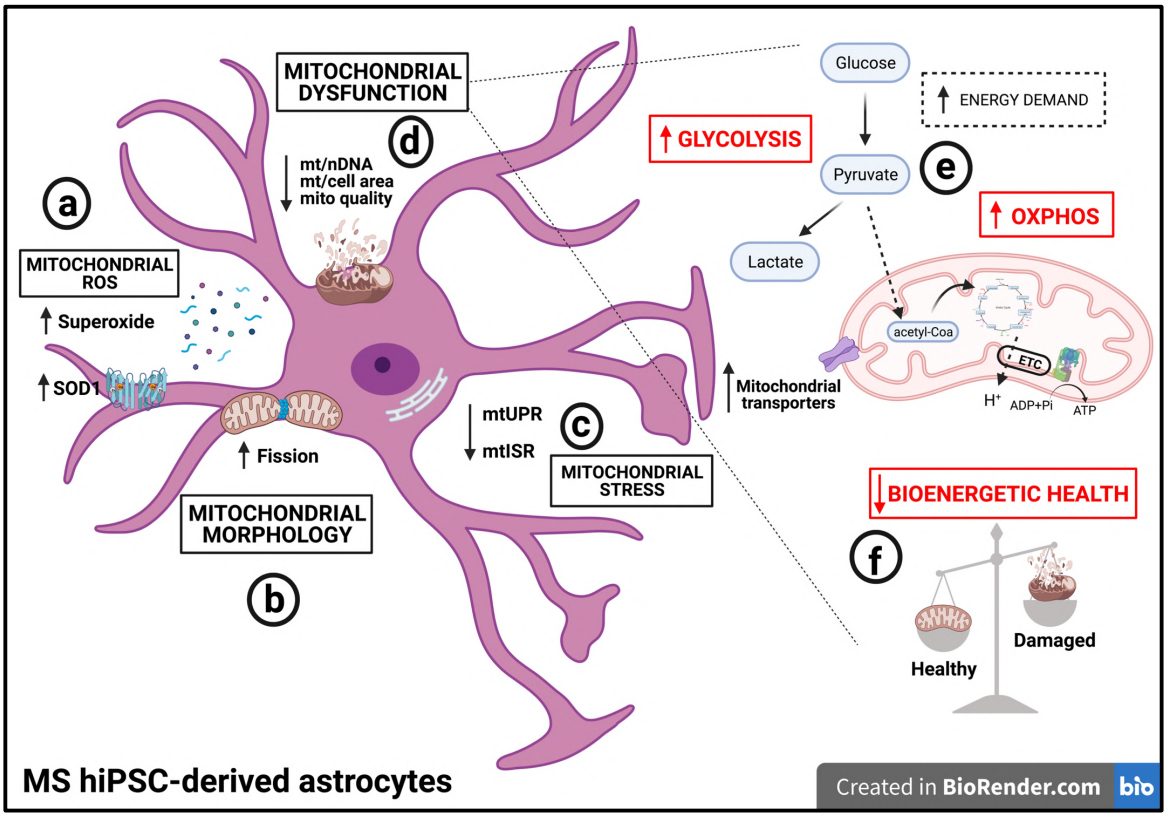


**Figure 21. Summary of study findings.** In this study we were able to successfully derive astrocytes from Multiple Sclerosis patients using the iPSC technology. When compared to controls, we observed in these cells changes in mitochondrial ROS, including increased superoxide production and SOD1 expression (**a**); changes in mitochondrial morphology (**b**), with increased mitochondrial fission; changes in mitochondrial stress (**c**), with a decreased expression of mtUPR and mtISR related genes, suggesting impaired activation of these protective pathways; mitochondrial dysfunction (**d**), with decreased mitochondrial/nuclear DNA ratio, mitochondrial/cell area ratio and mitochondrial quality. This mitochondrial dysfunction could be demonstrated in metabolic alterations, with enhanced glycolysis and OXPHOS in MS astrocytes, as well as increased expression of mitochondrial transporters, suggesting higher energy demands in these cells (**e**). It also was characterized by a reduced cell bioenergetic health with increased mitochondrial damage (**f**). SOD1 – superoxide dismutase 1; mtUPR – mitochondrial Unfolded Protein Response; mtISR – mitochondrial integrated stress response; mt/nDNA – mitochondrial to nuclear DNA ratio; mt/cell area – mitochondrial to cell area; mito quality – mitochondrial quality; ETC – electron transport chain; Pi – inorganic phosphate. The figure was generated using the Biorender software.

## 7. BIBLIOGRAPHIC REFERENCES


1. Reich, D.S., C.F. Lucchinetti, and P.A. Calabresi, Multiple Sclerosis. N Engl J Med, 2018. **378**(2): p. 169-180.

2. da Gama Pereira, A.B., et al., Prevalence of multiple sclerosis in Brazil: A systematic review. Mult Scler Relat Disord, 2015. **4**(6): p. 572-9.

3. Dendrou, C.A., Fugger, L. and Friese M.A., Immunopathology of multiple sclerosis. Nature Reviews Immunology, 2015. **15**(9): p. 545-58.

4. Thompson, A.J., et al., Multiple sclerosis. Lancet, 2018. **391**(10130): p. 1622-1636.

5. Trapp, B.D. and K.A. Nave, Multiple sclerosis: an immune or neurodegenerative disorder? Annu Rev Neurosci, 2008. **31**: p. 247-69.

6. Soares J.L.S., Oliveira, E.M.L. and Pontillo, A. Variants in NLRP3 and NLRC4 inflammasome associate with susceptibility and severity of multiple sclerosis. Multiple Sclerosis and Related Disorders, 2019. **29**: p. 26-34.

7. Raine, C.S., Multiple sclerosis: immune system molecule expression in the central nervous system. J Neuropathol Exp Neurol, 1994. **53**(4): p. 328-37.

8. Louveau, A., et al., CNS lymphatic drainage and neuroinflammation are regulated by meningeal lymphatic vasculature. Nat Neurosci, 2018. **21**(10): p. 1380-1391.

9. Van Der Voorn, P., et al., Expression of MCP-1 by reactive astrocytes in demyelinating multiple sclerosis lesions. Am J Pathol, 1999. **154**(1): p. 45-51.

10. Krumbholz, M., et al., BAFF is produced by astrocytes and up-regulated in multiple sclerosis lesions and primary central nervous system lymphoma. J Exp Med, 2005. **201**(2): p. 195-200.

11. The IFNβ Multiple Sclerosis Study Group. Interferon beta-1b is effective in relapsing–remitting multiple sclerosis. I. Clinical results of a multicenter, randomized, double-blind, placebo-controlled trial. Neurology, 1993. **43**: p.655–661.

12. Jacobs, L. D. et al. Intramuscular interferon beta-1a for disease progression in relapsing multiple sclerosis. Ann. Neurol. , 1996. **39**: p.285–294.

13. Johnson, K. P. et al. Copolymer 1 reduces relapse rate and improves disability in relapsing–remitting multiple sclerosis: results of a phase III multicenter, double-blind placebo-controlled trial. Neurology, 1995. **45**: p.1268–1276.

14. Sheremata, W. A. et al. A safety and pharmacokinetic study of intravenous natalizumab in patients with MS. Neurology, 1999. **52**: p. 1072–1074 .

15. Miller, D. H. et al. A controlled trial of natalizumab for relapsing multiple sclerosis. N. Engl. J. Med., 2003. **348**: p.15–23.

16. Langer-Gould, A. et al. Progressive multifocal leukoencephalopathy in a patient treated with natalizumab. N. Engl. J. Med., 2005. **353**: p.375–381.

17. Polman, C. H. et al. A randomized, placebo-controlled trial of natalizumab for relapsing multiple sclerosis. N. Engl. J. Med., 2006. **354**: p.899–910.

18. Kappos, L. et al. A placebo-controlled trial of oral fingolimod in relapsing multiple sclerosis. N. Engl. J. Med., 2010. **362**: p.387–401.

19. O'Connor, P. et al. Randomized trial of oral teriflunamide for relapsing multiple sclerosis. N. Engl. J. Med., 2011. **365**: p.1293–1303.

20. Gold, R. et al. Placebo-controlled phase 3 study of oral BG-12 for relapsing multiple sclerosis. N. Engl. J. Med., 2012. **367**: p.1098–1107.

21. Giovannoni, G. et al. A placebo-controlled trial of oral cladribine for relapsing multiple sclerosis. N. Engl. J. Med., 2010. **362**: p.416–426.

22. Hauser, S. L. et al. B-cell depletion with rituximab in relapsing–remitting multiple sclerosis. N. Engl. J. Med., 2008. **358**: p.676–688.

23. Hauser, S. L. et al. Ocrelizumab versus interferon beta-1a in relapsing multiple sclerosis. N. Engl. J. Med., 2017. **376**: p.221–234.

24. Atkins, H. L. et al. Immunoablation and autologous haematopoietic stem-cell transplantation for aggressive multiple sclerosis: a multicentre single-group phase 2 trial. Lancet , 2016. **388**: p.576–585.

25. Kappos, L. et al. Siponimod versus placebo in secondary progressive multiple sclerosis (EXPAND): a double-blind, randomised, phase 3 study. Lancet, 2018. **391**: p.1263–1273.

26. Xie YZ, Zhang RX. Neurodegenerative diseases in a dish: the promise of iPSC technology in disease modeling and therapeutic discovery. Neurol Sci., 2015. **36**(1): p.21–27.

27. Li L, Chao J, Shi Y. Modeling neurological diseases using iPSC-derived neural cells : iPSC modeling of neurological diseases. Cell Tissue Res. 2018;**371**(1):p.143-151.

28. Kang X, Yu Q, Huang Y, et al. Effects of Integrating and Non-Integrating Reprogramming Methods on Copy Number Variation and Genomic Stability of Human Induced Pluripotent Stem Cells. PLoS One. 2015;10(7):e0131128. Published 2015 Jul 1. doi:10.1371/journal.pone.0131128

29. Wang H. Modeling Neurological Diseases With Human Brain Organoids. Front Synaptic Neurosci. 2018;10:15.

30. Suga M, Kondo T, Inoue H. Modeling Neurological Disorders with Human Pluripotent Stem Cell-Derived Astrocytes. Int J Mol Sci., 2019. **20**(16):3862.

31. Di Ruscio, A., Patti, F., Welner, R. et al. Multiple sclerosis: getting personal with induced pluripotent stem cells. Cell Death Dis, 2015. **6:** e1806.

32. Orack JC, Deleidi M, Pitt D, et al. Modeling Multiple Sclerosis with Stem Cell Biological Platforms: Toward functional validation of cellular and molecular phenotypes. Stem Cells Transl Med. 2015 Jan 15.

33. Brennand KJ, Simone A, Jou J, et al. Modelling schizophrenia using human induced pluripotent stem cells [published correction appears in Nature. 2011 Nov 24;479(7374):556].

34 Israel MA, Yuan SH, Bardy C, et al. Probing sporadic and familial Alzheimer's disease using induced pluripotent stem cells. Nature. 2012;482(7384):216-220. Published 2012 Jan 25. doi:10.1038/nature10821

35 Sánchez-Danés A, Richaud-Patin Y, Carballo-Carbajal I, et al. Disease-specific phenotypes in dopamine neurons from human iPS-based models of genetic and sporadic Parkinson's disease. EMBO Mol Med. 2012;4(5):380-395.

36 Fujimori, K., Ishikawa, M., Otomo, A. et al. Modeling sporadic ALS in iPSC-derived motor neurons identifies a potential therapeutic agent. Nat Med 24, 1579–1589 (2018).

37 Song B, Sun G, Herszfeld D et al. Neural differentiation of patient specific iPS cells as a novel approach to study the pathophysiology of multiple sclerosis, Stem Cell Research, Volume 8, Issue 2, 2012, Pages 259-273.

38 Douvaras P, Wang J, Zimmer M et al. Efficient generation of myelinating oligoden-drocytes from primary progressive multiplesclerosis patients by induced pluripotent stemcells. Stem Cell Reports 2014;3:250–259.

39 Nicaise A, Wagstaff L, Willis C, et al. Cellular senescence in progenitor cells contributes to diminished remyelination potential in progressive multiple sclerosis. Proceedings of the National Academy of Sciences Apr 2019, 116 (18)

40 Perriot S et al. Human Induced Pluripotent Stem Cell-Derived Astrocytes Are Differentially Activated by Multiple Sclerosis-Associated Cytokines. Stem Cell Reports 2018, Volume 11, Issue 5, 1199 – 1210.

41 Ponath, G., Lincoln, M.R., Levine-Ritterman, M. et al. Enhanced astrocyte responses are driven by a genetic risk allele associated with multiple sclerosis. Nat Commun 9, 5337 (2018).

42 Cheung, G., et al., Activity-Dependent Plasticity of Astroglial Potassium and Glutamate Clearance. Neural Plast, 2015. **2015**: p. 109106.

43 Ponath, G., C. Park, and D. Pitt, The Role of Astrocytes in Multiple Sclerosis. Front Immunol, 2018. **9**: p. 217.

44 Halassa, M.M., T. Fellin, and P.G. Haydon, The tripartite synapse: roles for gliotransmission in health and disease. Trends Mol Med, 2007. **13**(2): p. 54-63.

45 Wheeler, M.A. and F.J. Quintana, Regulation of Astrocyte Functions in Multiple Sclerosis. Cold Spring Harb Perspect Med, 2018.

46 Chao, C.C., Gutiérrez-Vazquez, C., Rothhammer, V., et al. Metabolic Control of Astrocyte Pathogenic Activity via cPLA2-MAVS. Cell, 2019. 179 (7): p. 1483-1498.

47 Wheeler, M.A., Clark, I.C., Tjon, E.C. et al. MAFG-driven astrocytes promote CNS inflammation. Nature, 2020. **578**: p.593–599.

48 Witte, M.E., et al., Mitochondrial dysfunction contributes to neurodegeneration in multiple sclerosis. Trends Mol Med, 2014. **20**(3): p. 179-87.

49. Su, K., D. Bourdette, and M. Forte, Mitochondrial dysfunction and neurodegeneration in multiple sclerosis. Front Physiol, 2013. **4**: p. 169.

50 Cha, M.Y., D.K. Kim, and I. Mook-Jung, The role of mitochondrial DNA mutation on neurodegenerative diseases. Exp Mol Med, 2015. **47**: p. e150.

51 Howell, N., et al., mtDNA mutations and common neurodegenerative disorders. Trends Genet, 2005. **21**(11): p. 583-6.

52 Mills EL, Kelly B, O'Neill LAJ. Mitochondria are the powerhouses of immunity. Nature Immunology 2017; **18**(5): p. 488-498.

53 Belanger, M., I. Allaman, and P.J. Magistretti, Brain energy metabolism: focus on astrocyte-neuron metabolic cooperation. Cell Metab, 2011. **14**(6): p. 724-38.

54 Rambold, A.S. and E.L. Pearce, Mitochondrial Dynamics at the Interface of Immune Cell Metabolism and Function. Trends Immunol, 2018. **39**(1): p. 6-18.

55 Archer, SL. Mitochondrial Dynamics – Mitochondrial Fission and Fusion in Human Diseases. N Engl J Med 2013; 369:2236-2251

56 Róna-Vörös K, Weydt P. The role of PGC-1α in the pathogenesis of neurodegenerative disorders. Curr Drug Targets. 2010 Oct;11(10):1262-9.

57 Zhang Z, Yan J, Chang Y, ShiDu Yan S, Shi H. Hypoxia inducible factor-1 as a target for neurodegenerative diseases. Curr Med Chem. 2011;18(28):4335-4343.

58 Kowaltowski AJ, Menezes-Filho SL, Assali EA et al. Mitochondrial morphology regulates organellar Ca2+ uptake and changes cellular Ca2+ homeostasis. FASEB Journal 2019; 33: p.1-13.

59 Draheim, T., Liessem, A., Scheld, M., et al. Activation of the astrocytic Nrf2/ARE system ameliorates the formation of demyelinating lesions in a multiple sclerosis animal model. Glia, 2016. 64: p.2219-2230.

60 Motori, E., et al., Inflammation-induced alteration of astrocyte mitochondrial dynamics requires autophagy for mitochondrial network maintenance. Cell Metab, 2013. **18**(6): p. 844-59.

61. Schouten JP, et al. Relative quantification of 40 nucleic acid sequences by multiplex ligation-dependent probe amplification, Nucleic Acids Research, Volume 30, Issue 12, 15 June 2002.

62 Chen EY, Tan CM, Kou Y, Duan Q, Wang Z, Meirelles GV, Clark NR, Ma'ayan A. Enrichr: interactive and collaborative HTML5 gene list enrichment analysis tool. BMC Bioinformatics. 2013;128(14).

63 Kuleshov MV, Jones MR, Rouillard AD, Fernandez NF, Duan Q, Wang Z, Koplev S, Jenkins SL, Jagodnik KM, Lachmann A, McDermott MG, Monteiro CD, Gundersen GW, Ma'ayan A. Enrichr: a comprehensive gene set enrichment analysis web server 2016 update. Nucleic Acids Research 2016.

64 Xiao B, Deng X, Zhou W and Tan E-K (2016) Flow Cytometry-Based Assessment of Mitophagy Using MitoTracker. Front. Cell. Neurosci. 10:76.

65 Brookens, S. K., Cho, S. H., Basso, P. J., & Boothby, M. R. AMPKα1 in B Cells Dampens Primary Antibody Responses yet Promotes Mitochondrial Homeostasis and Persistence of B Cell Memory. The Journal of Immunology 2020.

66 Lendahl U, Zimmerman LB, McKay RD. CNS stem cells express a new class of intermediate filament protein. Cell. 1990 Feb 23;60(4):585-95.

67 Soubannier V, Maussion G, Chaineau M, et al. Characterization of human iPSC-derived astrocytes with potential for disease modeling and drug discovery. Neuroscience Letters, Volume 731, 135028, 2020.

68 Trindade, P, Loiola, EC, Gasparotto, J, et al. Short and long TNF-alpha exposure recapitulates canonical astrogliosis events in human-induced pluripotent stem cells-derived astrocytes. Glia. 2020; 68: 1396– 1409.

69 Joshi, A.U., Minhas, P.S., Liddelow, S.A. et al. Fragmented mitochondria released from microglia trigger A1 astrocytic response and propagate inflammatory neurodegeneration. Nat Neurosci 22, 1635–1648 (2019).

70 Chavez-Valdez R, Flock DL, Martin LJ, Northington FJ. Endoplasmic reticulum pathology and stress response in neurons precede programmed necrosis after neonatal hypoxia-ischemia. Int J Dev Neurosci. 2016;48:58-70.

71 Anderson N, et al. Folding the Mitochondrial UPR into the Integrated Stress Response. Trends in Cell Biology, Volume 30, Issue 6, 428 – 439

72 Moehle EA, Shen K, Dillin A. Mitochondrial proteostasis in the context of cellular and organismal health and aging. J Biol Chem. 2019;294(14):5396-5407.

73 Pérez, M.J., Ivanyuk, D., Panagiotakopoulou, V. et al. Loss of function of the mitochondrial peptidase PITRM1 induces proteotoxic stress and Alzheimer's disease-like pathology in human cerebral organoids. Mol Psychiatry (2020).

74 Pellegrino MW, Haynes CM. Mitophagy and the mitochondrial unfolded protein response in neurodegeneration and bacterial infection. BMC Biol. 2015;13:22.

75 Chacko BK, Kramer PA, Ravi S, et al. The Bioenergetic Health Index: a new concept in mitochondrial translational research. Clin Sci (Lond). 2014;127(6):367-373.

76 Chacko BK, Zhi D, Darley-Usmar VM, Mitchell T. The Bioenergetic Health Index is a sensitive measure of oxidative stress in human monocytes. Redox Biol. 2016;8:43-50.

77 Rentzos, M., Nikolaou, C., Rombos, A. et al. Tumour necrosis factor alpha is elevated in serum and cerebrospinal fluid in multiple sclerosis and inflammatory neuropathies. J Neurol 243, 165–170 (1996).

78 Frankola KA, Greig NH, Luo W, Tweedie D. Targeting TNF-α to elucidate and ameliorate neuroinflammation in neurodegenerative diseases. CNS Neurol Disord Drug Targets. 2011;10(3):391-403. doi:10.2174/187152711794653751

79 Cabral-Costa JV and Kowaltowski AJ. Neurologic disorders and mitochondria. Molecular Aspects of Medicine, volume 71, 100826 (2020).

80 de Oliveira LG, Angelo YdS, Iglesias AH and Peron JPS (2021). Unraveling the Link Between Mitochondrial Dynamics and Neuroinflammation. Front. Immunol. 12:624919.

81 Mahad D, Ziabreva I, Lassmann H, Turnbull D. Mitochondrial defects in acute multiple sclerosis lesions. Brain. 2008 Jul;131(Pt 7):1722-35.

82 Witte ME, Bø L, Rodenburg RJ, Belien JA, Musters R, Hazes T, Wintjes LT, Smeitink JA, Geurts JJ, De Vries HE, van der Valk P, van Horssen J. Enhanced number and activity of mitochondria in multiple sclerosis lesions. J Pathol. 2009 Oct;219(2):193-204.

83 Wentling M, Lopez-Gomez C, Park HJ, Amatruda M, Ntranos A, Aramini J, Petracca M, Rusielewicz T, Chen E, Tolstikov V, Kiebish M, Fossati V, Inglese M, Quinzii CM, Katz Sand I, Casaccia P. A metabolic perspective on CSF-mediated neurodegeneration in multiple sclerosis. Brain. 2019 Sep 1;142(9):2756-2774.

84 Sun S, Tang Y, Lou X, et al. UXT is a novel and essential cofactor in the NF-kappaB transcriptional enhanceosome. J Cell Biol. 2007;178(2):231-244.

85 Robb, JL, Hammad, NA, Weightman Potter, PG, Chilton, JK, Beall, C, Ellacott, KLJ. The metabolic response to inflammation in astrocytes is regulated by nuclear factor-kappa B signaling. Glia. 2020; 68: 2246– 2263.

86 De Vos K, Goossens V, Boone E, et al. The 55-kDa tumor necrosis factor receptor induces clustering of mitochondria through its membrane-proximal region. J. Biol. Chem. 1998;273:9673–9680.

87 Thomas WD, Zhang XD, Franco AV, et al. TNF-related apoptosis-inducing ligand-induced apoptosis of melanoma is associated with changes in mitochondrial membrane potential and perinuclear clustering of mitochondria. J. Immunol. 2000;165:5612–5620.

88 Moss TN, Vo A, McKeehan WL, Liu L. UXT (Ubiquitously Expressed Transcript) causes mitochondrial aggregation. In Vitro Cell Dev Biol Anim. 2007;43(3-4):139-146. doi:10.1007/s11626-007-9016-6

89 Babenko, V.N., Smagin, D.A., Galyamina, A.G. et al. Altered Slc25 family gene expression as markers of mitochondrial dysfunction in brain regions under experimental mixed anxiety/depression-like disorder. BMC Neurosci 19, 79 (2018).

90 Macco, R., Pelizzoni, I., Consonni, A. et al. Astrocytes acquire resistance to iron-dependent oxidative stress upon proinflammatory activation. J Neuroinflammation 10, 897 (2013).

91 Delivani P, Adrain C, Taylor RC, Duriez PJ, Martin SJ. Role for CED-9 and Egl-1 as regulators of mitochondrial fission and fusion dynamics. Mol Cell. 2006 Mar 17;21(6):761-73.

92 Rolland SG, Conradt B. New role of the BCL2 family of proteins in the regulation of mitochondrial dynamics. Curr Opin Cell Biol. 2010;22(6):852-858.

93 Sheridan C, Delivani P, Cullen SP, Martin SJ. Bax- or Bak-induced mitochondrial fission can be uncoupled from cytochrome C release. Mol Cell. 2008 Aug 22;31(4):570-85.

94 Garrido, C., Galluzzi, L., Brunet, M. et al. Mechanisms of cytochrome c release from mitochondria. Cell Death Differ 13, 1423–1433 (2006).

95 Takahashi, Y., Meyerkord, C. & Wang, HG. Bif-1/Endophilin B1: a candidate for crescent driving force in autophagy. Cell Death Differ 16, 947–955 (2009).

96 Karbowski M, Jeong SY, Youle RJ. Endophilin B1 is required for the maintenance of mitochondrial morphology. J Cell Biol. 2004 Sep 27;166(7):1027-39.

97 Sokol AM, Sztolsztener ME, Wasilewski M, Heinz E, Chacinska A. Mitochondrial protein translocases for survival and wellbeing. FEBS Lett. 2014 Aug 1;588(15):2484-95.

98 Srivastava S, Savanur MA, Sinha D, et al. Regulation of mitochondrial protein import by the nucleotide exchange factors GrpEL1 and GrpEL2 in human cells. J Biol Chem. 2017;292(44):18075-18090.

99 Burri L, Strahm Y, Hawkins CJ, et al. Mature DIABLO/Smac is produced by the IMP protease complex on the mitochondrial inner membrane. Mol Biol Cell. 2005;16(6):2926-2933. doi:10.1091/mbc.e04-12-1086

100 Alonzo JR, Venkataraman C, Field MS, Stover PJ. The mitochondrial inner membrane protein MPV17 prevents uracil accumulation in mitochondrial DNA. J Biol Chem. 2018;293(52):20285-20294.

101 Patergnani S, Castellazzi M, Bonora M, et al. Autophagy and mitophagy elements are increased in body fluids of multiple sclerosis-affected individuals. Journal of Neurology, Neurosurgery & Psychiatry 2018;89:439-441.

102 Castellazzi M, Patergnani S, Donadio M, et al. Correlation between auto/mitophagic processes and magnetic resonance imaging activity in multiple sclerosis patients. J Neuroinflammation. 2019;16(1):131. Published 2019 Jun 27.

103 Shai, N., Yifrach, E., van Roermund, C.W.T. et al. Systematic mapping of contact sites reveals tethers and a function for the peroxisome-mitochondria contact. Nat Commun 9, 1761 (2018).

104 Fransen M, Nordgren M, Wang B, Apanasets O. Role of peroxisomes in ROS/RNS-metabolism: implications for human disease. Biochim Biophys Acta. 2012 Sep;1822(9):1363-73.

105 Ofengeim D, Ito Y, Najafov A, et al. Activation of necroptosis in multiple sclerosis. Cell Rep. 2015;10(11):1836-1849.

106 Sadeghian, M., Mastrolia, V., Rezaei Haddad, A. et al. Mitochondrial dysfunction is

an important cause of neurological deficits in an inflammatory model of multiple sclerosis. Sci Rep 6, 33249 (2016).

107 Haile Y, Deng X, Ortiz-Sandoval C, et al. Rab32 connects ER stress to mitochondrial defects in multiple sclerosis. J Neuroinflammation. 2017;14(1):19. Published 2017 Jan 23.

108 Jadiya, P., Kolmetzky, D.W., Tomar, D. et al. Impaired mitochondrial calcium efflux contributes to disease progression in models of Alzheimer's disease. Nat Commun 10, 3885 (2019).

109 Chavez-Valdez R, Flock DL, Martin LJ, Northington FJ. Endoplasmic reticulum pathology and stress response in neurons precede programmed necrosis after neonatal hypoxia-ischemia. Int J Dev Neurosci. 2016;48:58-70.

110 Sorrentino, V., Romani, M., Mouchiroud, L. et al. Enhancing mitochondrial proteostasis reduces amyloid-β proteotoxicity. Nature 552, 187–193 (2017).

111 Anderson CJ, Bredvik K, Burstein SR, et al. ALS/FTD mutant CHCHD10 mice reveal a tissue-specific toxic gain-of-function and mitochondrial stress response. Acta Neuropathol. 2019;138(1):103-121.

112 Fischer MT, Sharma R, Lim JL, et al. NADPH oxidase expression in active multiple sclerosis lesions in relation to oxidative tissue damage and mitochondrial injury. Brain. 2012;135(Pt 3):886-899.

113 Kondadi AK, Anand R, Reichert AS. Functional Interplay between Cristae Biogenesis, Mitochondrial Dynamics and Mitochondrial DNA Integrity. International Journal of Molecular Sciences. 2019; 20(17):4311.

114 Pike Winer LS, Wu M. Rapid analysis of glycolytic and oxidative substrate flux of cancer cells in a microplate. PLoS One. 2014;9(10):e109916.

115 Royds JA, Timperley WR, Taylor CB. Levels of enolase and other enzymes in the cerebrospinal fluid as indices of pathological change. J Neurol Neurosurg Psychiat (1981) 44:1129–35.

116 Kölln J, Zhang Y, Thai G, Demetriou M, Hermanowicz N, Duquette P, et al. Inhibition of glyceraldehyde-3-phosphate dehydrogenase activity by antibodies present in

the cerebrospinal fluid of patients with multiple sclerosis. J Immunol (2010) 185:1968–75.

117 McArdle B, Mackenzie ICK, Webster GR. Studies on intermediate carbohydrate metabolism in multiple sclerosis. J Neurol Neurosurg Psychiat (1960) 23:127.

118 Henneman DH, Altschule MD, Goncz RM, Alexander L. Carbohydrate metabolism in brain disease. I. Glucose metabolism in multiple sclerosis. A.M.A. Arch. Neurol. Psychiat. (1954) 72(6):688–95.

119 Iñarrea P, Alarcia R, Alava MA, Capablo JL, Casanova A, Iñiguez C, et al. Mitochondrial complex enzyme activities and cytochrome c expression changes in multiple sclerosis. Mol Neurobiol (2014) 49(1):1–9.

120 Smith KJ, Lassmann H. The role of nitric oxide in multiple sclerosis. Lancet Neurol (2002) 1(4):232–41.

121 Camacho-Pereira J, Tarragó MG, Chini CCS, et al. CD38 Dictates Age-Related NAD Decline and Mitochondrial Dysfunction through an SIRT3-Dependent Mechanism. Cell Metab. 2016;23(6):1127-1139.

122 Tradewell ML, Durham HD, Mushynski WE, Gentil BJ. Mitochondrial and axonal abnormalities precede disruption of the neurofilament network in a model of charcot-marie-tooth disease type 2E and are prevented by heat shock proteins in a mutant-specific fashion. J Neuropathol Exp Neurol. 2009 Jun;68(6):642-52.

123 Tegelberg, S., Tomašić, N., Kallijärvi, J. et al. Respiratory chain complex III deficiency due to mutated BCS1L: a novel phenotype with encephalomyopathy, partially phenocopied in a Bcs1l mutant mouse model. Orphanet J Rare Dis 12, 73 (2017).

124 Ruiz, A., Alberdi, E., and Matute, C. (2018). Mitochondrial division inhibitor 1 (mdivi-1) protects neurons against excitotoxicity through the modulation of mitochondrial function and intracellular Ca2+ Signaling. Front. Mol. Neurosci. 11:3.

125 Sabouny R, Shutt TE. Reciprocal Regulation of Mitochondrial Fission and Fusion. Trends Biochem Sci. 2020 Jul;45(7):564-577.

126 Tsuruta F, Masuyama N, Gotoh Y. The phosphatidylinositol 3-kinase (PI3K)-Akt

pathway suppresses Bax translocation to mitochondria. J Biol Chem. 2002 Apr 19;277(16):14040-7.

127 Wu D, Sanin DE, Everts B, Chen Q, Qiu J, Buck MD, et al. Type 1 Interferons Induce Changes in Core Metabolism that Are Critical for Immune Function. Immunity (2016) 44:1325–36.

128 Chang MJ, Zhong F, Lavik AR, Parys JB, Berridge MJ, Distelhorst CW. Feedback regulation mediated by Bcl-2 and DARPP-32 regulates inositol 1,4,5-trisphosphate receptor phosphorylation and promotes cell survival. Proc Natl Acad Sci U S A. 2014 Jan 21;111(3):1186-91.

**SUPPLEMENTARY DATA**

## Supplementary table 1. Genes contained in Human Mitochondria PCR array

| Gen Bank | Symbol | Description |
|---|---|---|
| NM_032797 | *AIFM2* | Apoptosis-inducing factor, mitochondrion-associated, 2 |
| NM_003977 | *AIP* | Aryl hydrocarbon receptor interacting protein |
| NM_001188 | *BAK1* | BCL2-antagonist/killer 1 |
| NM_014417 | *BBC3* | BCL2 binding component 3 |
| NM_000633 | *BCL2* | B-cell CLL/lymphoma 2 |
| NM_138578 | *BCL2L1* | BCL2-like 1 |
| NM_001196 | *BID* | BH3 interacting domain death agonist |
| NM_004052 | *BNIP3* | BCL2/adenovirus E1B 19kDa interacting protein 3 |
| NM_000077 | *CDKN2A* | Cyclin-dependent kinase inhibitor 2A (melanoma, p16, inhibits CDK4) |
| NM_001303 | *COX10* | COX10 homolog, cytochrome c oxidase assembly protein, heme A: farnesyltransferase (yeast) |
| NM_173827 | *COX18* | COX18 cytochrome c oxidase assembly homolog (S. cerevisiae) |
| NM_004377 | *CPT1B* | Carnitine palmitoyltransferase 1B (muscle) |
| NM_000098 | *CPT2* | Carnitine palmitoyltransferase 2 |
| NM_005690 | *DNM1L* | Dynamin 1-like |
| NM_016068 | *FIS1* | Fission 1 (mitochondrial outer membrane) homolog (S. cerevisiae) |
| NM_012192 | *FXC1* | Fracture callus 1 homolog (rat) |
| NM_025196 | *GRPEL1* | GrpE-like 1, mitochondrial (E. coli) |
| NM_001017963 | *HSP90AA1* | Heat shock protein 90kDa alpha (cytosolic), class A member 1 |
| NM_002156 | *HSPD1* | Heat shock 60kDa protein 1 (chaperonin) |
| NM_144981 | *IMMP1L* | IMP1 inner mitochondrial membrane peptidase-like (S. cerevisiae) |
| NM_032549 | *IMMP2L* | IMP2 inner mitochondrial membrane peptidase-like (S. cerevisiae) |
| NM_133259 | *LRPPRC* | Leucine-rich PPR-motif containing |
| NM_033540 | *MFN1* | Mitofusin 1 |
| NM_014874 | *MFN2* | Mitofusin 2 |
| NM_005932 | *MIPEP* | Mitochondrial intermediate peptidase |
| NM_002437 | *MPV17* | MpV17 mitochondrial inner membrane protein |
| NM_018116 | *MSTO1* | Misato homolog 1 (Drosophila) |
| NM_006554 | *MTX2* | Metaxin 2 |
| NM_006158 | *NEFL* | Neurofilament, light polypeptide |
| NM_130837 | *OPA1* | Optic atrophy 1 (autosomal dominant) |
| NM_021127 | *PMAIP1* | Phorbol-12-myristate-13-acetate-induced protein 1 |
| NM_018307 | *RHOT1* | Ras homolog gene family, member T1 |
| NM_138769 | *RHOT2* | Ras homolog gene family, member T2 |
| NM_006142 | *SFN* | Stratifin |
| NM_016009 | *SH3GLB1* | SH3-domain GRB2-like endophilin B1 |
| NM_005984 | *SLC25A1* | Solute carrier family 25 (mitochondrial carrier; citrate transporter), member 1 |
| NM_012140 | *SLC25A10* | Solute carrier family 25 (mitochondrial carrier; dicarboxylate transporter), member 10 |
| NM_003705 | *SLC25A12* | Solute carrier family 25 (mitochondrial carrier, Aralar), member 12 |
| NM_014251 | *SLC25A13* | Solute carrier family 25, member 13 (citrin) |
| NM_003951 | *SLC25A14* | Solute carrier family 25 (mitochondrial carrier, brain), member 14 |
| NM_014252 | *SLC25A15* | Solute carrier family 25 (mitochondrial carrier; ornithine transporter) member 15 |
| NM_152707 | *SLC25A16* | Solute carrier family 25 (mitochondrial carrier; Graves disease autoantigen), member 16 |
| NM_006358 | *SLC25A17* | Solute carrier family 25 (mitochondrial carrier; peroxisomal membrane protein, 34kDa), member 17 |
| NM_021734 | *SLC25A19* | Solute carrier family 25 (mitochondrial thiamine pyrophosphate carrier), member 19 |
| NM_031947 | *SLC25A2* | Solute carrier family 25 (mitochondrial carrier; ornithine transporter) member 2 |
| NM_000387 | *SLC25A20* | Solute carrier family 25 (carnitine/acylcarnitine translocase), member 20 |
| NM_030631 | *SLC25A21* | Solute carrier family 25 (mitochondrial oxodicarboxylate carrier), member 21 |
| NM_024698 | *SLC25A22* | Solute carrier family 25 (mitochondrial carrier: glutamate), member 22 |

| | | |
|---|---|---|
| NM_024103 | *SLC25A23* | Solute carrier family 25 (mitochondrial carrier; phosphate carrier), member 23 |
| NM_013386 | *SLC25A24* | Solute carrier family 25 (mitochondrial carrier; phosphate carrier), member 24 |
| NM_052901 | *SLC25A25* | Solute carrier family 25 (mitochondrial carrier; phosphate carrier), member 25 |
| NM_004277 | *SLC25A27* | Solute carrier family 25, member 27 |
| NM_002635 | *SLC25A3* | Solute carrier family 25 (mitochondrial carrier; phosphate carrier), member 3 |
| NM_001010875 | *SLC25A30* | Solute carrier family 25, member 30 |
| NM_031291 | *SLC25A31* | Solute carrier family 25 (mitochondrial carrier; adenine nucleotide translocator), member 31 |
| NM_016612 | *SLC25A37* | Solute carrier family 25, member 37 |
| NM_001151 | *SLC25A4* | Solute carrier family 25 (mitochondrial carrier; adenine nucleotide translocator), member 4 |
| NM_001152 | *SLC25A5* | Solute carrier family 25 (mitochondrial carrier; adenine nucleotide translocator), member 5 |
| NM_000454 | *SOD1* | Superoxide dismutase 1, soluble |
| NM_000636 | *SOD2* | Superoxide dismutase 2, mitochondrial |
| NM_006804 | *STARD3* | StAR-related lipid transfer (START) domain containing 3 |
| NM_000116 | *TAZ* | Tafazzin |
| NM_012456 | *TIMM10* | Translocase of inner mitochondrial membrane 10 homolog (yeast) |
| NM_006335 | *TIMM17A* | Translocase of inner mitochondrial membrane 17 homolog A (yeast) |
| NM_005834 | *TIMM17B* | Translocase of inner mitochondrial membrane 17 homolog B (yeast) |
| NM_013337 | *TIMM22* | Translocase of inner mitochondrial membrane 22 homolog (yeast) |
| NM_006327 | *TIMM23* | Translocase of inner mitochondrial membrane 23 homolog (yeast) |
| NM_006351 | *TIMM44* | Translocase of inner mitochondrial membrane 44 homolog (yeast) |
| NM_001001563 | *TIMM50* | Translocase of inner mitochondrial membrane 50 homolog (S. cerevisiae) |
| NM_004085 | *TIMM8A* | Translocase of inner mitochondrial membrane 8 homolog A (yeast) |
| NM_012459 | *TIMM8B* | Translocase of inner mitochondrial membrane 8 homolog B (yeast) |
| NM_012460 | *TIMM9* | Translocase of inner mitochondrial membrane 9 homolog (yeast) |
| NM_014765 | *TOMM20* | Translocase of outer mitochondrial membrane 20 homolog (yeast) |
| NM_020243 | *TOMM22* | Translocase of outer mitochondrial membrane 22 homolog (yeast) |
| NM_006809 | *TOMM34* | Translocase of outer mitochondrial membrane 34 |
| NM_006114 | *TOMM40* | Translocase of outer mitochondrial membrane 40 homolog (yeast) |
| NM_032174 | *TOMM40L* | Translocase of outer mitochondrial membrane 40 homolog (yeast)-like |
| NM_014820 | *TOMM70A* | Translocase of outer mitochondrial membrane 70 homolog A (S. cerevisiae) |
| NM_000546 | *TP53* | Tumor protein p53 |
| NM_000714 | *TSPO* | Translocator protein (18kDa) |
| NM_021833 | *UCP1* | Uncoupling protein 1 (mitochondrial, proton carrier) |
| NM_003355 | *UCP2* | Uncoupling protein 2 (mitochondrial, proton carrier) |
| NM_003356 | *UCP3* | Uncoupling protein 3 (mitochondrial, proton carrier) |
| NM_004182 | *UXT* | Ubiquitously-expressed transcript |
| NM_001101 | *ACTB* | Actin, beta |
| NM_004048 | *B2M* | Beta-2-microglobulin |
| NM_002046 | *GAPDH* | Glyceraldehyde-3-phosphate dehydrogenase |
| NM_000194 | *HPRT1* | Hypoxanthine phosphoribosyltransferase 1 |
| NM_001002 | *RPLP0* | Ribosomal protein, large, P0 |

## Suplemmentary table 2. Significant p-values for GO Biological Process 2018

| Name | p value | q value |
|---|---|---|
| mitochondrion morphogenesis (GO:0070584) | 0.000027 | 5.075895e-04 |
| mitochondrial fragmentation involved in apoptotic process (GO:0043653) | 0.000027 | 5.075895e-04 |
| cell part morphogenesis (GO:0032990) | 0.000042 | 7.150710e-04 |
| mitochondrion transport along microtubule (GO:0047497) | 0.000050 | 7.963699e-04 |
| positive regulation of intrinsic apoptotic signaling pathway (GO:2001244) | 0.000130 | 1.822294e-04 |
| protein import into mitochondrial matrix (GO:0030150) | 0.000130 | 1.438956e-03 |
| regulation of protein oligomerization (GO:0032459) | 0.000191 | 1.729392e-03 |
| establishment of mitochondrion localization, microtubule-mediated (GO:0034643) | 0.005389 | 3.952111e-04 |
| negative regulation of endoplasmic reticulum calcium ion concentration (GO:0032471) | 0.005389 | 2.790042e-02 |
| adenine nucleotide transport (GO:0051503) | 0.006284 | 3.952111e-04 |
| ornithine transport (GO:0015822) | 0.006284 | 2.790042e-02 |
| amino-acid betaine transport (GO:0015838) | 0.006284 | 2.790042e-02 |
| carnitine transport (GO:0015879) | 0.006284 | 2.790042e-02 |
| outer mitochondrial membrane organization (GO:0007008) | 0.006284 | 2.790042e-02 |
| purine ribonucleotide transport (GO:0015868) | 0.006284 | 3.952111e-04 |
| inner ear receptor stereocilium organization (GO:0060122) | 0.006284 | 2.790042e-02 |
| positive regulation of mitochondrial calcium ion concentration (GO:0051561) | 0.007179 | 2.811660e-02 |
| vasodilation (GO:0042311) | 0.008073 | 2.811660e-02 |
| dynamin family protein polymerization involved in mitochondrial fission (GO:0003374) | 0.008073 | 2.811660e-02 |
| mitochondrial protein processing (GO:0034982) | 0.008073 | 2.811660e-02 |
| positive regulation of autophagosome assembly (GO:2000786) | 0.008073 | 2.811660e-02 |
| cellular response to superoxide (GO:0071451) | 0.008073 | 2.811660e-02 |
| protein localization to vacuole (GO:0072665) | 0.008073 | 2.811660e-02 |
| dynamin family protein polymerization involved in membrane fission (GO:0003373) | 0.008073 | 2.811660e-02 |
| removal of superoxide radicals (GO:0019430) | 0.008073 | 2.811660e-02 |
| peroxisome fission (GO:0016559) | 0.008073 | 5.075895e-04 |
| positive regulation of vacuole organization (GO:0044090) | 0.008966 | 3.015685e-02 |
| positive regulation of cellular component organization (GO:0051130) | 0.008966 | 1.081578e-01 |
| chaperone-mediated protein transport (GO:0072321) | 0.008966 | 3.015685e-02 |

| Name | p value | q value |
|---|---|---|
| anterograde axonal transport (GO:0008089) | 0.008966 | 5.364380e-02 |
| organelle transport along microtubule (GO:0072384) | 0.009858 | 2.880018e-03 |
| response to axon injury (GO:0048678) | 0.009858 | 3.039526e-02 |
| carnitine shuttle (GO:0006853) | 0.009858 | 3.039526e-02 |
| macromolecule modification (GO:0043412) | 0.009858 | 4.655455e-02 |
| receptor catabolic process (GO:0032801) | 0.009858 | 4.655455e-02 |
| apoptotic mitochondrial changes (GO:0008637) | 0.009858 | 3.345160e-03 |
| fatty acid transmembrane transport (GO:1902001) | 0.009858 | 3.039526e-02 |
| regulation of T cell differentiation in thymus (GO:0033081) | 0.010750 | 3.269037e-02 |
| regulation of protein targeting to membrane (GO:0090313) | 0.010750 | 4.894812e-02 |
| axonal transport (GO:0098930) | 0.011641 | 5.715099e-02 |
| placenta development (GO:0001890) | 0.011641 | 3.356060e-02 |
| coenzyme biosynthetic process (GO:0009108) | 0.011641 | 5.158289e-02 |
| regulation of superoxide anion generation (GO:0032928) | 0.011641 | 3.356060e-02 |
| mitochondrial genome maintenance (GO:0000002) | 0.011641 | 3.356060e-02 |
| myelination in peripheral nervous system (GO:0022011) | 0.011641 | 3.356060e-02 |
| response to alcohol (GO:0097305) | 0.011641 | 4.664457e-02 |
| cofactor biosynthetic process (GO:0051188) | 0.012531 | 5.364380e-02 |
| positive regulation of establishment of protein localization to mitochondrion (GO:1903749) | 0.012531 | 1.093151e-01 |
| cellular response to starvation (GO:0009267) | 0.012531 | 1.081578e-01 |
| receptor metabolic process (GO:0043112) | 0.012531 | 7.441943e-02 |
| positive regulation of mitochondrial fission (GO:0090141) | 0.012531 | 1.023734e-03 |
| necroptotic process (GO:0070266) | 0.012531 | 3.392400e-02 |
| thymus development (GO:0048538) | 0.012531 | 3.392400e-02 |
| positive regulation of catalytic activity (GO:0043085) | 0.012531 | 5.420351e-02 |
| response to ethanol (GO:0045471) | 0.012531 | 3.392400e-02 |
| positive regulation of cellular catabolic process (GO:0031331) | 0.013420 | 1.081578e-01 |
| regulation of mitochondrial membrane potential (GO:0051881) | 0.013420 | 3.423732e-03 |
| intracellular lipid transport (GO:0032365) | 0.013420 | 3.546669e-02 |
| regulation of developmental growth (GO:0048638) | 0.013420 | 5.286277e-02 |

| Name | p value | q value |
|---|---|---|
| mitochondrion localization (GO:0051646) | 0.013420 | 3.546669e-02 |
| superoxide metabolic process (GO:0006801) | 0.014309 | 5.158289e-02 |
| programmed necrotic cell death (GO:0097300) | 0.014309 | 3.609622e-02 |
| retina homeostasis (GO:0001895) | 0.014309 | 5.885117e-02 |
| guanosine-containing compound metabolic process (GO:1901068) | 0.014309 | 3.609622e-02 |
| regulation of autophagosome assembly (GO:2000785) | 0.014309 | 5.420351e-02 |
| mitochondrial fusion (GO:0008053) | 0.014309 | 1.264259e-03 |
| negative regulation of steroid biosynthetic process (GO:0010894) | 0.014309 | 3.609622e-02 |
| regulation of multicellular organism growth (GO:0040014) | 0.015196 | 3.790523e-02 |
| protein localization to membrane (GO:0072657) | 0.015196 | 1.479999e-01 |
| positive regulation of autophagy (GO:0010508) | 0.015196 | 8.238900e-02 |
| organelle fusion (GO:0048284) | 0.016083 | 1.431302e-03 |
| organelle fission (GO:0048285) | 0.016083 | 2.435109e-03 |
| cellular response to glucose starvation (GO:0042149) | 0.016083 | 5.420351e-02 |
| endoplasmic reticulum calcium ion homeostasis (GO:0032469) | 0.016083 | 3.839242e-02 |
| regulation of oxidative stress-induced intrinsic apoptotic signaling pathway (GO:1902175) | 0.016083 | 3.839242e-02 |
| release of cytochrome c from mitochondria (GO:0001836) | 0.016083 | 1.431302e-03 |
| positive regulation of macroautophagy (GO:0016239) | 0.016083 | 6.255269e-02 |
| positive regulation of intracellular protein transport (GO:0090316) | 0.016083 | 2.811660e-02 |
| regulation of cell division (GO:0051302) | 0.016083 | 8.102274e-02 |
| calcium-mediated signaling using intracellular calcium source (GO:0035584) | 0.016083 | 3.839242e-02 |
| anion transmembrane transport (GO:0098656) | 0.016083 | 3.839242e-02 |
| mitochondrial calcium ion homeostasis (GO:0051560) | 0.016970 | 3.965535e-02 |
| regulation of T cell differentiation (GO:0045580) | 0.016970 | 5.420351e-02 |
| regulation of mitochondrial fission (GO:0090140) | 0.016970 | 1.438956e-03 |
| mitochondrial transport (GO:0006839) | 0.016970 | 2.274473e-13 |
| regulation of macroautophagy (GO:0016241) | 0.017855 | 1.143919e-01 |
| mitochondrial fission (GO:0000266) | 0.017855 | 1.604780e-03 |
| mitochondrion disassembly (GO:0061726) | 0.017855 | 5.885117e-02 |
| hydrogen peroxide metabolic process (GO:0042743) | 0.017855 | 4.118066e-02 |

| Name | p value | q value |
|---|---|---|
| positive regulation of mitochondrion organization (GO:0010822) | 0.018740 | 1.729392e-03 |
| GTP metabolic process (GO:0046039) | 0.018740 | 4.245185e-02 |
| cellular response to amino acid starvation (GO:0034198) | 0.018740 | 5.898107e-02 |
| positive regulation of protein targeting to membrane (GO:0090314) | 0.019624 | 4.400548e-02 |
| autophagy of mitochondrion (GO:0000422) | 0.019624 | 5.910387e-02 |
| RNA modification (GO:0009451) | 0.019624 | 7.176495e-02 |
| macromolecule catabolic process (GO:0009057) | 0.019624 | 5.536105e-02 |
| positive regulation of protein oligomerization (GO:0032461) | 0.020508 | 4.552636e-02 |
| peroxisome organization (GO:0007031) | 0.020508 | 1.729392e-03 |
| heart contraction (GO:0060047) | 0.020508 | 6.255269e-02 |
| regulation of cytokinesis (GO:0032465) | 0.021390 | 9.139507e-02 |
| positive regulation of reactive oxygen species metabolic process (GO:2000379) | 0.021390 | 5.898107e-02 |
| regulation of cell cycle process (GO:0010564) | 0.021390 | 9.783864e-02 |
| positive regulation of protein targeting to mitochondrion (GO:1903955) | 0.021390 | 9.202875e-02 |
| regulation of cholesterol biosynthetic process (GO:0045540) | 0.022272 | 5.910387e-02 |
| positive regulation of organelle assembly (GO:1902117) | 0.022272 | 6.531306e-02 |
| regulation of intrinsic apoptotic signaling pathway (GO:2001242) | 0.022272 | 5.781882e-03 |
| regulation of protein targeting to mitochondrion (GO:1903214) | 0.022272 | 9.739581e-02 |
| response to hydrogen peroxide (GO:0042542) | 0.023153 | 6.205628e-02 |
| protein complex assembly (GO:0006461) | 0.024033 | 3.392400e-02 |
| positive regulation of protein complex assembly (GO:0031334) | 0.025792 | 9.739581e-02 |
| interleukin-12-mediated signaling pathway (GO:0035722) | 0.025792 | 6.440725e-02 |
| cellular response to interleukin-12 (GO:0071349) | 0.025792 | 6.440725e-02 |

## Supplementary table 3. Significant p-values for GO Molecular Function 2018

| Name | p value | q value |
|---|---|---|
| adenine nucleotide transmembrane transporter activity (GO:0000295) | 0.000021 | 0.000002 |
| ADP transmembrane transporter activity (GO:0015217) | 0.000034 | 0.000002 |
| antiporter activity (GO:0015297) | 0.000103 | 0.001032 |
| amino-acid betaine transmembrane transporter activity (GO:0015199) | 0.005389 | 0.022452 |
| carnitine transmembrane transporter activity (GO:0015226) | 0.005389 | 0.022452 |
| L-ornithine transmembrane transporter activity (GO:0000064) | 0.005389 | 0.022452 |
| ATP transmembrane transporter activity (GO:0005347) | 0.008073 | 0.000403 |
| adenyl-nucleotide exchange factor activity (GO:0000774) | 0.009858 | 0.030806 |
| adenyl nucleotide binding (GO:0030554) | 0.009858 | 0.030806 |
| protein channel activity (GO:0015266) | 0.009858 | 0.030806 |
| Rac GTPase binding (GO:0048365) | 0.012531 | 0.067887 |
| nuclease activity (GO:0004518) | 0.013420 | 0.080954 |
| protein transmembrane transporter activity (GO:0008320) | 0.014309 | 0.042084 |
| beta-tubulin binding (GO:0048487) | 0.014309 | 0.002208 |
| organic cation transmembrane transporter activity (GO:0015101) | 0.017855 | 0.046987 |
| copper ion binding (GO:0005507) | 0.020508 | 0.067183 |
| endonuclease activity (GO:0004519) | 0.021390 | 0.088509 |

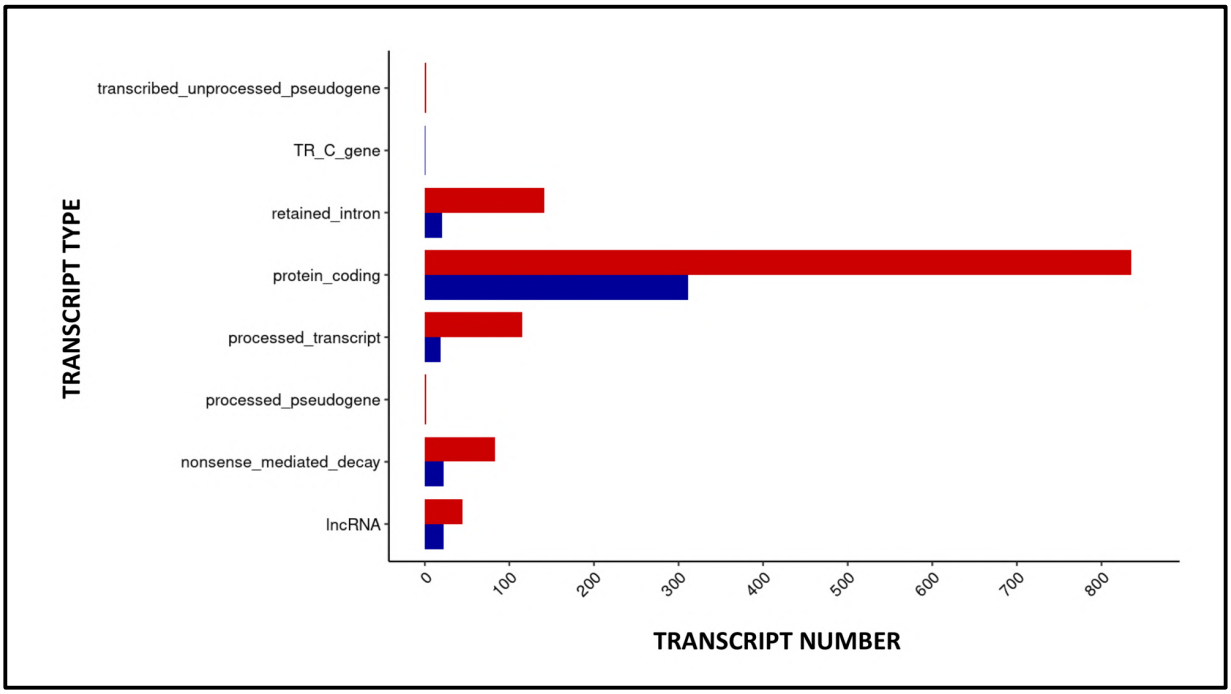


**Supplementary figure 1. Type and number of differentially expressed transcripts found in RNAseq analysis.** Graph showing the transcript type on the y-axis and the transcript number on the x-axis, filtered by FDR<0.05 using DESeq2 package analysis. lncRNA – long non-coding RNA, TR_C_gene – constant chain T cell receptor gene that undergoes somatic recombination before transcription.

**APPENDIX**

The following documents are attached as appendix in the following order:

a) Academic transcript (Master program in Immunology)

**Publications in the period:**

***Book Chapter:***

b) **Ghirotto, Bruno**; Olsen Saraiva Câmara, Niels. Regulação da Dinâmica Mitocondrial em Doenças Renais: Abordagens e Perspectivas. Atualidades em Nefrologia 16. Editora Sarvier, 2020. ISBN: 9786556860069.

***Published papers:***

c) **Ghirotto B**, Terra FF, Câmara NOS, Basso PJ. Sirtuins in B lymphocytes metabolism and function. *World J Exp Med*. 2019;9(1):1-13.

***In review papers:***

d) Leite JA, **Ghirotto B**, Targhetta VP, Lima J, Câmara NOS. Sirtuins as pharmacological targets in neurodegenerative and neuropsychiatric disorders. British Journal of Pharmacology (submitted).
e) Foresto-Neto O, **Ghirotto B**, Câmara NOS. The kidney as a sensor for short-chain fatty acids. Kidney 360 (submitted).
f) Basso PJ, Sales-Campos H, Nardini V, Alves VBF, Bonfá G, Rodrigues CC, **Ghirotto B**, Chica JEL, Nomizo A, Cardoso CRB. Peroxisome Proliferator-activated Receptor alpha (PPAR-alpha) mediates the beneficial effects of Atorvastatin in experimental colitis. Frontiers in Immunology (submitted).
g) Breda CNS, Breda LCD, Carvalho LAC, Amano MT, Terra FF, Silva RC, Fragas MG, Forni MF, Venturini G, Feitosa ACM, **Ghirotto B**, Cruz MC, Cunha FF, Ignacio A, Latância M, Castoldi A, Andrade-Oliveira V, Silva EM, Hiyane MI, Pereira AC, Festuccia WTL, Meotti FC, Câmara NOS. Loss of Rictor in neutrophils impairs fusion of granules and affects cellular metabolism favoring increased bacterial burden in sepsis. The Journal of Immunology (submitted).

Universidade de São Paulo
Brasil

# FICHA DO ALUNO

Janus

**42133 - 9303859 / 1 - Bruno Ghirotto Nunes**

| | |
|---|---|
| **Email:** | bruno.ghirotto.nunes@usp.br |
| **Data de Nascimento:** | 05/07/1996 |
| **Cédula de Identidade:** | RG - 50.012.141-2 - SP |
| **Local de Nascimento:** | Estado de São Paulo |
| **Nacionalidade:** | Brasileira |
| **Graduação:** | Bacharel em Ciências Biológicas - Instituto de Biociências - Universidade de São Paulo - São Paulo - Brasil - 2019 |

| | |
|---|---|
| **Curso:** | Mestrado |
| **Programa:** | Imunologia |
| **Data de Matrícula:** | 10/01/2019 |
| **Início da Contagem de Prazo:** | 10/01/2019 |
| **Data Limite para o Depósito:** | 12/07/2021 |
| **Orientador Acadêmico:** | Prof(a). Dr(a). Niels Olsen Saraiva Câmara - 10/01/2019 até 16/04/2019 Email: niels@icb.usp.br |
| **Orientador:** | Prof(a). Dr(a). Niels Olsen Saraiva Câmara - 17/04/2019 até o presente Email: niels@icb.usp.br |

**Proficiência em Línguas:**

Inglês, Aprovado em 10/01/2019

| | |
|---|---|
| **Data de Aprovação no Exame de Qualificação:** | Aprovado em 23/04/2020 |

**Data do Depósito do Trabalho:**

**Título do Trabalho:**

**Data Máxima para Aprovação da Banca:**

**Data de Aprovação da Banca:**

**Data Máxima para Defesa:**

**Data da Defesa:**

**Resultado da Defesa:**

**Histórico de Ocorrências:** Primeira Matrícula em 10/01/2019
Aluno matriculado no Regimento da Pós-Graduação USP (Resolução nº 6542 em vigor de 20/04/2013 até 28/03/2018).

**Última ocorrência:** Matrícula de Acompanhamento em 15/03/2021

| Sigla | Nome da Disciplina | Início | Término | Carga Horária | Cred. | Freq. | Conc. | Exc. | Situação |
|---|---|---|---|---|---|---|---|---|---|
| BMI5897-2/2 | Imunidade Inata e Adaptativa no Sistema Nervoso Central | 04/02/2019 | 03/03/2019 | 60 | 4 | 100 | A | N | Concluída |
| BMI5881-6/2 | Regulação da Resposta Imune | 11/03/2019 | 05/05/2019 | 120 | 8 | 100 | A | N | Concluída |
| QBQ5789-4/2 | Bioenergética Mitocondrial: Abordagens in situ e in vivo (Instituto de Química - Universidade de São Paulo) | 22/03/2019 | 02/05/2019 | 60 | 4 | 100 | A | N | Concluída |
| MCM5919-2/3 | Imunoterapia para Doenças Neoplásicas (Faculdade de Medicina - Universidade de São Paulo) | 17/06/2019 | 23/06/2019 | 30 | 2 | 100 | A | N | Concluída |
| ICB5726-2/1 | Imunodeficiências Primárias e Doenças Autoinflamatórias | 01/08/2019 | 04/09/2019 | 120 | 8 | 100 | A | N | Concluída |
| BMI5863-9/3 | Seminário Didático-Cientifico em Imunologia II | 08/08/2019 | 20/11/2019 | 60 | 4 | 100 | A | N | Concluída |
| IBI5073-2/1 | Biologia de Sistemas para Ciências da Vida (Curso Interunidades: Bioinformática - Universidade de São Paulo) | 26/09/2019 | 18/12/2019 | 60 | 4 | 100 | A | N | Concluída |

| | Créditos mínimos exigidos | | Créditos obtidos |
|---|---|---|---|
| | Para exame de qualificação | Para depósito da dissertação | |
| **Disciplinas:** | 16 | 32 | 34 |
| **Estágios:** | | | |
| **Total:** | 16 | 32 | 34 |

**Créditos Atribuídos à Dissertação:** 64

**Conceito a partir de 02/01/1997:**

A - Excelente, com direito a crédito; B - Bom, com direito a crédito; C - Regular, com direito a crédito; R - Reprovado; T - Transferência.

Um(1) crédito equivale a 15 horas de atividade programada.

# 3

# REGULAÇÃO DA DINÂMICA MITOCONDRIAL EM DOENÇAS RENAIS: ABORDAGENS E PERSPECTIVAS

Bruno Ghirotto
Niels Olsen Saraiva Câmara

*A participação das mitocôndrias na fisiopatologia das doenças renais vem se evidenciando ao longo dos estudos realizados nos últimos anos. No entanto, pouca ênfase foi atribuída ao processo de dinâmica mitocondrial e sua importância na regulação dos processos inflamatórios e de estresse oxidativo que acometem os rins dos pacientes afetados por essas comorbidades. Sabe-se hoje em dia que as mitocôndrias são organelas totalmente dinâmicas, alterando suas morfologias de acordo com as necessidades bioenergéticas das células, o que leva a uma alteração de suas funções, podendo ser benéfico ou prejudicial à funcionalidade dos órgãos. Dada a importância do fenômeno em diversas doenças já descritas, sobretudo nas neurodegenerativas, este capítulo busca trazer uma atualização sobre a regulação da dinâmica mitocondrial no campo da nefrologia, trazendo uma breve introdução sobre o tema e, posteriormente, detalhando como esse processo pode interferir na patologia das doenças renais, utilizando como referência estudos bastante relevantes de literatura científica, que podem trazer futuras aplicações clínicas aos nefrologistas.*

## INTRODUÇÃO

As mitocôndrias são organelas com uma arquitetura altamente organizada, apresentando alto grau de compartimentalização que é essencial para sua função. A mitocôndria é composta por duas membranas, uma externa e outra interna, esta última onde está localizada a cadeia de transporte de elétrons. O principal papel das mitocôndrias nas células é o acoplamento da oxidação de substratos pelo ciclo do ácido tricarboxílico (TCA) à fosforilação oxidativa (OXPHOS), o que resulta em alta taxa de produção de ATP (até 36 moléculas de ATP para cada molécula de glicose) pela cadeia de elétrons. Além disso, outro papel importante dessas organelas é a utilização de intermediários do ciclo do TCA em reações anabólicas ou regulatórias. Não obstante, a atividade metabólica mitocondrial também culmina na produção de ROS mitocondriais (mtROS), que podem funcionar tanto como sinalizadores celulares como promover dano celular, principalmente por meio de lesões no DNA[1].

Ao contrário do que se pensava, as mitocôndrias não são organelas estáticas, mas sim altamente dinâmicas, modificando seus padrões bioenergéticos de acordo com as necessidades metabólicas das células. As mudanças nos padrões de arquitetura mitocondrial são divididas em dois processos-chave, a fusão e a fissão. Elas garantem a segregação efetiva do DNA mitocondrial bem como regulam os níveis de produção de mtROS, a homeostase de cálcio e a OXPHOS.

A fusão mitocondrial é um processo ainda pouco compreendido, mas sabe-se que ocorre em duas etapas: primeiramente, a fusão da membrana externa é regulada pela interação entre duas proteínas chamadas mitofusinas 1 e 2 (Mfn1 e Mfn2), enquanto a fusão da membrana

World Journal of Experimental Medicine

Submit a Manuscript: https://www.f6publishing.com

*World Journal of Experimental Medicine* 2019 January 16; 9(1): 1-13

DOI: 10.5493/wjem.v9.i1.1

ISSN 2220-315x (online)

*MINIREVIEWS*

# Sirtuins in B lymphocytes metabolism and function

Bruno Ghirotto, Fernanda Fernandes Terra, Niels Olsen Saraiva Câmara, Paulo José Basso

**ORCID number:** Bruno Ghirotto (0000-0001-6835-3329); Fernanda Fernades Terra (0000-0002-2860-5365); Niels Olsen Saraiva Camara (0000-0001-5436-1248); Paulo Jose Basso (0000-0003-4856-9207).

**Author contributions:** Ghirotto B wrote the manuscript, edited, generated the table and performed the literature review; Terra FF wrote the manuscript, generated the figures and performed the literature review; Câmara NOS contributed to review the manuscript and approval of the final version; Basso PJ designed the aim of the minireview, wrote, edited and contributed to final approval of the final version.

**Supported by** Fundação de Amparo à Pesquisa de São Paulo (FAPESP) under Agreements, No. 2015/26682-6, No. 2017/03248-4 and No. 2017/05264-7. This study was financed in part by the Coordenação de Aperfeiçoamento de Pessoal de Nível Superior – Brasil (CAPES) – Finance Code 001.

**Conflict-of-interest statement:** The authors hereby declare to have no potential conflicts of interest.



**Bruno Ghirotto, Fernanda Fernandes Terra, Niels Olsen Saraiva Câmara, Paulo José Basso,** Department of Immunology, Institute of Biomedical Sciences, University of São Paulo, São Paulo 05508-000, Brazil

**Niels Olsen Saraiva Câmara,** Division of Nephrology, School of Medicine, Federal University of São Paulo, São Paulo 04023-062, Brazil

**Niels Olsen Saraiva Câmara,** Laboratory of Renal Physiology (LIM 16), School of Medicine, University of São Paulo, São Paulo 01246-903, Brazil

**Corresponding author:** Niels Olsen Saraiva Câmara, MD, PhD, Research Scientist, Department of Immunology, Institute of Biomedical Sciences, University of São Paulo, Av. Prof. Lineu Prestes, 1730 Cid. Universitaria, São Paulo 05508-000, Brazil. niels@icb.usp.br
**Telephone:** +55-11-30917388
**Fax:** +55-11-30917224

## Abstract

Sirtuins (SIRTs) are NAD$^+$-dependent histone deacetylases and play a role in virtually all cell biological processes. As SIRTs functions vary according to their subtypes, they can either activate or inhibit signaling pathways upon different conditions or tissues. Recent studies have focused on metabolic effects performed by SIRTs in several cell types since specific metabolic pathways (*e.g.*, aerobic glycolysis, oxidative phosphorylation, β-oxidation, glutaminolysis) are used to determine the cell fate. However, few efforts have been made to understand the role of SIRTs on B lymphocytes metabolism and function. These cells are associated with humoral immune responses by secreting larger amounts of antibodies after differentiating into antibody-secreting cells. Besides, both the SIRTs and B lymphocytes are potential targets to treat several immune-mediated disorders, including cancer. Here, we provide an outlook of recent studies regarding the role of SIRTs in general cellular metabolism and B lymphocytes functions, pointing out the future perspectives of this field.

**Key words:** B cells; Metabolic sensors; Histone deacetylases; Cancer



**Core tip:** Current studies have focused on understanding which intracellular molecules coordinate the metabolic flux within the cells. In addition to metabolism, sirtuins play a role in virtually all cell biological processes, but they have not been properly described in B lymphocytes function and metabolism, despite the importance of these immune cells in health and disease. Here we discuss studies that associate sirtuins and B lymphocytes, highlight the gaps found in the literature and point out the future research